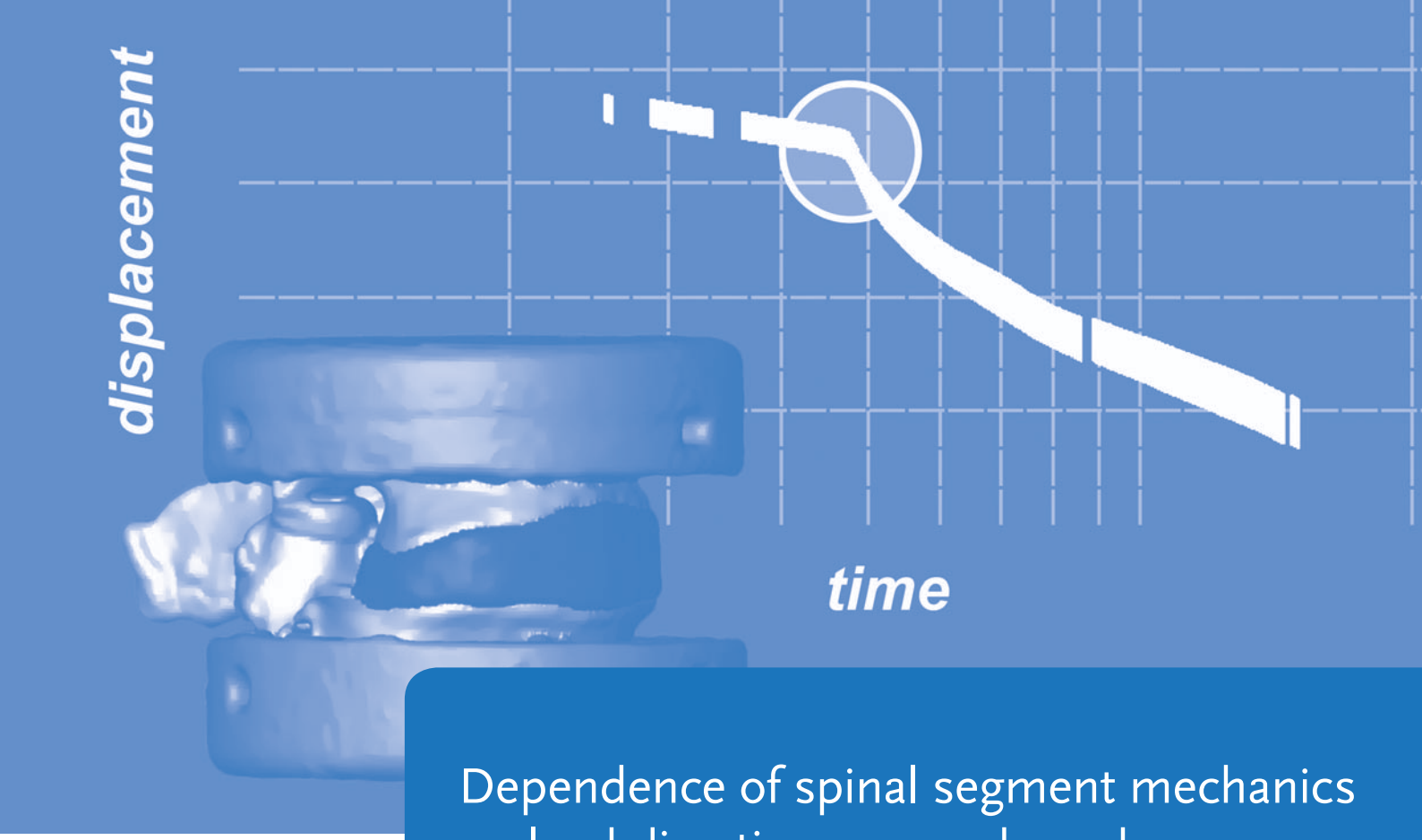

Dependence of spinal segment mechanics on load direction, age and gender

K. Nagel, A. Klein, K. Püschel, M. Morlock, G. Huber

baua:
Federal Institute for Occupational Safety and Health

Research
Project F 2059

K. Nagel
A. Klein
K. Püschel
M. Morlock
G. Huber

Dependence of spinal segment mechanics on load direction, age and gender

Dortmund/Berlin/Dresden 2013

This publication is the final report of the project ‘Dependence of spinal segment mechanics on load direction, age and gender’ – Project F 2059 – on behalf of the Federal Institute for Occupational Safety and Health.
The responsibility for the contents of this publication lies with the authors.

Authors: Dipl.-Ing. Katrin Nagel
Prof. Dr. Michael M. Morlock
Dr.-Ing. Gerd Huber
TUHH - Hamburg University of Technology
Institute of Biomechanics
Denickestr. 15, 21073 Hamburg, Germany

Dr. med. Anke Klein
Prof. Dr. Klaus Püschel
University Medical Center Hamburg-Eppendorf
Department of Legal Medicine
Butenfeld 34, 22529 Hamburg, Germany

Cover figure: Gerd Huber, TUHH, Hamburg University of Technology

Cover design: Susanne Graul,
Federal Institute for Occupational Safety and Health

Production: Bonifatius GmbH, Paderborn

Publisher: Federal Institute for Occupational Safety and Health
Friedrich-Henkel-Weg 1-25, 44149 Dortmund, Germany
Telephone +49 231 9071-0
Fax +49 231 9071-2454
poststelle@baua.bund.de
www.baua.de

Berlin:
Nöldnerstr. 40-42, 10317 Berlin, Germany
Telephone +49 30 51548-0
Fax +49 30 51548-4170

Dresden:
Fabricestr. 8, 01099 Dresden, Germany
Telephone +49 351 5639-50
Fax +49 351 5639-5210

ISBN 978-3-88261-008-6

www.baua.de/dok/4532702

List of Contents

Dependence of spinal segment mechanics on load direction, age and gender

Abstract

Whole body vibrations (WBV) are a potential source for low back pain. The mechanism that associates external WBV and internal spinal overload is still unknown, but might be investigated through joint approaches using numerical simulations and in vitro studies. Knowledge about the mechanical behaviour of the spinal structures is essential for this approach. This study aims to determine the influence of frequency and loading magnitude on the spinal stiffness and of loading magnitude on the numbers of cycles to failure. Functional spinal units (L2-L3, L4-L5) from three donor groups were collected: Midlife Male, Midlife Female and Young Male. Characteristic parameters e.g. endplate area (AREA) and bone mineral density (BMD) were determined. Vertebral Capacity (VC), the product of both, was used as principal influencing factor. In vitro testing was performed in tempered saline solution. 6 specimens underwent ultimate strength testing, enabling comparison of the test pool with previously published measurements. 36 specimens endured cyclic testing. Tests started with non-destructive loading (0.005-12 Hz) in axial compression (<2 kN) and shear (<0.3 kN), followed by fatigue loading (<300,000 cycles, 5°Hz), either in shear (n = 6) or axially (n = 30). For axial loading, the specimens were assigned to three groups with different peak-to-peak loads (0-2 kN, 0-3 kN and 1-3 kN). High BMD of the Young Male group and small AREA of the Midlife Female group resulted in greater VC (37%) for the former group ($p < 0.001$). Ultimate strength results were similar to former studies. Analysis of stiffness parameters revealed that stiffness is non-linear in both load directions, axial stiffness was reduced by shear preload ($p < 0.001$), anterior shear stiffness was larger with a superimposed anterior offset ($p = 0.005$). Midlife Females exhibited a 23% smaller axial stiffness than Midlife Males ($p < 0.001$); shear stiffness for Young Males was larger than for Midlife Males ($p = 0.005$). Stiffness increased with frequency (axial, 19%, $p < 0.001$ and shear, 25%, $p < 0.001$). For the 0-2 kN fatigue loading, endplate failure occurred occasionally (4 of 8), and frequently for 0-3 kN (10 of 13; 1 excluded). Loading with high peak but small amplitude (1-3 kN) lead to occasional specimen failure (4 of 7; 1 excluded). Higher loading amplitudes reduced cycles to failure compared to smaller amplitude, even though the maximum peak (3 kN) was the same. The characteristic creep curves for shear fatigue loading exhibited minor and major discontinuities and separation of the annulus from the endplates, and failure of the bony posterior elements (1 excluded) appeared. The specimens exhibited a large inner- and intra-group variation in VC. AREA serves as a scaling factor for converting axial compressive force to stress. BMD is known to be related to Young's modulus of the vertebral bony structure. The testing of parameters delivered a broad database for numerical analysis, focusing on passive loading as whole body vibrations and load bearing, rather than different postures and voluntarily performed flexion. A cyclic load magnitude of 40-50% of the respective ultimate strength results in fatigue failure for most axially loaded specimens and all shear loaded specimens. Axial failure appears to be predictable using VC; however no correlation was found for shear failure. Other than peak loading, the amplitudes of the cyclic loading dominantly influence fatigue fracture.

Key words: spine, dynamic, axial, shear, fatigue, in vitro, age

Mechanik von Wirbelsäulenbewegungssegmenten – Abhängig von Lastrichtung, Alter und Geschlecht

Kurzreferat

Ganzkörpervibrationen (GKV) sind ein potentieller Auslöser für Schmerzen im Lumbalbereich. Der mechanische Zusammenhang zwischen GKV und interner Überlastung der Wirbelsäule ist unbekannt, könnte jedoch durch Kombination von numerischen Simulationen und in-vitro-Studien untersucht werden. Hierfür muss jedoch das mechanische Verhalten dieser Strukturen bekannt sein. Ziel dieser Studie war es, den Einfluss von Lastfrequenz und -größe auf die Steifigkeit und den Einfluss der Lastgröße auf die Dauerfestigkeit zu ermitteln. Bewegungssegmente (L2-L3, L4-L5) dreier Spendergruppen wurden gesammelt: Mittelalt-Männlich, Mittelalt-Weiblich und Jung-Männlich. Charakteristika wie die Endplattenfläche (AREA) und die Knochendichte (BMD) wurden bestimmt. Deren Produkt, die Vertebrale Kapazität (VC), wurde als Haupteinflussfaktor verwendet. Die Testung wurde in temperierter Salzlösung durchgeführt. 6 Präparate wurden auf ihre Bruchfestigkeit getestet, um Vergleiche mit publizierten Daten zu ermöglichen. 36 Präparate wurden zyklisch belastet. Zunächst wurde zerstörungsfrei (0,005-12 Hz) in Axial- (<2 kN) und Schubrichtung (<0,3 kN) belastet. Anschließend wurde die Dauerfestigkeit (<300.000 Zyklen, 5 Hz) in Schub- bzw. Axialrichtung (n = 6 bzw. n = 30) bestimmt. Im Falle der axialen Dauerlast wurden Gruppen mit verschiedenen Spitze-Spitze-Lasten gebildet (0-2 kN, 0-3 kN und 1-3 kN). Das VC der Jung-Männlich-Gruppe war größer (37 %, $p < 0,001$) als das der Mittelalt-Weiblich-Gruppe; aufgrund der hohen BMD der ersten und der geringeren AREA der zweiten Gruppe. Die Bruchfestigkeit war vergleichbar mit anderen Studien. Beide Lastrichtungen wiesen eine nichtlineare Steifigkeit auf. Die axiale Steifigkeit wurde durch eine überlagerte Schublast verringert ($p < 0,001$) und die anteriore Schubsteifigkeit war bei überlagerter anteriorer Vorlast größer ($p = 0,005$). Die axiale Steifigkeit war für Mittelalt-Weiblich um 23 % geringer als die von Mittelalt-Männlich ($p < 0,001$); während die Schubsteifigkeit von Jung-Männlich größer war als die von Mittelalt-Männlich ($p = 0,005$). Die Steifigkeit stieg mit steigender Frequenz (Axial, 19 %, $p < 0,001$ und Schub, 25 %, $p < 0,001$). 0-2 kN Dauerlast führten zu gelegentlichem (4 von 8) und 0-3 kN zu häufigem (10 von 13, 1 ausgeschlossen) Versagen der Endplatte. Belastung mit der gleichen Maximallast, aber kleineren Amplituden (1-3 kN), führte hingegen zu gelegentlichem Versagen (4 von 7, 1 ausgeschlossen). Das Kriechverhalten für Schubdauerlast zeigten geringfügige und wesentliche Diskontinuitäten. Der Annulus löste sich von den Endplatten und die posterioren Elemente versagten (1 ausgeschlossen). Innerhalb und zwischen den Spendergruppen war VC sehr unterschiedlich. Mittels AREA wird die axiale Kompressionskraft skaliert und in Spannung umgerechnet, während BMD mit dem E-Modul der knöchernen Struktur zusammenhängt. Die Parametermessungen liefern eine Datenbasis für numerische Analysen welche sich mit passiven Lasten wie GKV und dem Heben von Gewichten befassen. Verschiedene Haltungen und Flexion wurden nicht untersucht. Eine zyklische Last von 40-50 % der entsprechenden Bruchlast führt zum Ermüdungsbruch der meisten axial belasteten und aller auf Schub belasteten Präparate. Axiales Versagen, aber nicht Schubversagen, scheint über VC berechenbar zu sein. Abgesehen vom Spitzenwert der zyklischen Last war deren Amplitude ein dominierender Faktor.

Schlüsselwörter: Wirbelsäule, dynamisch, Axial, Schub, Ermüdung, in vitro, Alter

1 Introduction

Exposure to whole body vibrations at workplaces may increase the prevalence of low back pain. This coherency is well known from epidemiological studies and has consequently been addressed in the EU directive 2002/44/EG, which was put into place to protect employees from hazards generated by vibration and noise. The directive covers the exposure and threshold levels for vibrations in the three main directions of movement. Directional multiplying factors are used to compensate for the directional sensibility of the spine. So far, however, no data have been acquired to approve these factors. Furthermore, neither the age nor gender of the employees is taken into account in the directives even though it is known that spinal integrity depends on the bone mineral density and the geometry of the spinal elements, as shown by Brinckmann et al. (1989) and Huber & Mischke et al. (2010).

Although the critical aspects of repeated load cycles for disc degeneration and various diseases of the spine are known, there is lack of scientific investigation in this area. The mechanism of how external whole body vibrations cause internal spinal overload is unknown. Co-activities between numerical simulations and in vitro studies are promising in terms of investigating this mechanism. This can help evaluate the load acting on the spine. However, knowledge about the fatigue strength of the spine exhibited by this loading is also vague, especially with respect to loading direction, the worker's age and gender.

Investigations of the dynamic conditions carried out so far mainly focus on the superior-inferior axis of the spine. However, it is known that in the workplace there are important aspects of loading in the horizontal plane, which needs to be considered as well – especially for heavy working machines. With regard to the shear direction, however, in vitro data on the dynamic properties and failure strength of human spinal specimens are rare.

Dynamic shear load tests with porcine specimens were carried out by van Dieën et al. (2006). Transmission to human functional spinal units (FSUs) is limited. Porcine specimens were also used by van Solinge et al. (2010) to measure shear ultimate strength. In addition, Cripton et al. (1995) and Skrzypiec et al. (2012) conducted experiments on shear ultimate strength using different load rates and different donor groups, respectively. The ultimate shear strength of spinal specimens was determined to be 2.9 kN for midlife population and 3.6 kN for a younger population. However, to the author's knowledge, fatigue experiments in lateral shear direction with human specimens have not been conducted yet.

To gain knowledge regarding these aspects of occupational safety and health, the current study covers three major comparisons: First, high-cycle fatigue experiments with lumbar spine specimens of young male subjects exposed to shear fatigue loading and axial fatigue loading are performed. Second, the gender aspect is examined with the FSUs of midlife male and female donors exposed to fatigue testing according to Huber et al., 2010. Third, specimens from young male donors underwent fatigue experiments with high amplitudes and offsets to investigate whether mainly the cyclic load amplitude (largely independent from the offset) or the cyclic peak load (maximum compression or shear load, which is dependent on offset and amplitude) is decisive for specimen failure.

2 Material and Methods

2.1 Specimens

For the scheduled experiments, three groups of functional spinal units (FSUs) consisting of two vertebrae and one intervertebral disc (IVD) were needed: 12 FSUs of Midlife Male donors, 12 FSUs of Midlife Female donors and 18 FSUs of Young Male donors. The term Midlife corresponds to an age of 45 to 65 years and Young corresponds to an age of 25 to 44 years. These 42 FSUs from the lumbar spine (either L2-L3 or L4-L5) were collected by the Department of Legal Medicine, University Medical Centre Hamburg-Eppendorf (Hamburg, Germany). The specimens were rendered anonymous before they were handed over to the TUHH personnel. The only information available pertained to gender, age and anthropometrical data. The following anthropometrical data were acquired from the donors: body height, body weight, acromial height, elbow height, ankle diameter, knee joint diameter, elbow joint diameter and wrist joint diameter (Tab. 2-1 and Fig. 2-1). The parameters collected were in accordance with those of two preceding projects F 1899 (Huber et al., 2005) and F 2069 (Huber & Mischke et al., 2010).

Tab. 2-1 Anthropometrical data of donors determined, including abbreviations and chosen measurement devices.

denotation	abbreviation	measurement device
body weight	m_B	scales
body height	h_B	tape measure
acromial height	h_{AC}	tape measure
elbow height	h_{EB}	tape measure
ankle diameter	d_{AN}	anthropometer
knee joint diameter	d_{KN}	anthropometer
elbow joint diameter	d_{EB}	anthropometer
wrist joint diameter	d_{WR}	anthropometer

Immediately after explantation, the spinal specimens were wrapped in saline soaked gauze, which was double sealed in plastic bags and kept frozen (< -20°C) until the day of testing. This storage method did not alter creep behaviour significantly (Dhillon et al., 2001) or the stiffness (Gleizes et al., 1998) of the human spinal specimens.

The frozen specimens underwent computed tomography scanning (Department of Legal Medicine, Mx8000 IDT 16, Philips Healthcare, DA Best, NL). The scans were used to determine the quality and usability of the specimens. Numerical processing and examination was performed by using commercial visualisation software (Avizo 5.0, VSG, Merignac, France).

Numerical processing included the generation of 3D models of each lumbar spine. Apart from the assessment of the specimens' suitability, these models were used to derive geometrical parameters, like endplate area and intervertebral disc height. In addition, numerical processing was used to determine the bone mineral density of each vertebra.

Several characteristic parameters of the specimens were determined by two independent observers and a coefficient of determination (R^2) above 0.75 was requested. If systematic errors of measurement between the observers are not existent, the slope of the linear regression between the values of the two observers should not significantly differ from 1. This was statistically tested by a linear regression between the differences of the values (Δ) received by the two observers versus the values of one observer. If the regression of this Δ did not exhibit a slope significantly different from 0, the systematic difference between the observers was regarded as negligible.

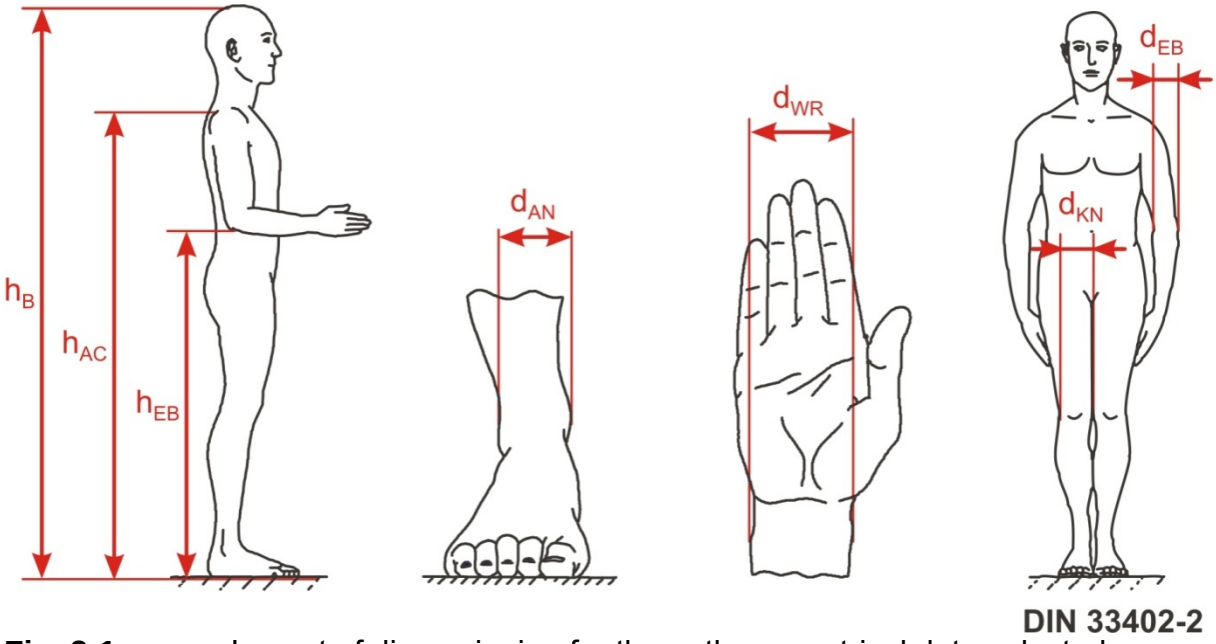

Fig. 2-1 Layout of dimensioning for the anthropometrical data selected (Huber & Mischke et al. (2010), adapted from DIN 33402-2).

2.1.1 Specimen Preparation

Each lumbar spine donated comprised two FSUs (L2-L3 and L4-L5). Separation of the two FSUs of the specimens in the frozen state was not possible because it was difficult to determine the cutting plane without the use of anatomical landmarks in the deep-frozen tissue. Therefore, the two FSUs had to be tested on two consecutive test days so that they would not have to be refrozen.

The specimens were allowed to thaw at room temperature for half a day prior to dissection. On the first day, the lumbar spine was separated into the two respective FSUs. To prepare a specimen for testing, the muscles of one segment were removed (the anterior and posterior longitudinal ligaments were kept intact), whereas the tissue around the second segment was kept on the specimen to prevent drying out during storage in the refrigerator at 4°C. On the following day, the second segment was dissected and tested.

The FSUs were embedded in metal holders using a positioning frame to ensure parallel alignment (Fig. 2-2). To do this, a two-component polymer resin (Ureol, Huntsman Advanced Materials, Everberg, Belgium) was used. In order to improve fixation in resin, screws were inserted to the facet joint bearing areas of the free

caudal and to the cranial facet joints of all the segments tested. Additional screws were inserted to the endplates and the vertebral bodies of the specimens were foreseen for the high cycle shear load. This was necessary to provide improved resistance to the moments that stressed the fixation interface due to anterior-posterior displacement (Fig. 2-3).

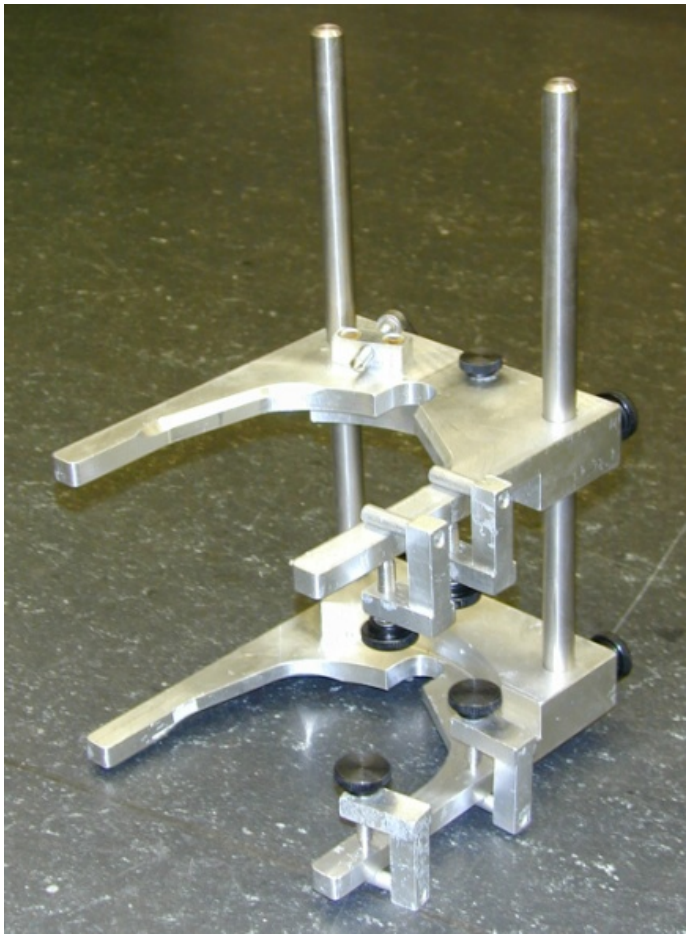

Fig. 2-2 Frame for potting and transporting the FSUs (Huber et al., 2005).

Fig. 2-3 Specimen 3012 L2-L3 with screws for improved fixation.

2.1.2 Endplate Area

The endplate area (AREA) of vertebrae is an important parameter in helping to classify the load bearing structure of the spine and can serve to accounts for the huge variation in human body size. In order to calculate the endplate area, the pre-test CT data were processed using 3D visualisation software (Avizo 5.0, VSG, Merignac, France).

After generating three-dimensional models of the bony structure, the endplate area was independently determined by two persons according to the following procedure: First, the planes to cut the vertebral body at the height of the superior and inferior endplates were selected. To find the correct plane, the cutting plane was positioned parallel to the apparent load bearing area of the vertebra and then moved towards the vertebra until it penetrated the surface so that a closed contour could be obtained. The contour coordinates were exported in a text file.

It was infeasible to obtain a closed contour for some of the extensively deformed vertebrae. This was especially the case with the midlife group because it was impossible to position the cutting plane in a way that allowed a contour to be generated without including parts of the pedicles (Fig. 2-4).

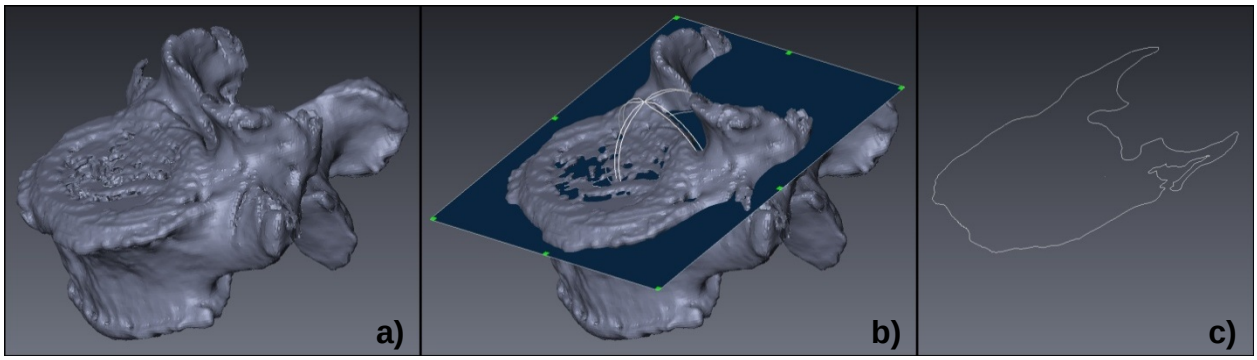

Fig. 2-4 Generating the endplate contour for deformed vertebrae using the regular method (left: 3D reconstruction of a deformed vertebra; middle: positioning of the cutting plane; right: resulting contour).

To determine a closed contour for these specimens, the 3D model of the vertebra was edited. The pedicles of the model were removed using volume editing tools. In order to place the cutting line, the apparent confinement of the endplate plateau was taken as the actual endplate area rim. After removing the pedicles, the cutting planes were selected according to the regular procedure and a closed contour could be obtained (Fig. 2-5). The modified method was applied if the endplate level was considerably below the upper pedicle attachment. The decision as to which procedure to use was made by the respective observer.

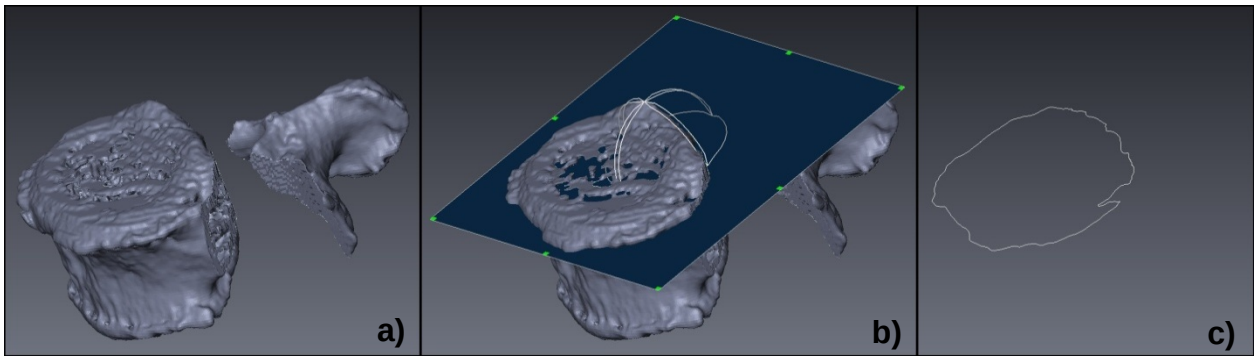

Fig. 2-5 Adapted method to generate the endplate contour for deformed vertebrae (left: model of deformed vertebra with removed pedicles; middle: positioning of the cutting plane; right: resulting contour).

The contour obtained had to undergo a further numerical process to calculate the endplate area (MATLAB, The MathWorks, Inc., Natick, MA, USA). However, this was not directly possible, because the contour line data consisted of several consecutive smaller sections arranged in arbitrary order in the data file, which was not appropriate to determine the enclosed area with the respective function (polyarea.m function). In project F 2069, this issue was dealt with using a MATLAB routine, which implemented a hullfit function (Huber & Mischke et al., 2010). This delivered a re-ordered lineset with a slightly decreased accuracy. In this project (F 2059), these single lines were connected using the 3D visualisation software until there was only one line left. Hence, the data file contained the data points in the correct order. After a coordinate transformation was performed to transform the data to the two-dimensional space, the enclosed area was computed (polyarea.m function). By using this procedure, the deformed endplate contours displaying undercuts and alternating coordinates (Fig. 2-6) did not have to be taken into account.

In order to gain confidence in the data gathered, the results of the two observers were compared. If deviation was greater than 10%, the measurement procedure was repeated by both researchers and the average of the final values of both was calculated.

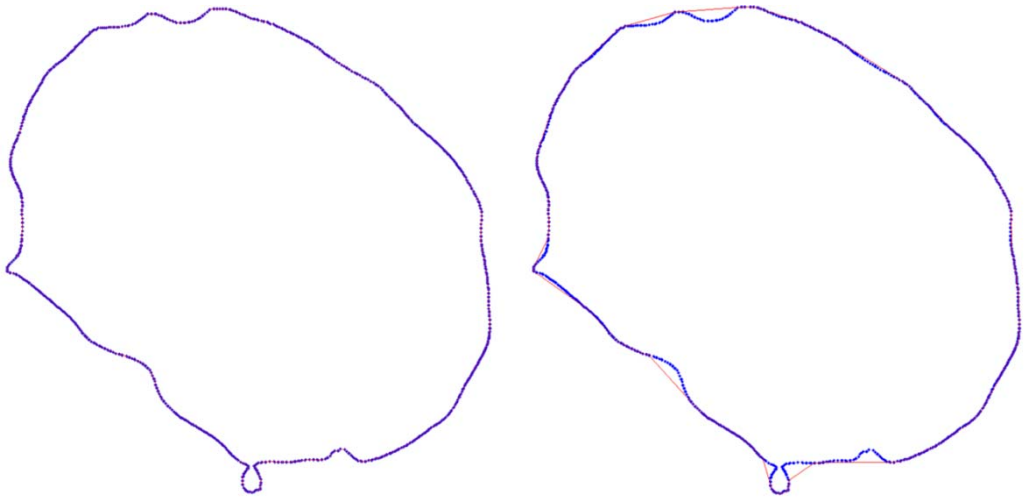

Fig. 2-6 Line set of deformed endplate processed with the two MATLAB procedures (left: polyarea function; right: hullfit function).

2.1.3 Bone Mineral Density

Ultimate strength is also related to bone mineral density (BMD). It is hypothesised that this might be true for the risk of fatigue fractures of vertebrae (Brinckmann et al., 1989). In this project, the BMD of the vertebrae was determined with the help of the CT scans. BMD was calculated based on the Hounsfield units (HU), which reflect the radiological attenuation caused by the material examined. Therefore, a dipotassium phosphate (K_2HPO_4) phantom with three vials was scanned in the CT together with each of the lumbar spines. The vials contained 0, 100 and 500 mg K_2HPO_4 per ml of distilled water. The HU value for each vertebra was determined using 3D visualisation software (Avizo 5.0, VSG, Merignac, France). A defined rectangular volume of about 1,100 mm³ was placed in the approximate centre of the numerical model of the vertebrae (Fig. 2-7) and the mean HU of the cancellous bone was computed. Since the voxel size differed depending on the field of view (FOV) of the CT scan, the number of voxels had to be adjusted for every scan to prevent reasonable changes in the volume analysed.

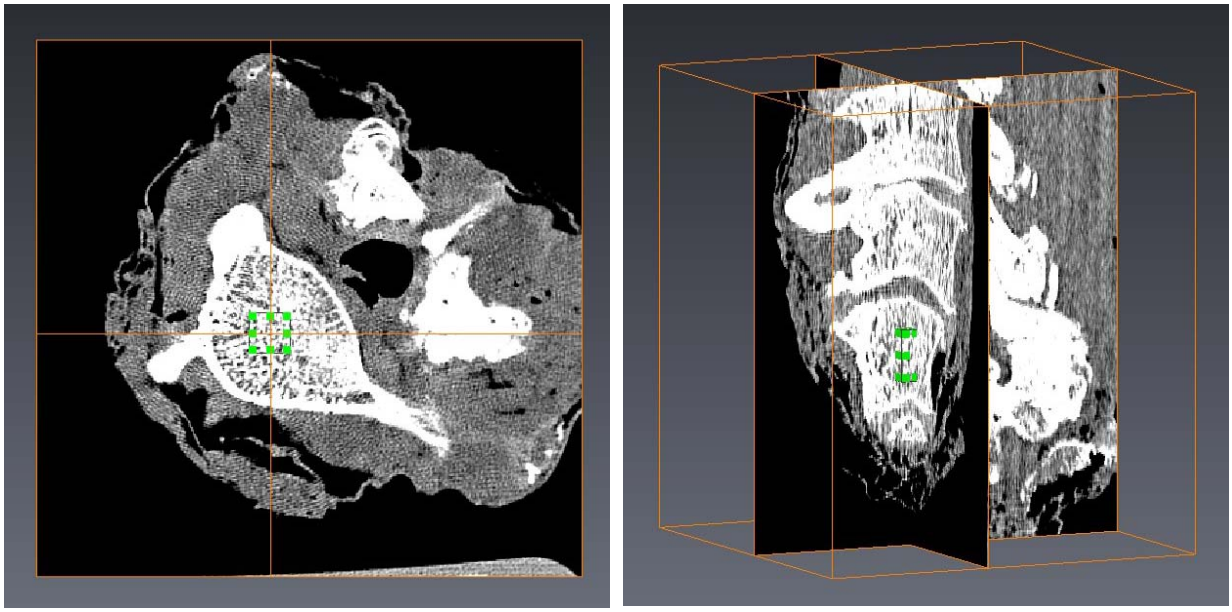

Fig. 2-7 Positioning of the evaluation volume (box with green margins) within a spinal vertebra shown in the longitudinal view (left) and frontal-lateral view (right).

To convert the obtained HU mean values into BMD values (mg K_2HPO_4/ml), the HU values of each vial of the phantom were determined for each lumbar spine in the same way it was done for the vertebrae. Hereby, a specimen-specific relationship between HU and mg K_2HPO_4 per ml was obtained. If the scanner exhibited an offset for vial with pure water, which should be zero by definition, the regression was corrected (Fig. 2-8).

The BMD values were determined by two observers and their results compared. Values with a deviation of greater than 15% were reviewed. This threshold is higher than the previously described 10% threshold to account for the high standard deviation of the inhomogeneous material. After revision, the results of the two researchers were averaged.

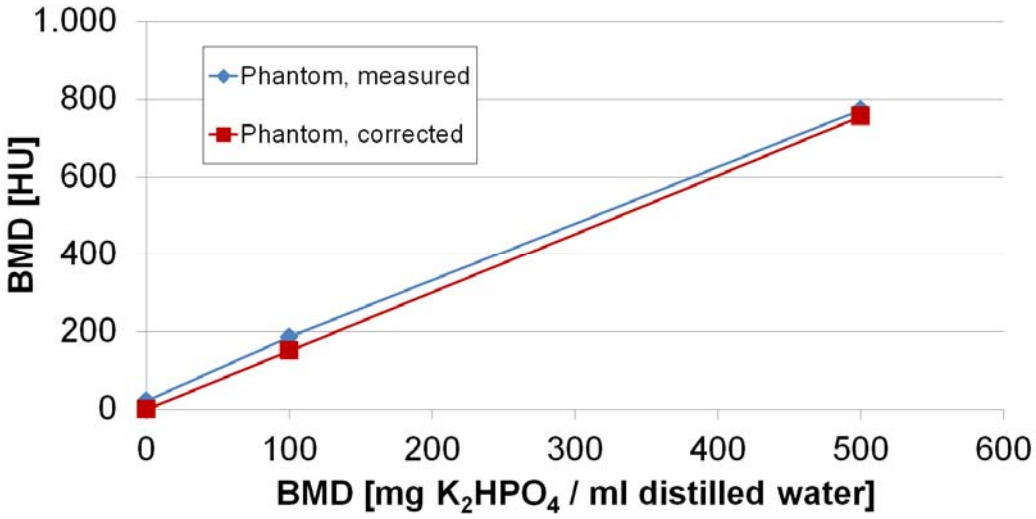

Fig. 2-8 Correction of the linear relationship between HU and mg K_2HPO_4/ml distilled water.

2.1.4 Intervertebral Disc Height – Frobin Classification

The state of degeneration of the spinal segments was quantified based on the intervertebral disc (IVD) height. Frobin et al., 1997 introduced a method to determine the IVD height from lateral radiographs. They evaluated 892 lumbar spines of female and male subjects between the ages of 15 and 57. With this method, the IVD height can be determined, while the influence of distortion, axial rotation and lateral tilt of the spine or vertebrae is compensated. The result is referred to as 'corrected relative disc height', a measure of disc height with respect to the anterior-posterior dimension of the adjacent cranial vertebra. The resulting database can be taken as reference values for healthy spines because pathologically deformed discs and vertebrae have been excluded. Comparing the IVD data with these references can give an impression of the status of degeneration of the respective sample. However, previous studies have shown that the comparison should be made with respect to the specimen within the experimental group since the height of the unloaded specimens in vitro appears to be higher than those in vivo.

The IVD height was determined using a semiautomatic numerical procedure (MATLAB, The MathWorks, Natick, MA) following the method of Frobin et al. (1997) (Fig. 2-9). The input data were lateral projections of the specimens based on the CT scans. A visualisation software (Avizo 5.0, VSG, Merignac, France) was used to generate the lateral projections (Frobin et al., 1997; Huber & Mischke et al., 2010). The determination was carried out by two observers with the help of the semiautomatic procedure. The results were compared and values with a deviation of more than 10% were revised. The data of the two observers was averaged.

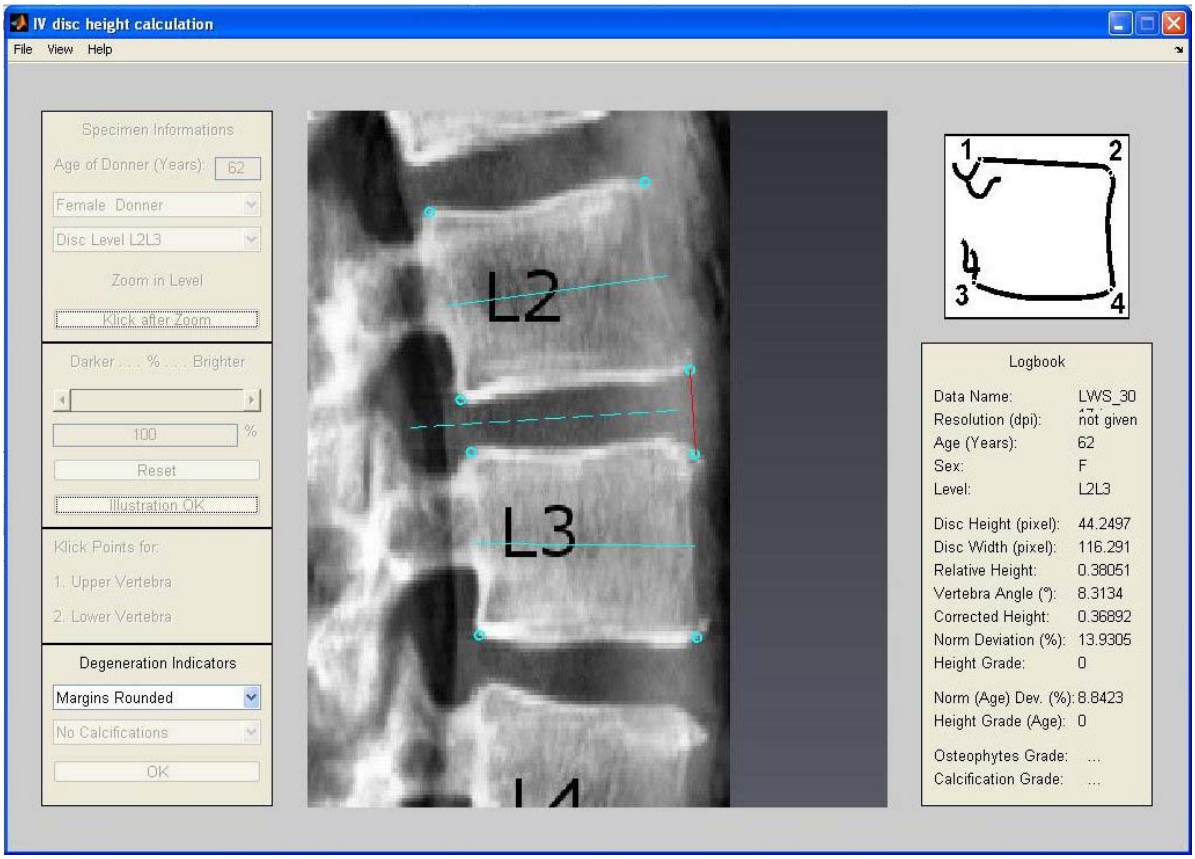

Fig. 2-9 User Interface for IVD height determination according to Frobin et al. (1997).

2.1.5 Post-Test Classification by CT and Thompson Grading

After mechanical testing, supplementary CT scans of each specimen were obtained. For specimens that were tested in shear mode, the failure mechanism was more difficult to evaluate due to the reversible deformation after removal of the shear load. Therefore, the respective specimens were deep frozen in a loaded position of about 18 mm shear deformation (Fig. 2-10), which was the deformation at the end of testing. This way, the fractured pedicles could be determined more clearly in the radiographs and CT scans which were taken afterwards.

Disc degeneration was graded after testing by means of a morphological section. Four aspects of the FSU were classified according to the grades I to V as follows: nucleus, annulus, endplate and vertebral body. The classification scheme according to Thompson et al. (1990) is given in Tab. 2-2.

To enable grading, the specimens were cut in the mid-sagittal plane by a band saw (EXAKT 3031 CP/N, EXAKT Advanced Technologies GmbH, Norderstedt, Germany). Debris was removed by briefly rinsing the sectional area. Care had to be taken to prevent the disc from resorbing fluid. Afterwards, photographs were taken and evaluated by two observers. The average of the four grading aspects was calculated for every specimen and observer and the mean between the two observers was taken as the result. No revision criterion was applied.

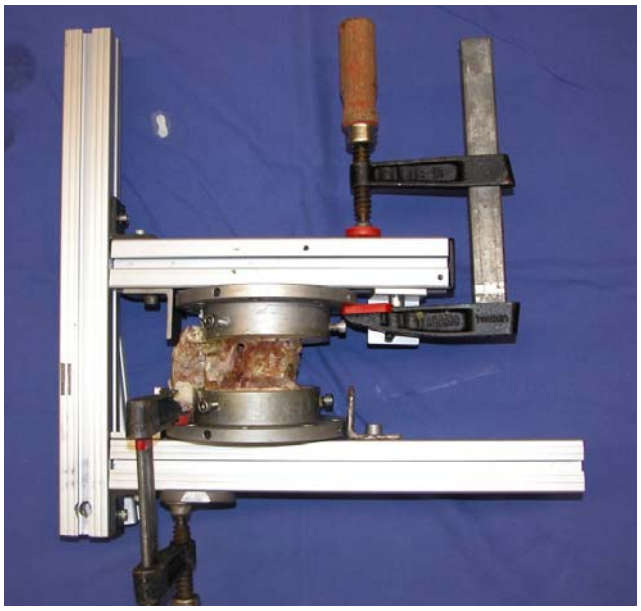

Fig. 2-10 Shear specimen fixed in a frame providing a displacement of about 18 mm of the upper fixation pot during deep freezing.

Tab. 2-2 Scheme for grading the degeneration of specimens according to Thompson et al. (1990).

Grade	Nucleus	Annulus	Endplate	Vertebral body
I	Bulging gel	Discrete fibrous lamellas	Hyaline, uniformly thick	Margins rounded
II	White fibrous tissue peripherically	Mucinous material between lamellas	Thickness irregular	Margins pointed
III	Consolidated fibrous tissue	Extensive mucinous infiltration; loss of annular-nucleus demarcation	Focal defects in cartilage	Early chondrophytes or osteophytes at margins
IV	Horizontal clefts parallel to endplate	Focal disruptions	Fibrocartilage extending from subchondral bone; irregularity and focal sclerosis in subchondral bone	Osteophytes less than 2 mm
V	Clefts extended through nucleus and annulus		Diffuse sclerosis	Osteophytes greater than 2 mm

2.1.6 Vertebral Capacity

According to (Brinckmann et al., 1989) the ultimate strength (F_{max}) of vertebrae can be estimated by considering the endplate area in combination with the bone mineral density:

$$F_{max} = 0.32\,\mathrm{kN} + 0.00308 \cdot \mathrm{AREA} \cdot \mathrm{BMD} \cdot \frac{\mathrm{kN}}{\mathrm{cm}^2 \cdot \frac{\mathrm{mg}\,K_2HPO_4}{\mathrm{ml}}} \qquad \textbf{2-1}$$

The product out of BMD and AREA is determining the resistance capability of the specimen. This might also be true for fatigue strength. Therefore, the Vertebral Capacity (VC) is used in this study to classify the FSUs and possible enable prediction of cycles to failure.

$$VC = AREA \cdot BMD \qquad \textbf{2-2}$$

However, Brinckmann et al. used the endplate area and BMD of the failed vertebrae. This is only possible for in vitro testing. In the context of this study, AREA is the mean area of the two endplates adjacent to the intervertebral disc of the FSU. BMD is the mean BMD value of the two vertebrae of the FSU.

2.2 Cyclic Testing

The specimens of donors of three different groups were included in this study: Young Male, Midlife Male and Midlife Female. Within each of the groups, half of the specimens were from level L2-L3 and half from L4-L5 FSUs, however, the group sizes were different. Specimens from each group were assigned to different load groups. The groups differed mainly with regard to the fatigue load applied. However, some of the specimens of Young Male donors were tested solely for ultimate strength without any cyclic testing (2.2.2.3). This was done in order to enable comparison of the actual test pool with specimens from other ultimate strength studies.

The test protocol for cyclic testing (36 FSUs) covered parameter testing of the specimens and subsequent fatigue testing. The initial steps of the parameter testing served as preconditioning. Parameter testing was obtained by quasistatic and frequency-dependent loading in compression and shear direction. The protocol also covered reference measurements at the beginning, between test steps and during fatigue testing after 1,000, 10,000, 100,000, 200,000 and 300,000 fatigue load cycles. At maximum, 300,000 load cycles in fatigue testing were applied. If a clear sign of failure was observed earlier, the measurements were completed after the next reference measurement cycles. Altogether, the measurements of unfailed specimen took up to 20.5 hours, which is slightly different from the 19.3 hours of project F 2069.

In Tab. 2-3, the measurement sequences for cyclic loading are listed. The order of frequency-dependent compression and shear load set was switched for half of the specimens of one load group. This decreases the influence of the testing order on the results. The ID number identifies the test steps specified below. These numbers were chosen based on project F 2069. Some of the measurements in this study have been omitted; therefore, some of the intermediate numbers are not given here.

Each load step was defined via mode of the cyclic function (waveform: ‘ramp’, ‘ramp around offset’, ‘sine’, ‘constant’), offset of the loading (F_{offset}), amplitude of the cyclic portion of the loading ($F_{amplitude}$) and frequency of the cycles (f), according to this equation:

$$F_{cyclic}(t) = F_{offset} + F_{amplitude} \cdot function(2 \cdot \pi \cdot f \cdot t) \qquad \textbf{2-3}$$

The ’ramp’ mode is a rather special case for ’ramp around offset‘ in which the amplitude and the offset have the same value. However, these modes differ with respect to the starting point of the periodical load (Fig. 2-11). Negative sign for amplitudes and offsets would analogously be used for compression in the axial direction and posterior orientation of the shear loading. In addition, the duration of every single loading ID is given. Two load directions (shear or compression) were performed for fatigue testing. Shear loading in parameter testing (sequence 2 and 4) was always in combination with constant axial load (Tab. 2-5).

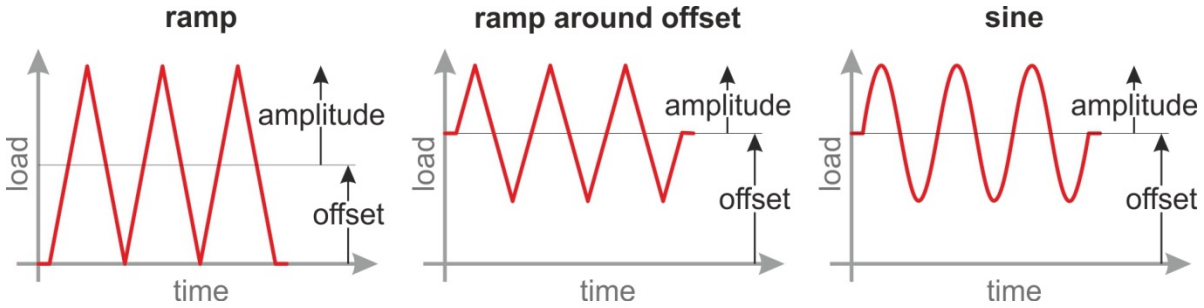

Fig. 2-11 Different modes for the shape of the cyclic loading have been used. Three cycles for ’ramp‘, ’ramp around offset‘ and ’sine‘ mode are illustrated.

Tab. 2-3 Measurement sequence for cyclic loading. The numbers are not following a continuous numerical order, because they are chosen to be consistent with the preceding projects (F1899 and F2069). The first two reference measurements were added in this project and have no separate number. The measurements are duplications of ID 1 (quasistatic) and ID 12 (dynamic). The suffix ref1 and ref2 helps to distinguish them.

Sequence	Protocol for…	ID No.	Duration [s]	Direction
1	Reference Measurements	1ref1, 12ref1	882	compression
2	Quasistatic Testing	1-5, 7	3,300	compression and shear
3	Reference Measurements	1ref2, 12ref2	882	compression
4	Frequency-Dep. Testing	12- 30, 7	2,556	compression and shear
5	Reference Measurements	33, 34	882	compression
6	Fatigue 1,000 Cycles	37	200	compression or shear
7	Reference Measurements	38, 39	882	compression
8	Fatigue 9,000 Cycles	42	1,800	compression or shear
9	Reference Measurements	43, 44	882	compression
10	Fatigue 90,000 Cycles	47	18,000	compression or shear
11	Reference Measurements	48, 49	882	compression
12	Fatigue 100,000 Cycles	52	20,000	compression or shear
13	Reference Measurements	53, 54	882	compression
14	Fatigue 100,000 Cycles	57	20,000	compression or shear
15	Reference Measurements	58, 59	882	compression

2.2.1 Parameter Measurements

Initial low cycle parameter measurements served several purposes. Firstly, the discs of the segments underwent a conditioning process with regard to mechanical characteristics. This conditioning process was needed because the cadaver specimens had not been loaded for an unphysiological amount of time and dissection and deep-freezing of the specimens altered the condition of the disc further. Moreover, these initial measurements were used to determine several characteristic parameters, e.g., quasistatic and dynamic stiffness in the axial and shear direction, as well as the frequency dependence of these parameters. The load sets for the initial cycles is given in Tab. 2-4 and Tab. 2-5.

All statistical analyses were carried out applying an error level of $\alpha = 0.05$ and using a statistical analysis software package (PASW 18, SPSS Inc./IBM Corporation, Armonk, NY, USA).

Tab. 2-4 Measurement protocol for quasistatic testing; load modes are 'constant' (---), 'ramp' (_/_) and 'ramp around offset' (-/\/-). Three cycles were applied for each loading ID.

ID No.	Axial load				Shear load				Time
	Mode [-]	Offset [N]	Freq. [Hz]	Ampl. [N]	Mode [-]	Offset [N]	Freq. [Hz]	Ampl. [N]	[s]
01	_/_	-1000	0.005	-1000[1]	---	0	/	/	600
02	_/_	-1000	0.005	-1000[1]	---	200	/	/	600
03	_/_	-1000	0.005	-1000[1]	---	-200	/	/	600
04	---	-800	/	/	-/\/-	0	0.005	200	600
05	---	-800	/	/	-/\/-	100	0.005	200	600
07	0	0	/	/	0	0	/	/	~300

2.2.1.1 Quasistatic Hysteresis

Quasistatic compression testing covered ramps from 0 to -2,000 N at 0.005 Hz (-1000 N offset, -1000 N amplitude) without anterior-posterior shear load (ID 01), as well as simultaneous constant shear loads (ID 02 and 03). Afterwards, the compression was constant at -800 N and shear load was applied with amplitudes of 200 N around an offset of 0 N and 100 N, respectively (ID No. 04 and 05, ramp around offset mode). Each step was executed for three cycles, which was one more than in the previous project (F 2069). The number of cycles was increased because creep was still present after two cycles and this was thought to have an influence on the segment behaviour determined. After the quasistatic test block, a period of 5 min without any load was added for spinal recovery. The number of different load levels decreased compared to F 2069; however, due to the additional cycles, the measurement time increased from 40 min to 50 min.

[1] For compression, the offset of the axial force is negative. To emphasise that the cyclic portion of the loading will even more compress the specimen, the amplitude is negative.

2.2.1.2 Frequency Dependent Hysteresis

Compared to previous projects F1899 and F2069, the frequency-dependent measurement protocol was reduced in terms of the number of load sets (amplitude-offset combinations). The remaining load sets appeared to be sufficient to analyse the influence of amplitude and offset. This reduced the number of load sets from 24 to 8 (Tab. 2-5). The frequency range covered was extended by lower frequencies, whereas the number of higher frequencies was reduced for project F 2059. This was done to cover the transition zone between quasistatic and dynamic and to keep the duration of the load set constant. The frequencies tested were 0.02, 0.05, 0.1, 0.2, 0.5, 1, 2, 3, 5, 7, 10 and 12 Hz. Each step was executed for three cycles or at least 3 seconds; this was also done to keep the duration of the test at a reasonable level. Consequently, each load set was reduced from 1,032 to 135 load cycles. In general, this implies a reduction from 24,768 to 1,080 load cycles with more slow cycles and fewer fast cycles during frequency-dependent testing. The testing time therefore increased from 1752 s to 2255 s.

Tab. 2-5 Measurement protocol for frequency-dependent testing; load modes are ‘constant’ (---) and ‘sine’ (~). For each loading ID, each of the 12 frequency steps was applied for at least three cycles or 3 seconds.

ID No.	Axial load				Shear load				Time
	Mode [-]	Offset [N]	Freq. [Hz]	Ampl. [N]	Mode [-]	Offset [N]	Freq. [Hz]	Ampl. [N]	[s]
12	~	-800	0.02–12	-550[1]	---	0	/	/	282
14	~	-1000	0.02–12	-200[1]	---	0	/	/	282
16	~	-1000	0.02–12	-550[1]	---	0	/	/	282
18	~	-1000	0.02–12	-1000[1]	---	0	/	/	282
21	---	-800	/	/	~	0	0.02–12	200	282
24	---	-800	/	/	~	100	0.02–12	200	282
28	---	-800	/	/	~	-100	0.02–12	50	282
30	---	-800	/	/	~	-100	0.02–12	200	282
07	0	0	/	/	0	0	/	/	~300

2.2.1.3 Reference Measurements

The reference measurement protocol was composed of ID 01 and ID 12 to cover quasistatic and frequency dependent parameters (Tab. 2-6). Reference measurements were applied at the beginning of testing (suffix ’ref1’), after quasistatic testing (suffix ’ref2’) and during fatigue testing (no suffix but own ID). The complete list of all reference measurement sequences can be found in Tab. 2-3.The reference measurements were to deliver information about changes in the specimen due to consecutive loading of the different groups of load sets. The initial reference load set was to display the null state of the segment since it was applied before any other load. However, the first cycles might still encounter initial creep. These reference measurements were the same for all load groups, regardless of whether the following fatigue testing involved axial compression with different loading types or anterior shear.

Tab. 2-6 Measurement protocol for reference measurements; load modes are 'constant' (---), 'ramp' (_/_) and 'sine' (~). For the quasistatic loading cycle (ID 01ref), three cycles were applied. Each of the 12 frequency steps was applied for at least three cycles or 3 seconds for the dynamic loading (ID 12ref).

ID No.	Axial load				Shear load				Time
	Mode [-]	Offset [N]	Freq. [Hz]	Ampl. [N]	Mode [-]	Offset [N]	Freq. [Hz]	Ampl. [N]	[s]
ID 01 ref	_/_	-1000	0.005	-1000[1]	---	0	/	/	600
ID12 ref	~	-800	0.02–12	-550[1]	---	0	/	/	282

2.2.1.4 Parameters

For evaluation of the quasistatic modes, the last complete load cycle was used to determine the characteristic parameters of the hysteresis. Data were filtered using a low pass 4th order Butterworth filter with a cut-off frequency of 0.5 Hz and 200 Hz for quasistatic and dynamic loading, respectively.

In the dynamic modes, the parameters were derived from the averaged hysteresis of the last two complete load cycles. Three parameters were used for evaluation: the overall apparent stiffness c_{app}, the stiffness at low negative displacement c_{inital}, and the stiffness at high negative displacement c_{peak} (Fig. 2-12). To calculate the apparent stiffness, the difference between minimum and maximum force (ΔF) was divided by the difference between minimum and maximum displacement (Δs). The stiffness at low displacement was calculated from the first third of data points close to the start displacement and the stiffness at high displacement was calculated from the last third of data points (see Fig. 2-12). These parameters were determined for every test frequency. For shear loading the stiffness at posterior displacement c_{post} and at anterior displacement c_{ant} were analogously determined (instead of $c_{initial}$ and c_{peak}).

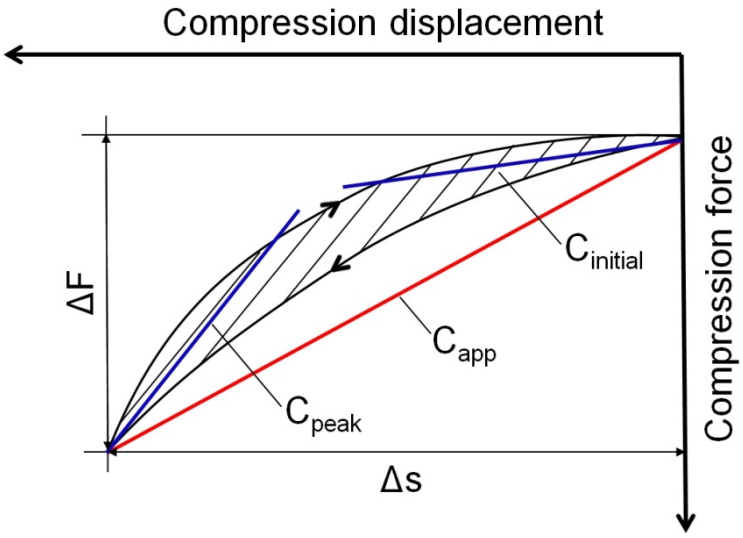

Fig. 2-12 Stiffness parameter:apparent stiffness (c_{app}),stiffness at low negative displacement (c_{inital}),stiffness at high negative displacement (c_{peak}).

2.2.2 Fatigue Measurements

Fatigue measurements were intended to yield data to analyse three aspects of lumbar FSUs. First, the influence of the magnitude of compression load on the number of fatigue cycles should be investigated. In this regard, it is unclear whether the peak load (maximum out of offset and Amplitude) or amplitude of a cyclic load is more determining for the number of fatigue cycles. Second, the intention was to compare the behaviour of lumbar FSUs in the z and x direction; one group underwent a cyclic load in the anterior shear direction. Finally, this study attempted to clarify whether gender has to be considered for predicting the fatigue behavior of FSUs, or if differences here can be attributed to size or BMD. The number of fatigue cycles measured was compared to the number of fatigue cycles calculated based on the following formula (Seidel et al., 2008, Huber et al., 2010):

$$N_{fatigue} = \left(\frac{F_{max} - F_{mean}}{0.5 \cdot F_{peak-to-peak}} \right)^6 \qquad \textbf{2-4}$$

where $N_{fatigue}$ is the number of fatigue cycles, F_{max} is the expected ultimate strength, F_{mean} is the mean value of the cyclic loading (offset) and $F_{peak\text{-}to\text{-}peak}$ is the peak-to-peak value of the loading (twice the amplitude). With respect to the terminology in this study (equation 2-3) this will lead to:

$$N_{fatigue} = \left(\frac{F_{max} - F_{Offset}}{F_{Amplitude}} \right)^6 \qquad \textbf{2-5}$$

The ultimate strength of the specimen can be calculated based on specimens' characteristics according to (Brinckmann et al., 1989) where VC is the vertebral capacity. (chapter 2.1.6):

$$F_{max} = 0.32\,kN + 0.00308 \cdot VC \cdot \frac{kN}{cm^2 \cdot \frac{mg\,K_2HPO_4}{ml}} \qquad \textbf{2-6}$$

The concept for the fatigue test design is displayed in Tab. 2-7. The number of L2-L3 and L4-L5 FSUs is expressed by the syntax A+B. A represents the number of L2-L3 FSUs and B the number of L4-L5 FSUs in the test group. The fatigue tests in this project should serve as an expansion of the database and a continuation of the fatigue tests conducted in F 2069, where a sinusoidal load of -1,000 N ± 1,000 N was applied. Eight FSUs (2+2 Midlife Male, 2+2 Midlife Female) were exposed to this load (NORM). Another 2+2 specimens of each of the midlife groups underwent loading with an offset of -2,000 N (OFFSET). This was done to investigate the impact of the amplitude on the number of fatigue cycles. Peak load is generally considered to be the factor with the highest influence, but according to Wöhler's laws (1870, cited in Schütz, 1996), the amplitudes are decisive for the cohesion of a material. According to (Huber et al., 2010), NORM load is not sufficient for the failure of the specimens of young donors within a reasonable range of cycles. Therefore, further testing of young specimens with NORM load was not performed.

Tab. 2-7 Measuring concept for fatigue testing.

Group	Number of FSUs in fatigue testing		Number of FSUs in the different loading groups			
	L2-L3	L4-L5	NORM	OFFSET	HIGH	SHEAR
Young Male	6	6	-	-	3+3	3+3
Midlife Male	6	6	2+2	2+2	2+2	-
Midlife Female	6	6	2+2	2+2	2+2	-

2.2.2.1 Axial Fatigue Load

Theoretical and experimental analyses were needed to find the required fatigue load, which is able to produce failures in specimens of young donors within 300,000 cycles. These numbers of cycles were a limit exhibited in project F 2069 at which degeneration of the specimen during in vitro testing stays in an acceptable range. In general, the lumbar vertebrae of young donors exhibited a VC of about 2,000 to 3,000 cm² mg K_2HPO_4/ml (Tab. 3-4). According to prediction of the fracture strength given above 2-6), this results in an estimated compressive strength of 6.5 kN to 9.6 kN. In (Brinckmann, Johannleweling, Hilweg, & Biggemann, 1987), the fracture probability after a certain number of load cycles with a fatigue load is based on 20–30%, 30–40%, 40–50%, 50–60% and 60–70% of the estimated compressive strength. The fracture probability was extrapolated for the theoretical analysis. The resulting curves are displayed in Fig. 2-13.

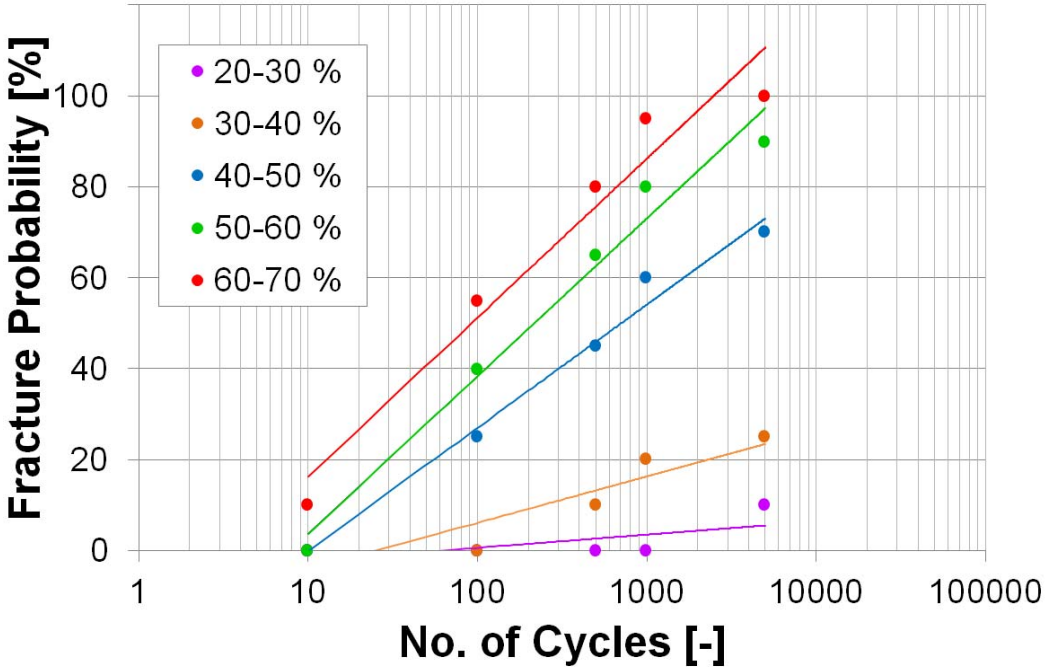

Fig. 2-13 Fracture probability of spinal motion segments after a certain number of cycles as a function of percentage of the ultimate compressive load (data adopted from Brinckmann et al., 1989).

According to the linear regression (Fig. 2-13), the fatigue load that most closely matched a fracture probability of 100% at about 100,000 cycles was about 40–50% of the ultimate compressive load. Hence, taking the estimated ultimate strength into account, peak fatigue load for the stated VC range was estimated at 2,600 N (40% of 6.5 kN) to 4,800 N (50% of 9.6 kN).

During pilot tests, a load of 1,500 N ± 1,500 N (HIGH) proved to be adequate for failure of the young donor group. Additionally, 8 midlife FSUs (2+2 Midlife Male, 2+2 Midlife Female) underwent HIGH loading as well. All compression fatigue loads were applied at 5 Hz and are displayed in Fig. 2-14.

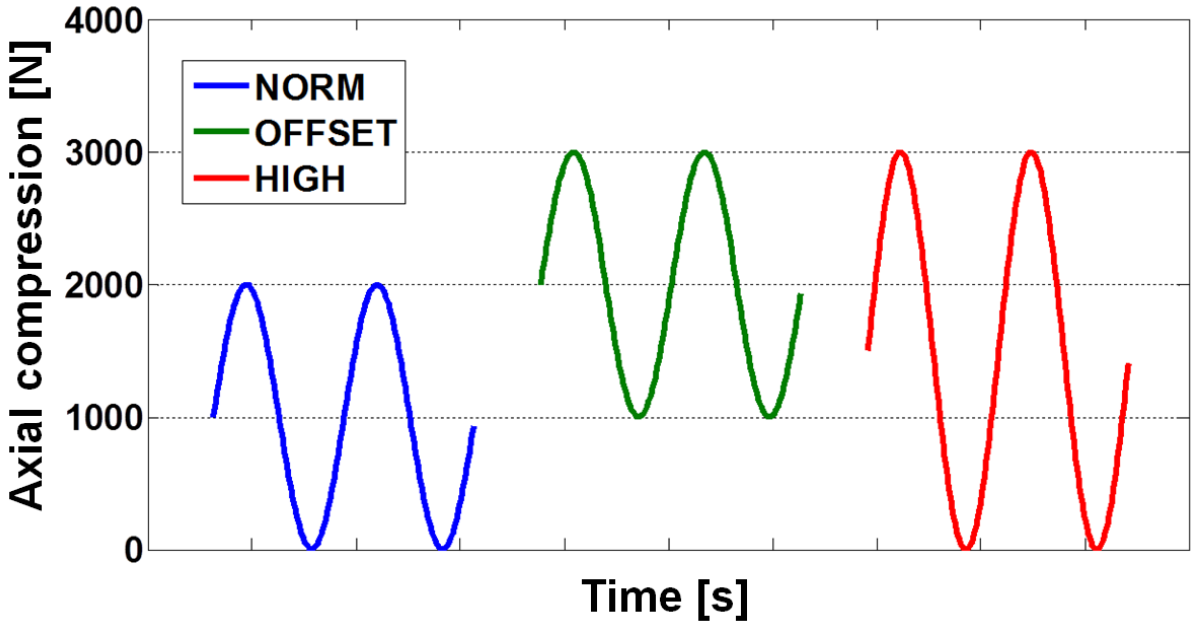

Fig. 2-14 Scheme of the three different sinusoidal compression fatigue load specifications; NORM and OFFSET have the same amplitudes, while OFFSET and HIGH reaches the same peak load. Compression means negative forces in the context of this study.

The determination of numbers of cycles to failure was done by using the fatigue creep curve (displacement signal) of the specimen (Fig. 2-15). Discontinuity in the curve was defined as failure and the number of cycles until failure was determined by two observers. If the results differed by more than 10%, the result was revised.

In order to analyse the fatigue failure a pure statistical linear black box model with no underlying theory was applied to predict the logarithmised cycles to failure. Amplitude and peak force (maximum absolute value out of offset and amplitude) of the load signals as well as VC were input variables in a multiple regression with backward removal of variables.

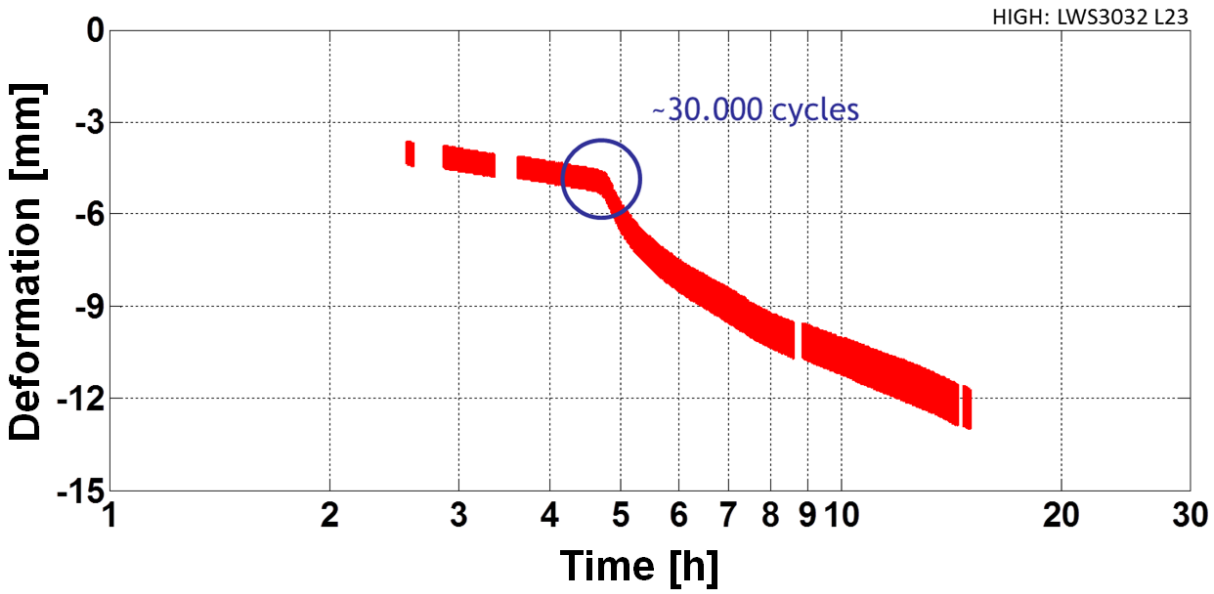

Fig. 2-15 Exemplary creep curve of a failed specimen exhibited to cyclic axial loading. The creep curve changed after 30,000 cycles (almost 5 h after the first loading), which was an indication of specimen failure.

2.2.2.2 Shear Fatigue Load

A reasonable load level for the in vitro shear fatigue load testing (SHEAR) was determined based on the ultimate strength in that direction. Analogous to the compression fatigue load, the shear fatigue load amounted to around 40% to 50% of the shear ultimate strength. Skrzypiec et al. (2012) determined a shear ultimate strength of about 3,570 N for FSUs with prior creeping (preconditioning). The peak shear load was therefore determined at 1,500 N. This resulted in a sinusoidal signal with 750 N ± 750 N in the anterior direction. There was no constant axial load during these tests. Six Young Male specimens were tested with this load.

Two different failure events were investigated: a discontinuity of peak-to-peak value is referred to as a ‘minor failure’ (No. 1 in Fig. 2-16); and a discontinuity of the mean value is referred to as a ‘major failure’ (No. 2 in Fig. 2-16).

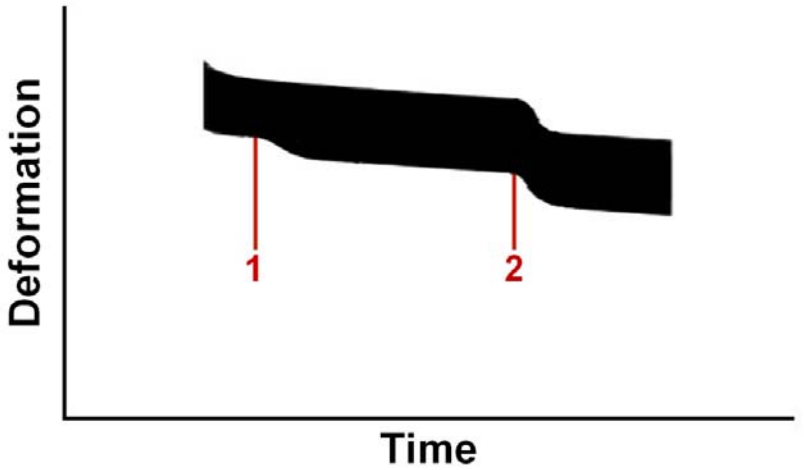

Fig. 2-16 Exemplary creep curve of a specimen exhibited to cyclic shear fatigue loading of two different types of failure were observed.

The fatigue shear experiments in this study were the first experiments of this type. Comparison data to verify the findings were not available, therefore additional analyses of the reaction components or, more precisely, the internal bending moment, were conducted. This was based on the known shearing force F_x. and the moment M_y recorded during testing by the load cell at the bottom of the specimen. The internal bending moment M_b at the edge of the upper and the lower metal holder was calculated according to the following equation:

$$M_b = F_x \cdot z - M_y, \qquad \textbf{2-7}$$

where z is the height in the z direction. M_b at edge of lower metal holder is as follows:

$$M_{b,low} = F_x \cdot z_0 - M_y, \qquad \textbf{2-8}$$

M_b at edge of upper metal holder:

$$M_{b,up} = F_x \cdot (z_0 + z_1) - M_y, \qquad \textbf{2-9}$$

The method is illustrated in Fig. 2-17 and Fig. 2-18. The internal bending moment is the two-fold integration of the bending curve and therefore has a zero point where the bending curve has a point of contraflexure. In theory, the point of contraflexure in shear loading should be positioned in the centre of the sheared structure. In the case of an FSU, the sheared structure is the intervertebral disc and the stable load case is indicated by the stable position of the point of contraflexure. For the experiments in this study, the position of the point of contraflexure and the zero point of bending moment should stay within the disc or shift only slightly.

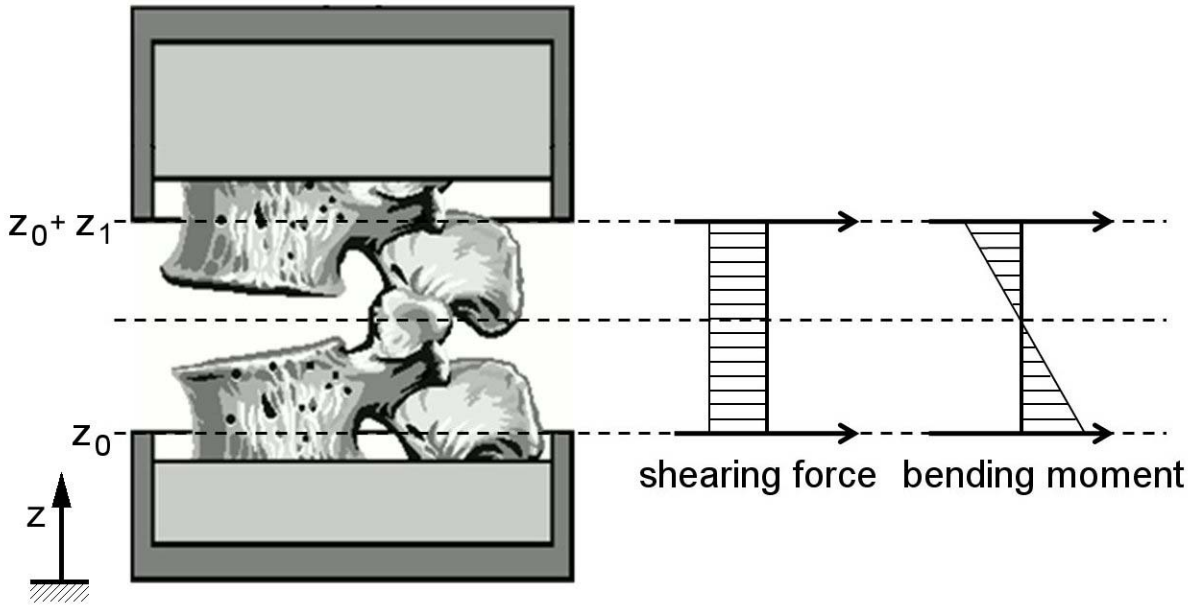

Fig. 2-17 Embedded FSU with corresponding qualitative shearing force and bending moment diagram.

In order to measure and rate the position of the zero point, the approximate height of the superior endplate of the caudal vertebra was used as a reference. The endplate height was determined from the CTs taken after testing. A disc height of 9 mm was assumed since 100% of all the specimens in the experiment group showed higher discs. In applying these measures, a zero point relative height of larger than 0 and smaller than 1 lies within the area of the intervertebral disc with sufficient certainty.

The shift of the point of contraflexure over the testing period was defined as the difference between the height at the beginning of fatigue loading and the height shortly after the last recorded failure (in millimetres).

Serious changes in the stress pattern would result in large shifts of the zero point of bending moment over the testing period or in a zero point lying clearly within the embedded region of the vertebrae.

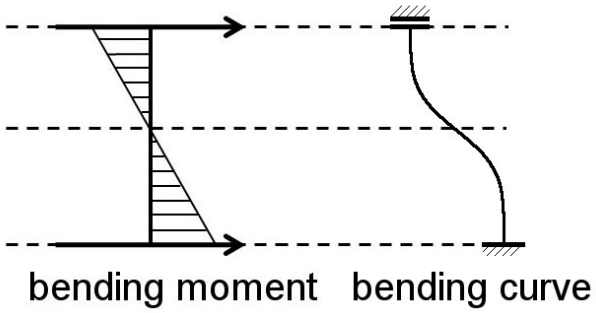

Fig. 2-18 Bending moment diagram and a bending curve with point of contraflexure displaying the bending pattern of a beam with one rigidly clamped end and one end with 1 degree of freedom. This figure merely illustrates the concept, but the bending curve was not calculated for the verification, only the bending moment.

2.2.2.3 Equivalent Cycles

Parameters, as well as reference measurements, cover a considerable number of cycles; these are summarized in Tab. 2-4 and Tab. 2-5. These load cycles might already contribute to the fatigue of the specimen and decrease the resisted numbers of cycles to failure in the fatigue experiments.

To assess the damage caused during these initial measurements with different load pattern, analyses for equivalent loading cycles were carried out. This has to be done with respect to the subsequent fatigue testing. If the influence is regarded to be meaningful, the equivalent cycles of the initial parameter testing could be added to the total cycles experienced by the specimen under the fatigue testing. This would also allow an enhanced comparison of the different parameter testing protocols of project F 2059 and F 2069 and their influence on the total life cycle of the specimen undergoing fatigue testing.

The proportion of cumulative fatigue damage (α_i) applied to a specimen under each cyclic loading (ID01 to ID30) can be expressed as a fraction of the loading cycles (n_i) under a certain load and the total number of cycles (N_i) at which failure is likely to occur for these load pattern (Miner 1945):

$$\alpha_i = \frac{n_i}{N_i} \qquad \textbf{2-10}$$

The total proportional damage accumulated by the specimen during parameter testing (including preconditioning) can thus be expressed as the sum of the proportional damage for every different load pattern:

$$\alpha_{parameter} = \sum_i \frac{n_i}{N_i} \qquad \textbf{2-11}$$

When testing the specimen for fatigue it has to be known, if the damage proportion of the parameter testing needs to be taken into account. This could be done by expressing the damage proportion $\alpha_{parameter}$ as equivalent loading cycles under the fatigue testing:

$$\frac{n_{equivalent}}{N_{equivalent}} = \alpha_{parameter} \qquad \textbf{2-12}$$

Solving for the number of equivalent cycles ($n_{equivalent}$) and inserting the loading cycles of the parameter testing yields:

$$n_{equivalent} = N_{equivalent} \cdot \sum_i \frac{n_i}{N_i} \qquad \textbf{2-13}$$

The number of cycles at which failure is likely to occur (N) can be expressed in terms of dependence on the testing conditions, such as the offset of the cyclic loading (F_{Offset}) and the amplitude ($F_{Amplitude}$) and the ultimate strength (F_{max}) of the specimen (equation 2-4). This equation is valid for every single loading step of the parameter testing:

$$N_i = \left(\frac{F_{max} - F_{Offset(i)}}{F_{Amplitude(i)}} \right)^6 \qquad \textbf{2-14}$$

In combination with the above part, this results in:

$$n_{equivalent} = \left(\frac{F_{max} - F_{Offset(equivalent)}}{F_{Amplitude(equivalent)}} \right)^6 \cdot \sum_i n_i \cdot \left(\frac{F_{Amplitude(i)}}{F_{max} - F_{Offset(i)}} \right)^6 \qquad \textbf{2-15}$$

The ultimate strength of lumbar vertebrae (F_{max}) might be predicted based on the VC of the specimen (Brinckmann et al., 1989,). For example; in accordance with equation 2-6, with an average VC of 2465 cm² mg K_2HPO_4/ml the ultimate strength of a segment would be:

$$F_{max} = 0.32\,kN + 0.00308 \cdot 2465 \cdot cm^2 \cdot \frac{mg\,K_2HPO_4}{ml} \cdot \frac{kN}{cm^2 \cdot \frac{mg\,K_2HPO_4}{ml}} \qquad 2\text{-}16$$

$$= 7.9\,kN$$

The equivalent load cycles of the two reference measurements (ID 01ref and ID 12ref, Tab. 2-6) with its 3 quasistatic and 135 dynamic load cycles are therefore:

$$n_{equivalent} = \left(\frac{7.9\,kN - 1kN}{1kN}\right)^6 \cdot \left[3 \cdot \left(\frac{1kN}{7.9\,kN - 1kN}\right)^6 + 135 \cdot \left(\frac{0.55\,kN}{7.9\,kN - 0.8\,kN}\right)^6\right] \qquad 2\text{-}17$$

$$= 6.1$$

These 6 equivalent cycles are valid for the NORM fatigue load. For HIGH or OFFSET, the first term will be lower. In this way, the equivalent loading cycles for fatigue testing ($n_{equivalent}$), which represent the damage initiated by the parameter testing (including compression quasistatic and frequency dependent testing and reference measurement), can be expressed as dependent on the vertebral capacity of each functional spine unit (Fig. 2-19).

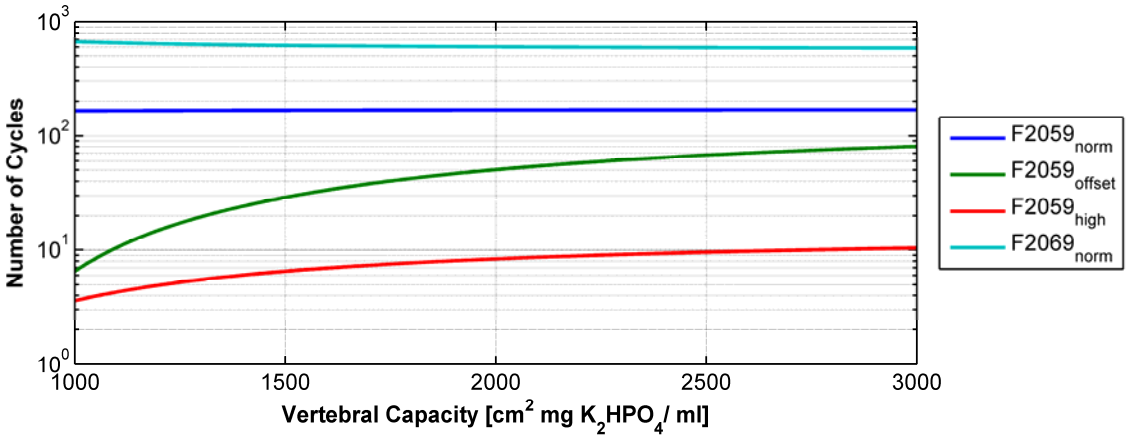

Fig. 2-19 Equivalent load cycles ($n_{equivalent}$) for parameter testing of the functional spine units in relation to vertebral capacity (VC) and the different fatigue protocols.

The equivalent number of cycles are smaller for the actual study (F 2059) than for the previous one (F 2069) and is rather small compared to the thousands of fatigue load cycles. The correction could be especially relevant for the weak specimens with low vertebral capacity. However, the exponential relation for fracture prediction based on the VC is still under debate, especially with regard to the exponent. Therefore, the sensitivity of equivalent numbers of cycles to failure with respect to the exponent in the equation was investigated. For an average vertebral capacity (for this graph, it is assumed to be 2465 cm² mg K_2HPO_4/ml), the equivalent number of cycles for the fatigue protocols were calculated with varying exponents (Fig. 2-20).

For the HIGH fatigue measurements the influence of the exponent appears to be more severe (manifold change of the numbers of cycles) than for NORM loading. This is related to the similarities in offsets and amplitudes between NORM and

parameter testing. However, the absolute amount of equivalent load cycles is very small for the HIGH group.

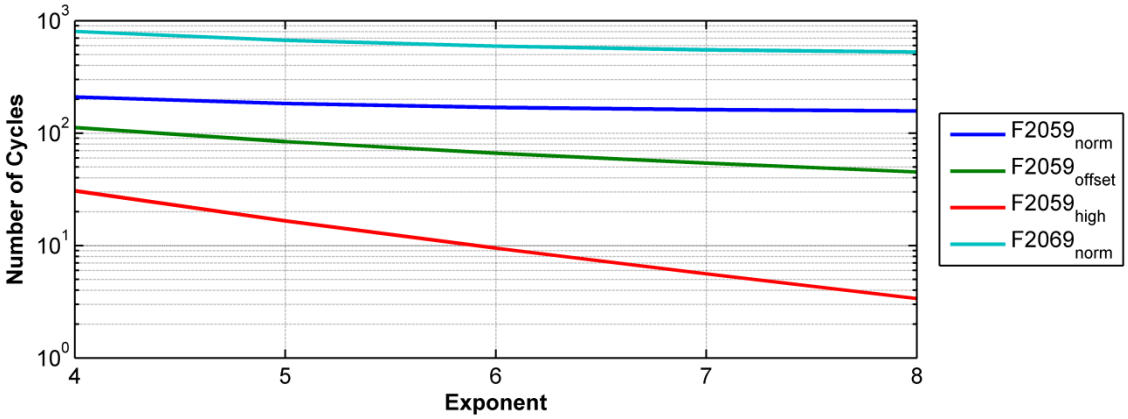

Fig. 2-20 Dependency of equivalent load cycles on the exponent of N_k.

2.3 Ultimate Strength Measurements

Monotonic quasistatic testing was carried out to determine the ultimate strength of the specimens of Young Male donors. A total of 6 specimens were tested using a measuring protocol adopted from Brinckmann et al. (1989). A preconditioning load of -1 kN (compression) was applied for 15 minutes. After removal of the preload, a monotonic compression load was applied at a rate of -0.5 mm/s. The loading was completed when a reasonable drop in the force was observed (Brinckmann et al., 1989). Measurement was stopped at about 10 mm after fracture. Determination of the fracture force was done using a semiautomatic numerical procedure (MATLAB, The MathWorks, Inc., Natick, MA, USA). The local force peak for the ultimate strength was determined based on 15 points before and after the point of fracture (Fig. 2-21).

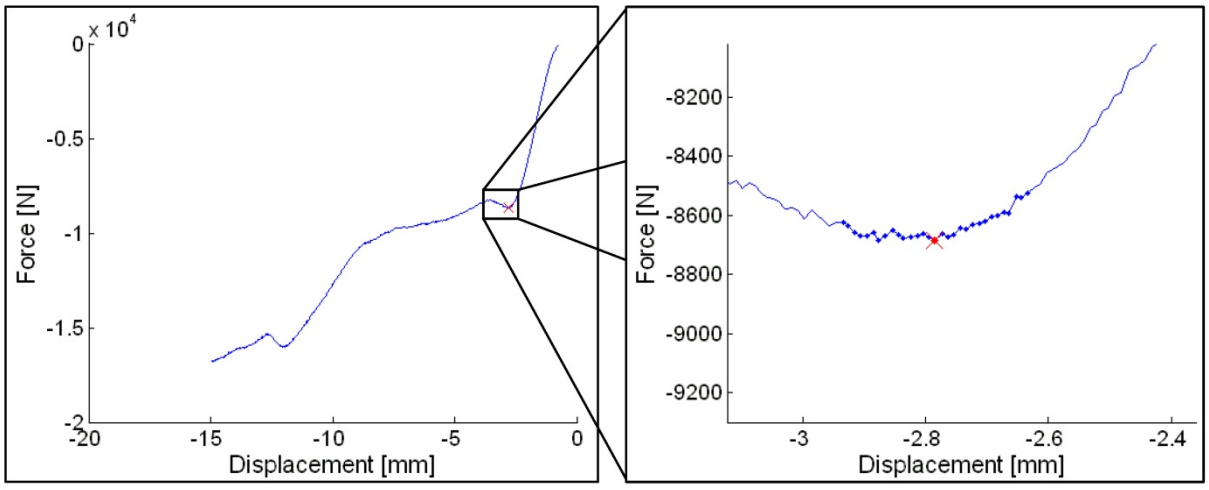

Fig. 2-21 Force displacement diagram resulting from ultimate strength testing of FSUs; the cross indicates the point of fracture and the cut-out shows the data points that are used to define the point of fracture (± 15 points). Note that the loading coordinates are negative. Therefore, the loading started in the upper right-hand corner of the diagram.

2.4 Test Setup

2.4.1 Test Rig for Cyclic Testing

For the measurements, a uniaxial servohydraulic testing machine (MTSBionix, 858.2, MTS, Eden Prairie, MN, USA) was supplemented with a second load axis in the horizontal direction to apply shear load to the specimen or to enable unrestricted anterior-posterior deformations. For this purpose, an additional servohydraulic cylinder (Type 120 10012-01, Hänchen, Ostfildern, Germany) and corresponding displacement sensor were attached to the standard testing device (analysis of the mechanical behaviour of the two axes can be found in Appendix 5.2). Rotation around all three axes and lateral translation was restricted. The specimens were mounted to the machine in an upright position. The lower fixation holder (see 2.1.1) was screwed to a six degree of freedom load cell (6DOF, SN 30 031, Huppert, Herrenberg, Germany) and the upper holder to the movable platform that was attached to both actuators. Coupling to the actuators was carried out by elastic elements (see Fig. 2-22), which allowed simultaneous movement of the platform in the z and x direction.

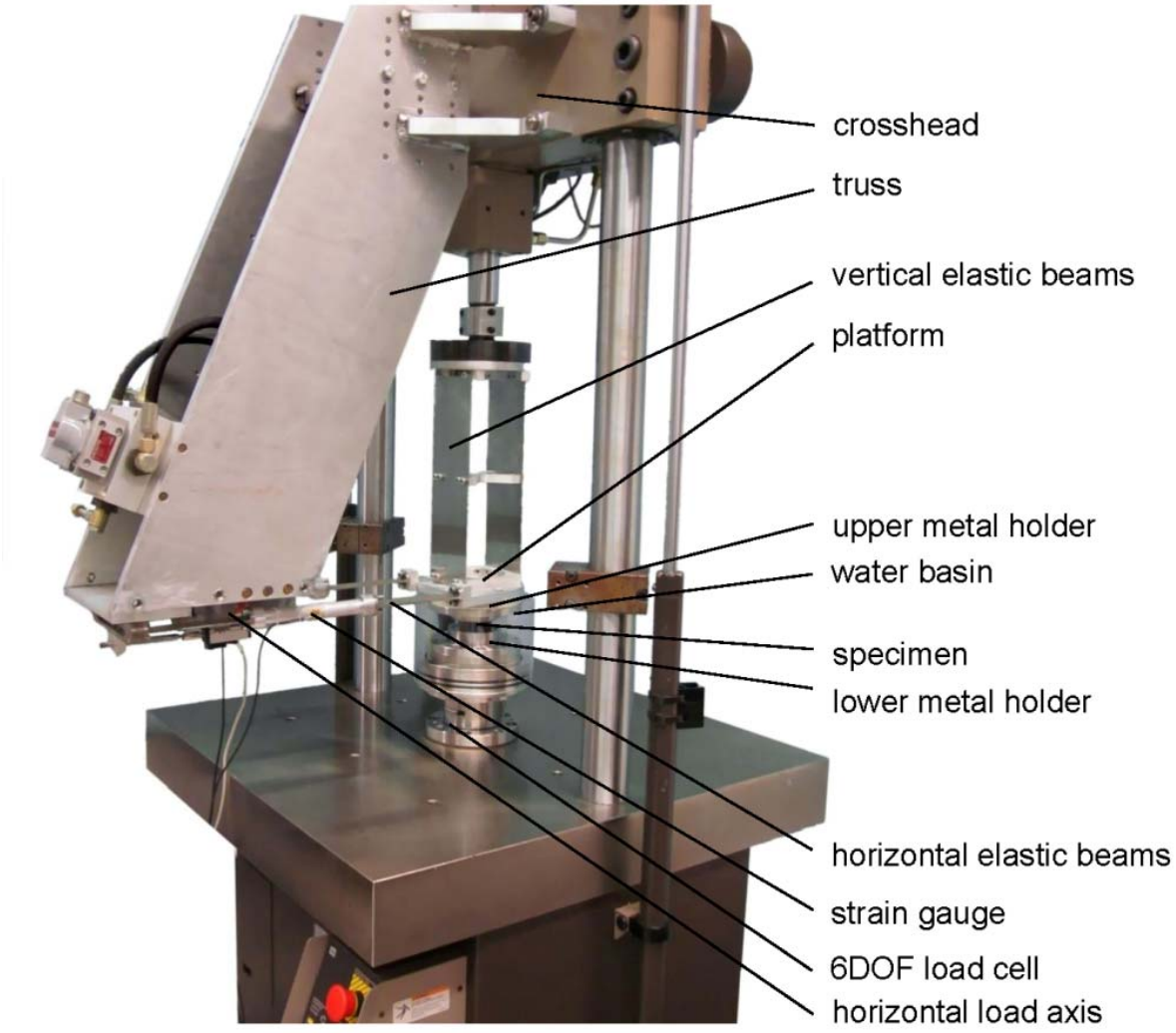

Fig. 2-22 Test rig for cyclic testing with horizontal load axis and specimen dummy (stiffening profiles unmounted).

Controlling of the additional axis was carried out by the test system's controller unit (FlexTest GT, MTS, Eden Prairie, MN, USA) of the testing machine. Testing was carried out in force controlled mode, based on the x and z force signals of the 6DOF. Strain gauges were installed at the horizontal coupling elements of the moveable platform to verify the load cell output. The six output signals of the 6DOF and the two signals from the strain gauges were processed by two synchronised carrier frequency amplifiers (Picas, Peekel Instruments, Bochum, Germany) and their output of the amplified measurement values was connected to the testing machine's analogue inputs (FlexTest GT, MTS, Eden Prairie, MN, USA).

Further details about the test rig can be found in Huber et al. (2005) and Huber & Mischke et al. (2010). For this project however, the additional horizontal axis had to be capable of applying a dynamic peak load of about 1,500 N (see 2.2.2). Compared to the previous project, minor structural modifications were necessary to achieve the necessary capability. The 4 vertical elastic bending elements were replaced by 2 wider ones exhibiting a higher second moment of inertia. The thickness of the two stiffening profiles was increased from 3 mm to 5 mm (Fig. 2-23). The occurring maximal dynamic load in the axial direction was -3,000 N.

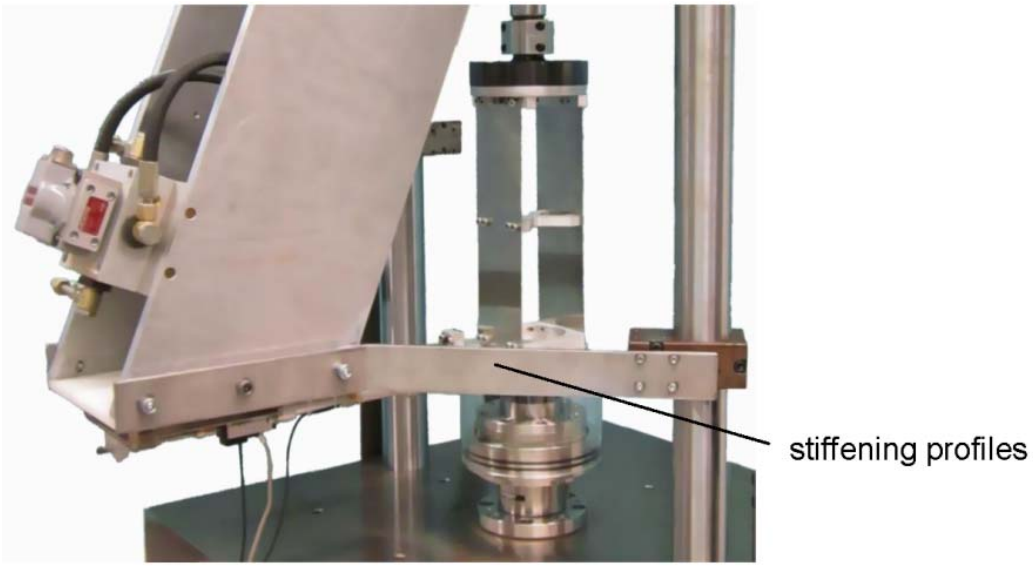

Fig. 2-23 Test rig for cyclic testing with mounted stiffening profiles for stiffness improvement.

The following convention is used to describe directions with respect to the spinal specimen (Fig. 2-24). Axial compression equates to the negative z direction and anterior shear is in the positive x direction. Anterior displacement of the cranial vertebra generates a positive force in axial fatigue loading.

For shear fatigue testing, the specimen was rotated at 180° around the z axis. By doing this, the high shear fatigue load could be applied using the pressure mode of the horizontal actuator, which exhibits a higher force capability than the pulling mode. In addition, the horizontal elastic beams were loaded under tension not compression, which prevents buckling. Hence, for shear trials, the negative x direction of the testing machine corresponded with the positive shear load.

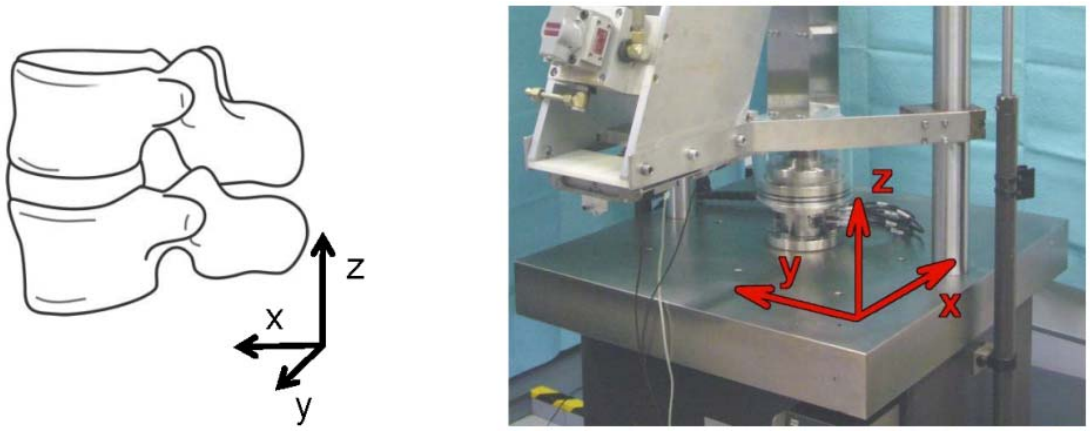

Fig. 2-24 Definition of the coordinate system of the specimen for axial fatigue loading. For shear loading, the specimens were rotated 180° around the z axes.

2.4.2 Test Rig for Ultimate Strength

Monotonic ultimate strength testing was carried out on the same servohydraulic testing machine as the cyclic tests, but without the additional actuator. The specimen was mounted within a water basin to keep the temperature constant at 37°C. Due to the tilted orientation of the facet joints the deformations of spinal specimens in x and z-direction are coupled. A two-dimensional unrestrained linear bearing was therefore mounted below the water basin to allow displacement in the anterior-posterior direction of the spine. The lateral direction was restricted. A rotational bearing allowed adjustment during rigging, but it has been restricted during testing (Fig. 2-25). A displacement sensor (T75a502, Novotechnik, Ostfildern-Ruit, Germany) detected the displacement in the anterior-posterior direction.

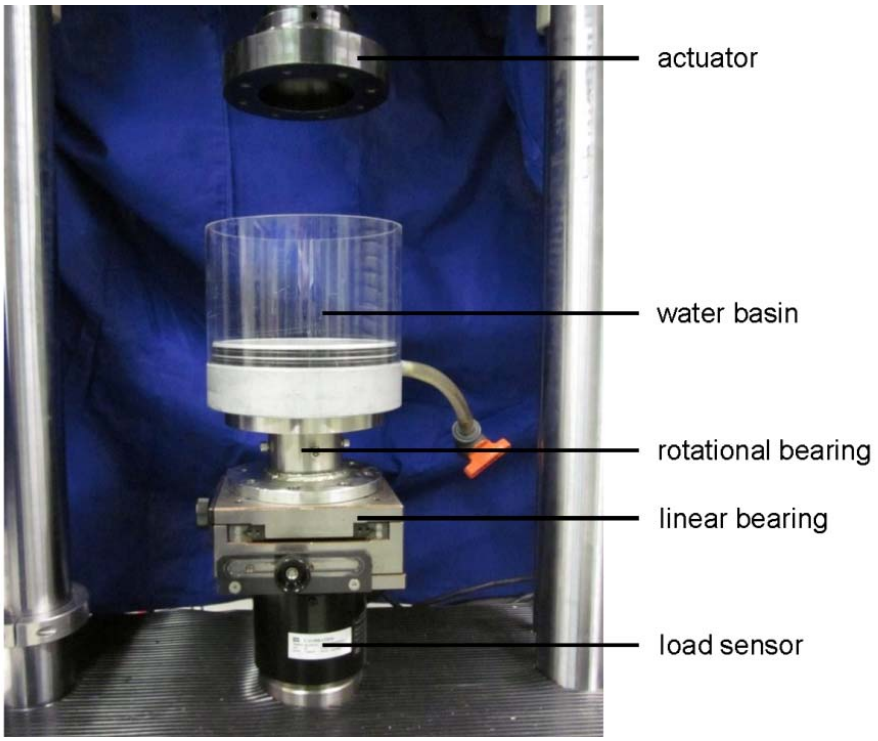

Fig. 2-25 Test setup for monotonic testing (the displacement sensor is mounted on the back side of the linear bearing).

2.4.3 Test Environment

Experiments were performed in an immersed saline (Ringer solution) environment. The temperature of the water basin was kept at 37°C for the entire duration of the measurements. The specimens were immersed in the basin for about 30 min prior to testing to reach physiological temperature until measurements started. This was needed because it is known from measurements of ovine spinal segments that the stiffness and consequently probably the fatigue behaviour as well, depends on the temperature of the specimen (Costi et al., 2002).

The saline solution was circulated by a tube system with a peristaltic pump (SR25, Rietschle Thomas Puchheim GmbH, Puchheim, Germany). The tube system passed a heat exchanger (copper coil) where the Ringer solution was heated by a water bath (F6/B5, Haake Messtechnik, Karlsruhe, Germany). The basin of the heat exchanger was held at about 42°C. The revolution speed and consequently the flux of the peristaltic pump was trimmed by a pulse width converter connected to the testing machine's controller (FlexTest GT, MTS, Eden Prairie, MN, USA). The converter also contained a diode that stopped the motor when the temperature exceeded 37°C. The temperature within the water basin was measured with a PT 100 sensor (DIN EN 60751, Type 104, LKM electronic GmbH, Geraberg, Germany). Fig. 2-26 shows the temperature control setup.

Micrographs of the Ringer solution were taken occasionally at the beginning and end of an experiment in order to check for the appearance of bacteria. Samples were examined using a microscope (Axiovert 40 CFL, Carl Zeiss MicroImaging GmbH, Göttingen, Germany). Photographs were taken with a microscopy camera (AxioCam ICc 1, Carl Zeiss MicroImaging GmbH, Göttingen, Germany).

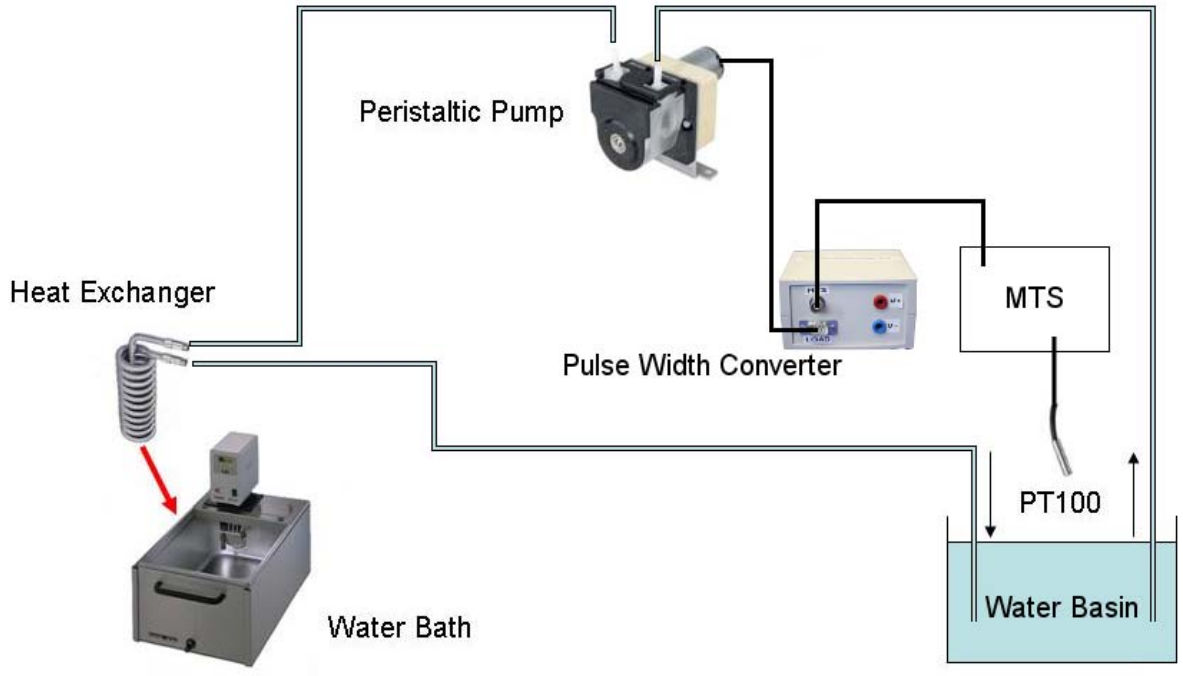

Fig. 2-26 Schema of the temperature control setup; the specimens were tested in a water basin headed in a closed circuit.

3 Results

The human FSUs underwent two different test procedures: 36 FSUs were used for the main experiment with parameter measurements carried out first, followed by fatigue testing; and 6 FSUs were used for ultimate strength measurements. To make these 42 FSUs (21 FSUs of level L2-L3 and 21 of level L4-L5) available, 32 lumbar spines (L2-L5) were provided by the Department of Legal Medicine, University Medical Center Hamburg-Eppendorf. These supernumerous specimens were needed because computer tomography scans exhibited that certain lumbar spines had been in an inappropriate (pathological) state for testing and two lumbar spines were needed for pilot experiments. The specimens were collected from February 2009 until August 2011. About 550 counselling interviews with the next of kin of the donors were conducted for this purpose. An overview about the specimens collected for the purpose of this study is given in the appendix (chapter 5.1).

3.1 Characterisation of the Specimens

Finally, specimens from 23 different donors were included in the study. From 19 donors, both segments have been used. From four donors, only one of the two FSUs was used, because the other one showed either pedicle fractures, bony bridging of the intervertebral gap or disc mineralisation. The following subchapters represent the basic characteristic parameters of the spinal specimens. They include anthropometrical information and CT-based measures (e.g., endplate area, BMD and disc height, morphometric investigations).

3.1.1 Anthropometrical Data

In Fig. 3-1 and Tab. 3-1, the main anthropometrical data, body weight and body height for the donors of the specimens included in the study are given. The data have been acquired during post-mortem examination.

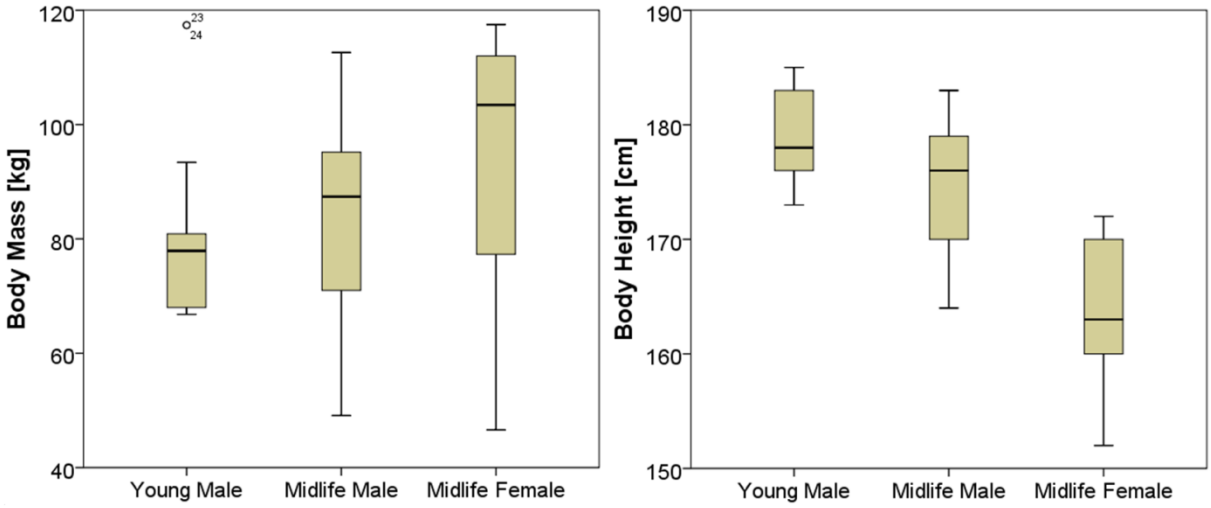

Fig. 3-1 Body mass (left,) and body height (right) of the FSUs included in this study ($n_{YoungMale}$ = 9, $n_{MidlifeMale}$ = 7, $n_{MidlifeFemale}$ = 7).

In Fig. 3-2, a comparison of the donors' body weight and body height are displayed for the 5th, 50th, and 95th percentile according to Jürgens (2004). Of note is that the

female donors did not represent a normal population because they exceeded the typical range for either body mass or body height, i.e., they were either heavier or less tall than the normal population.

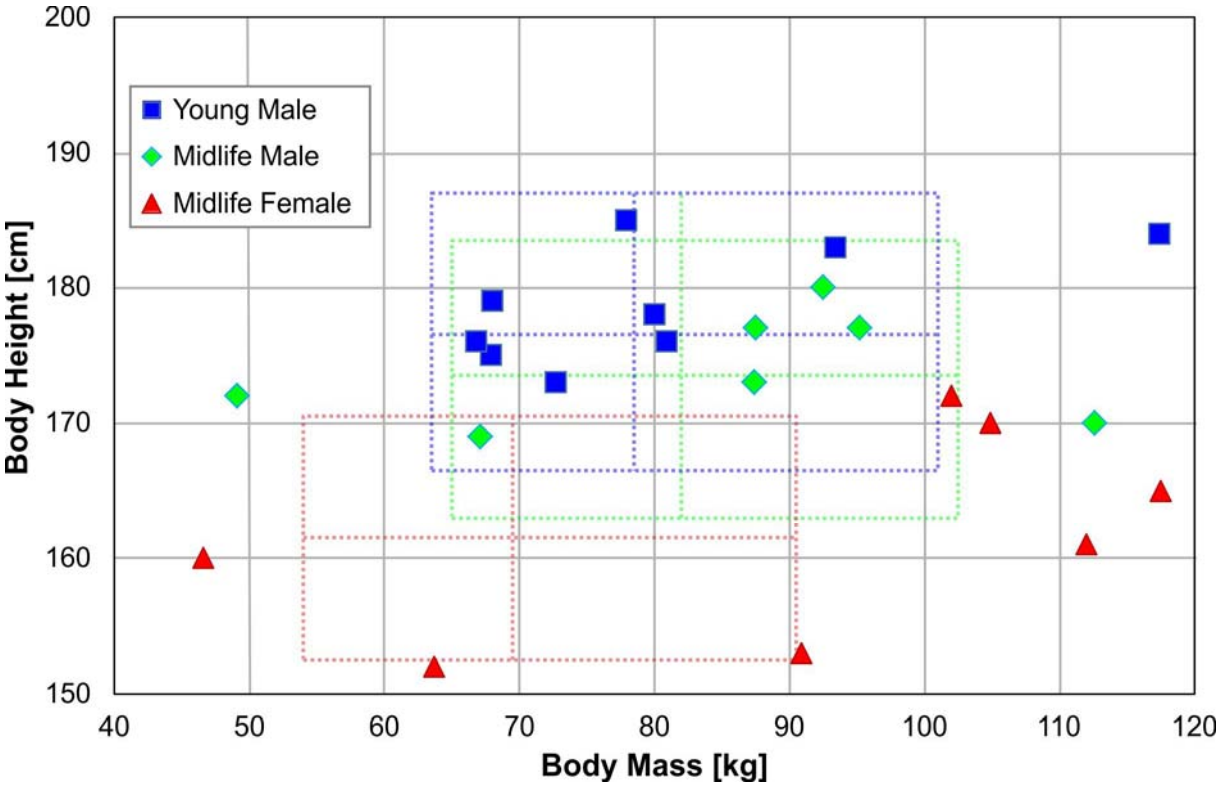

Fig. 3-2 Donor body weight and height of the specimens collected; squares and cross lines show the area of the 5th to 95th percentile and median, respectively (Jürgens, 2004).

Tab. 3-1 Anthropometrical data of donors whose FSUs were included in this study (m = male, f = female, hyphen indicates missing data, abbreviations are given in Tab. 2-1).

LWS	Gender	Age [yrs]	Days to explant.	m_B [kg]	h_B [cm]	h_{AC} [cm]	h_{EB} [cm]	d_{AN} [cm]	d_{KN} [cm]	d_{EB} [cm]	d_{WR} [cm]
3001	m	38	5	67.9	175	149	117.0	6.6	10.1	8.0	5.2
3004	f	56	3	102.0	172	153	125.0	7.7	10.8	8.5	5.4
3005	m	31	1	68.0	179	155	121.0	7.2	9.6	8.2	5.8
3006	m	54	4	87.5	177	149	117.5	6.8	9.8	7.8	5.7
3007	m	39	2	72.7	173	147	116.5	6.6	10.0	7.8	5.2
3009[2]	m	58	5	49.1	172	151	115.0	6.4	10.3	7.3	5.2
3011	f	55	5	46.6	160	138	109.0	5.9	8.1	6.4	4.8
3012	m	38	0	117.4	184	164	133.0	6.5	12.6	8.2	5.7
3013	m	38	5	80.9	176	156	124.0	6.6	9.5	7.5	5.4
3014	f	60	5	104.9	170	150	120.0	6.5	10.5	7.5	5.1
3016	m	60	3	112.6	170	156	122.0	7.5	12.0	8.6	6.2
3017	f	62	2	117.5	165	147	115.0	6.9	13.0	7.7	5.5
3018[2]	f	50	7	90.9	153	136	106.0	6.6	13.2	7.6	4.5
3019	m	33	4	93.4	183	165	131.0	6.7	11.2	7.7	5.4
3021	m	36	2	80.0	178	154	123.0	7.0	9.9	8.1	4.9
3023	m	54	6	92.5	180	154	122.0	6.8	10.8	8.2	5.5
3025[2]	m	63	3	65.0	164	-	-	-	-	-	-
3026	f	57	2	112.0	161	140	112.0	6.8	12.1	7.0	5.5
3027[2]	f	64	2	63.7	152	130	100.0	6.7	8.9	6.7	5.0
3028	m	54	2	87.4	173	144	113.0	6.7	9.3	8.0	5.2
3030	m	53	5	95.2	177	157	121.0	7.7	11.4	8.4	5.7
3031	m	42	4	77.9	185	160	127.0	7.5	10.4	8.5	5.8
3032	m	32	2	66.8	176	151	118.0	7.4	8.5	8.0	5.4

[2] Only one FSU of the respective lumbar spine is included in this study.

3.1.2 Endplate Area

Based on the CT scans of the explanted specimens, the endplate area (AREA) was determined by two independent observers. In most cases, the contour of the pedicles was present in the lineset file. Therefore, this structure in the spinal model had to be removed prior to determining the endplate area.

Linear regression between the findings of the two observers demonstrates the reproducibility of the evaluation method (Fig. 3-3). It showed a slope of 0.98 ($R^2 = 0.95$), which was not significantly different from 1 ($p = 0.179$).

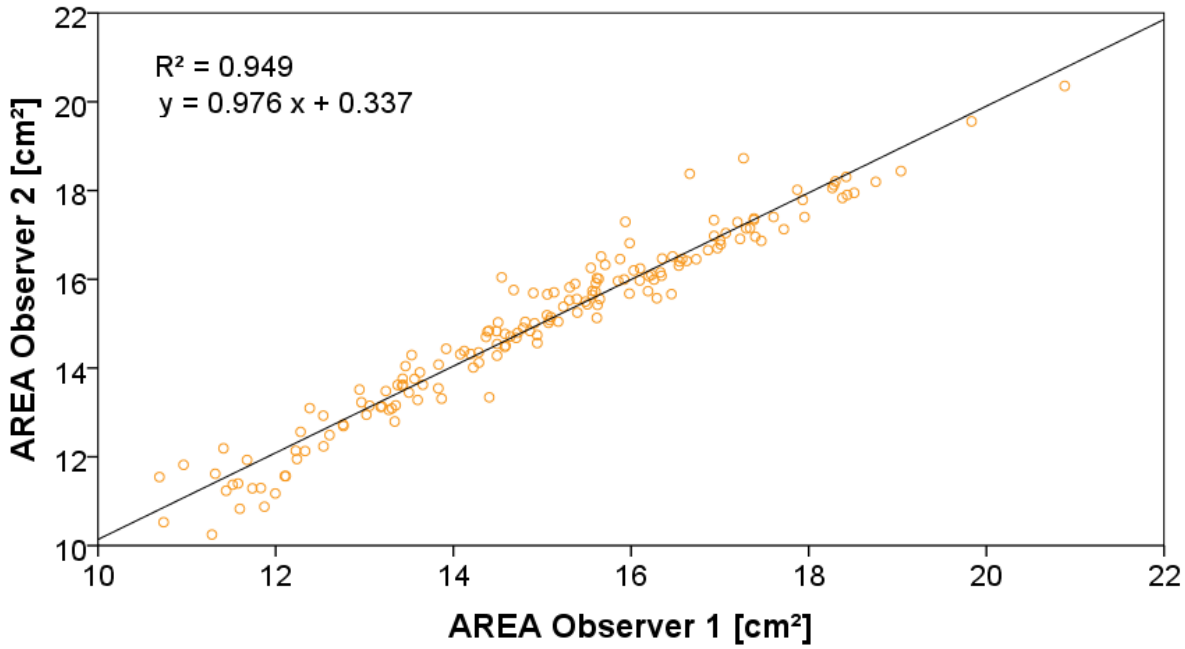

Fig. 3-3 Linear regression between endplate area results of Observer 1 and Observer 2.

In Fig. 3-4, the means of the superior and inferior endplate areas of the vertebral levels included in the analysis are displayed. The values obtained by Observer 1 and Observer 2 were averaged. With regard to AREA, the three-way ANOVA did not show any significant differences in terms of level dependence (L2, L3, L4, L5) or dependency on endplate location (inferior, superior) ($p > 0.124$). A significant difference was detected with regard to the donor groups ($p < 0.001$, Fig. 3-5). The AREA of Midlife Females accounts for 13.16 cm², which is significantly smaller than that of both Male groups ($p < 0.001$, Scheffe post-hoc). No difference was observed between the AREA of male groups of young donors of about 15.59 cm² and midlife donors of 15.81 cm² ($p = 0.803$, Scheffe post-hoc). In Tab. 3-2, the superior and inferior endplate areas of vertebrae L2 to L5 of the specimens tested are given in detail.

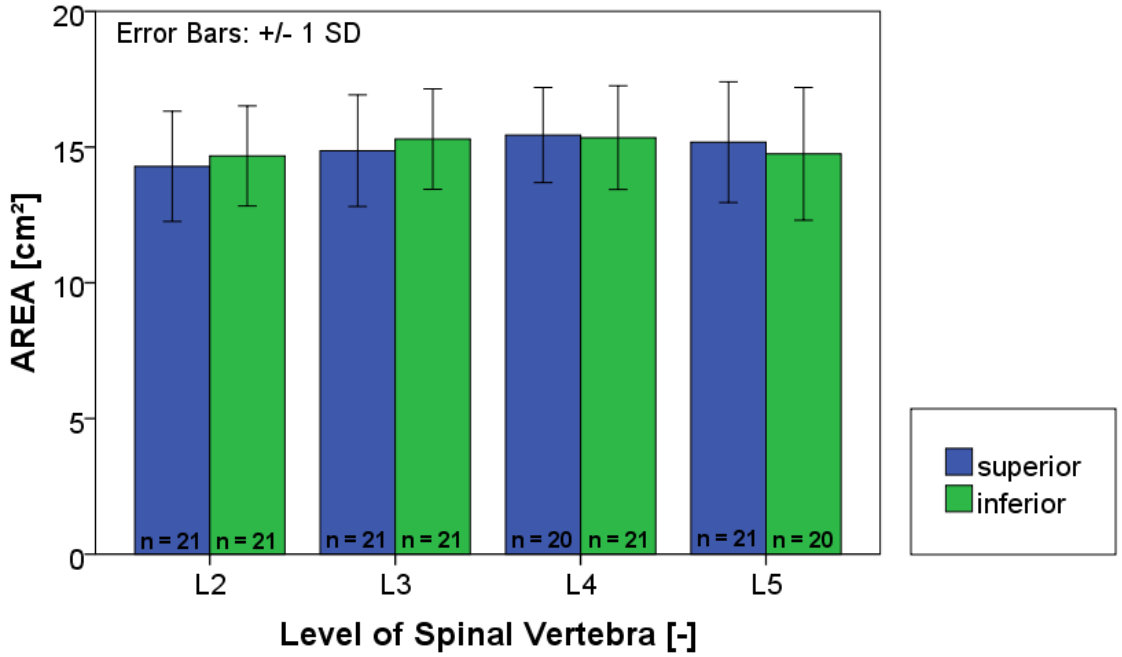

Fig. 3-4 Superior and inferior endplate area of the levels of spinal vertebrae investigated.

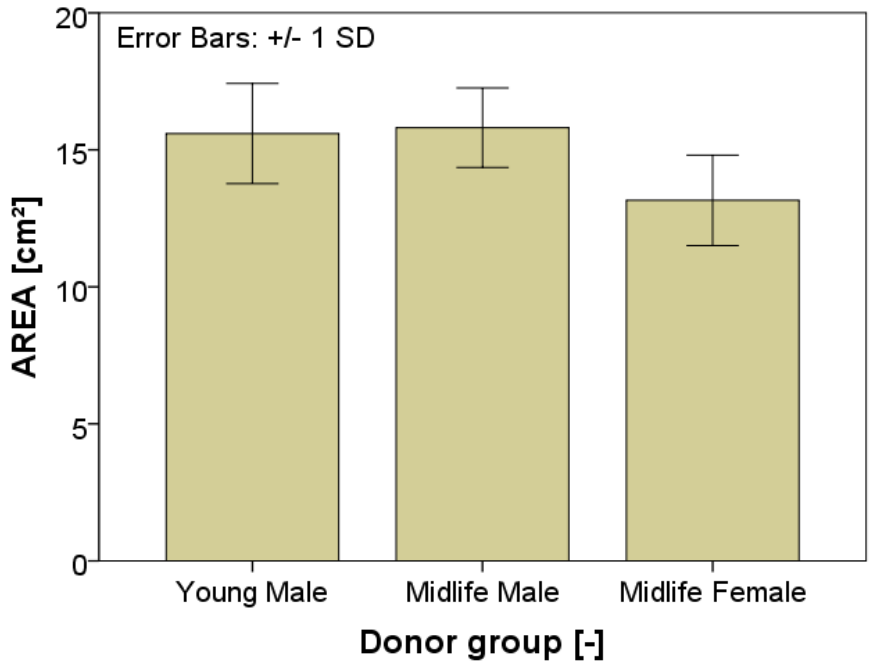

Fig. 3-5 Mean endplate area of the three donor groups. The AREA for Young Male (n = 72) and Midlife Male (n = 48) was significantly different from the AREA for Midlife Female (n = 46).

Tab. 3-2 Averaged endplate area of L2 to L5 (hyphen indicates endplates that were not evaluated because the corresponding discs were not tested).

LWS	L2		L3		L4		L5	
	superior [cm²]	inferior [cm²]	superior [cm²]	inferior [cm²]	superior [cm²]	inferior [cm²]	superior [cm²]	inferior [cm²]
3001	15.04	15.76	15.42	15.90	16.11	15.12	14.85	11.80
3004	13.66	13.76	13.59	14.12	13.23	13.15	12.98	11.51
3005	13.49	14.39	14.32	14.84	15.12	15.08	15.47	14.25
3006	16.02	14.52	13.96	15.82	15.29	15.63	15.60	14.92
3007	13.64	14.53	16.17	14.85	14.60	14.76	14.20	13.60
3009	14.69	15.91	17.18	16.59	-	-	-	-
3011	10.63	11.34	11.21	11.58	11.37	11.84	11.44	12.09
3012	16.52	16.94	16.90	17.36	17.38	17.22	17.25	16.06
3013	18.36	18.11	18.74	17.50	18.20	18.25	18.23	16.21
3014	14.75	15.96	15.11	15.93	15.83	15.37	13.87	13.44
3016	18.00	16.12	16.76	17.07	18.17	17.42	17.68	17.17
3017	12.18	12.23	13.17	12.55	13.47	11.83	12.73	11.49
3018	11.12	11.39	11.80	11.47	-	-	-	-
3019	12.74	13.20	13.16	13.26	13.10	12.74	13.10	12.39
3021	15.66	16.49	17.05	16.42	16.09	15.96	15.65	15.47
3023	13.91	14.19	14.66	15.32	15.42	15.60	15.56	13.51
3025	-	-	-	-	15.31	16.04	16.62	16.14
3026	12.42	13.36	13.75	14.96	15.22	15.36	15.30	17.13
3027	-	-	-	-	- [3]	13.69	10.76	- [3]
3028	12.73	13.07	11.56	16.24	16.40	17.94	17.24	18.48
3030	15.49	16.52	16.17	16.84	16.41	16.47	15.82	14.55
3031	15.52	16.17	16.96	17.86	17.52	18.16	19.70	20.62
3032	13.53	14.25	14.53	14.68	14.62	14.68	14.77	14.18

[3] AREA could not been determined due to severe osteophytes.

3.1.3 Bone Mineral Density

The BMD was also determined by two observers based on the CT scans of the frozen explanted specimens. The cuboid to determine the BMD was intended to be 1200 mm². Depending on the resolution of the CT scans the standard volume was about 30x30x25 voxels. With 25 voxels, the cranial-caudal axis of the vertebrae is represented. Degenerated vertebrae required a modification of the volume of interest for determination of the HU. This was carried out independently by the observers. After revising the data, which differed by more than 15% between the observers, a linear regression was carried out for their revised values (Fig. 3-6). The regression curve slope was 0.97 ($R^2 = 0.95$). There was no significant difference between this slope and a slope of 1 ($p = 0.168$). The underlying statistical test has been described in chapter 2.1.

The one-way ANOVA did not show a statistical difference between the levels ($p = 0.443$). In Fig. 3-7, the mean BMD of L2 to L5 is displayed. The subset data for the donor groups were not normally distributed, requiring non-parametric statistics. Due to the amount of non-parametric intra-specimen comparisons the α-level was corrected. The BMD for Young Male (146 mgK_2HPO_4/ml) was significantly larger than the BMD for Midlife Male ($p = 0.002$, Mann-Whitney Test, $\alpha/2 = 0.025$). No difference was detected between the male (124 mgK_2HPO_4/ml) and female (129 mgK_2HPO_4/ml) midlife groups ($p = 0.343$, Mann-Whitney Test, $\alpha/2 = 0.025$ Fig. 3-8). Tab. 3-1 displays the mean BMD values of Observer 1 and Observer 2 in detail.

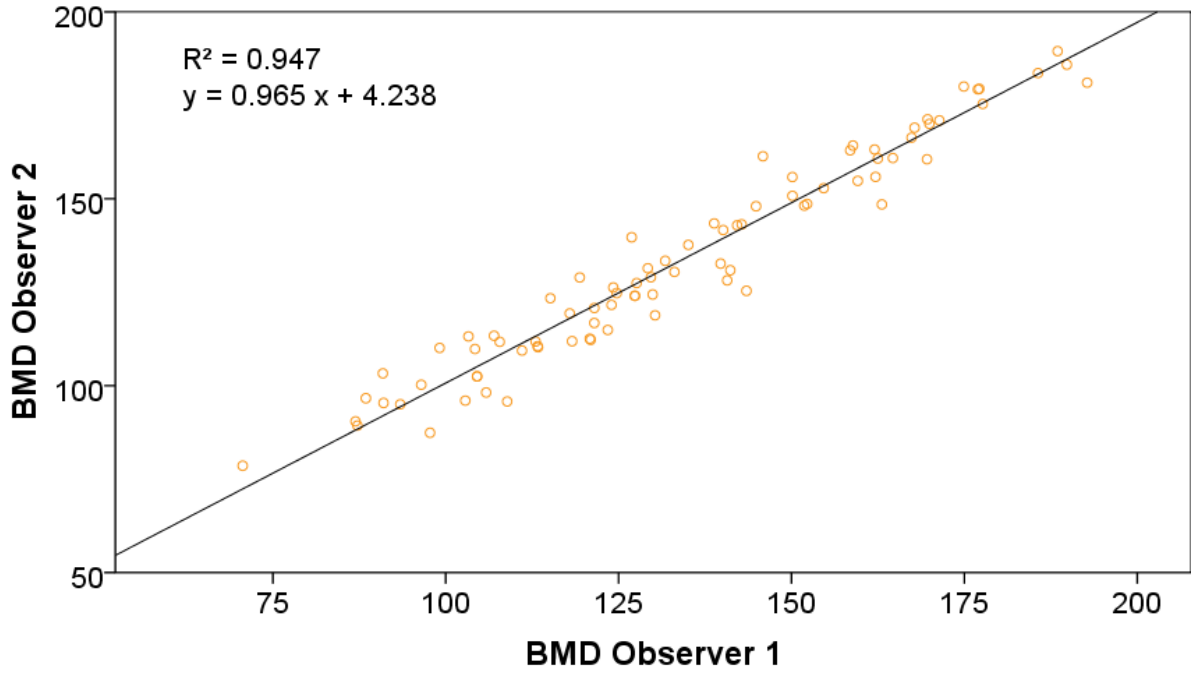

Fig. 3-6 Linear regression between bone mineral density results of Observer 1 and Observer 2 in K_2HPO_4 mg / ml.

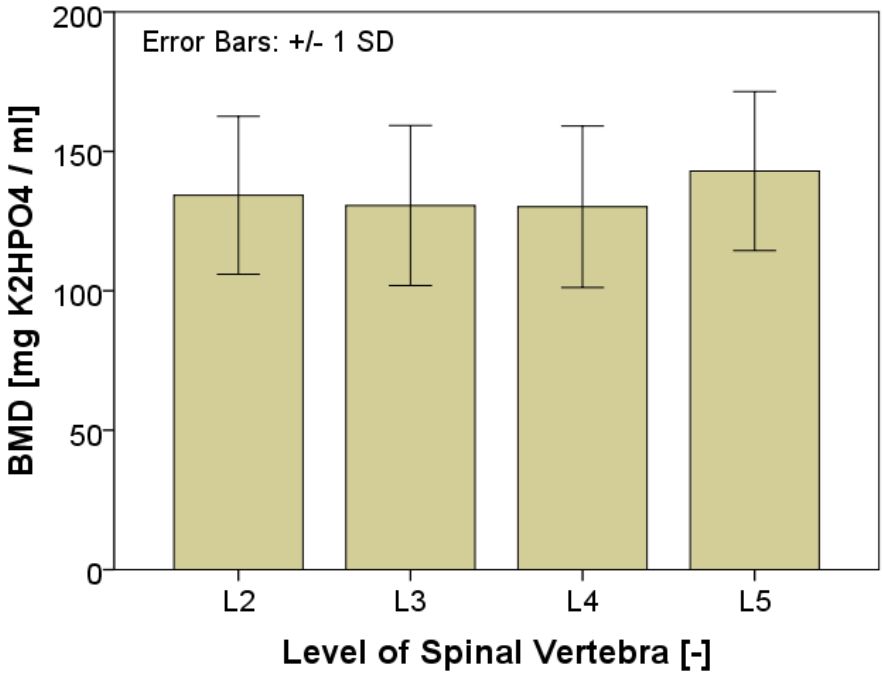

Fig. 3-7 Mean BMD of the four different levels included in this study; no significant differences were observed (n = 21 for each bar).

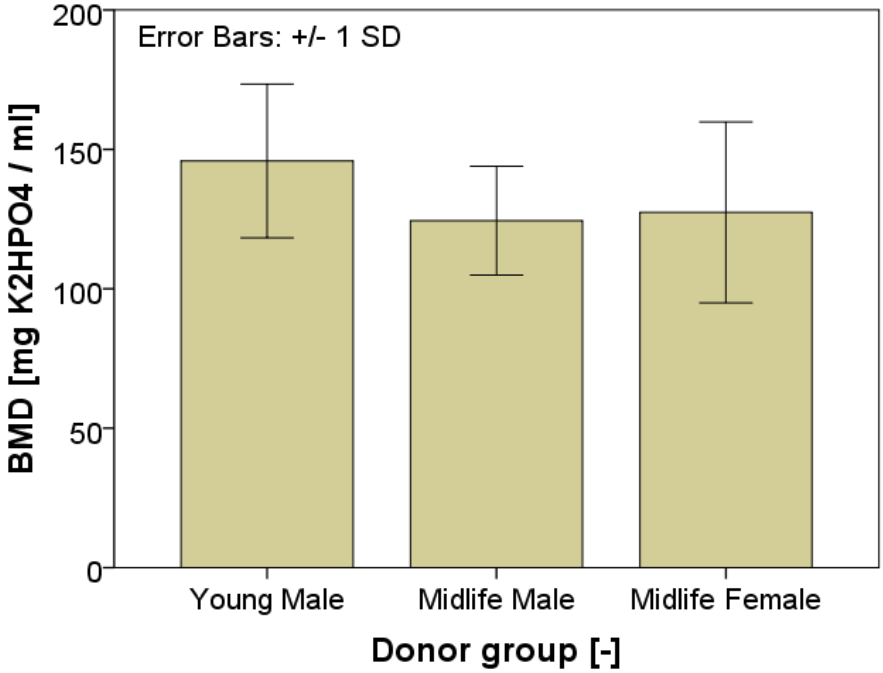

Fig. 3-8 Mean BMD of the three donor groups; BMD of young male group (n = 36) is significantly larger than that of the midlife donors (each group n = 24).

Tab. 3-3 Mean values of the bone mineral density determined by the two observers (hyphen indicates vertebrae that were not evaluated because the corresponding discs were not tested).

LWS	L2 [mg K_2HPO_4 / ml]	L3 [mg K_2HPO_4 / ml]	L4 [mg K_2HPO_4 / ml]	L5 [mg K_2HPO_4 / ml]
3001	165.08	161.64	166.86	176.50
3004	88.28	94.23	104.61	116.71
3005	157.19	150.01	150.46	159.02
3006	136.37	136.20	134.43	155.78
3007	146.44	161.57	153.62	160.71
3009	93.20	74.61	-	-
3011	116.61	119.26	103.50	125.69
3012	107.02	110.17	99.43	135.80
3013	92.54	97.10	92.57	109.77
3014	102.34	99.43	102.01	115.08
3016	122.79	119.13	119.17	134.44
3017	184.63	186.91	187.85	194.44
3018	162.60	153.75	-	-
3019	140.87	141.12	152.97	169.99
3021	177.47	168.40	178.12	188.99
3023	130.31	118.63	111.92	142.51
3025	-	-	98.35	88.70
3026	124.55	110.21	108.23	133.30
3027	-	-	111.82	112.41
3028	132.57	127.53	127.16	142.97
3030	136.02	124.16	129.34	150.44
3031	131.75	125.24	124.74	121.14
3032	170.48	162.78	171.17	178.29

3.1.4 Vertebral Capacity

The vertebral capacity (VC) was calculated for each FSU using the values determined for the endplate area and bone mineral density (Tab. 3-4). In combining the two characteristic parameters, a two-way ANOVA detected that VC was 37% greater for Young Males compared to Midlife Females ($p < 0.001$, Scheffe post-hoc); no other differences for the donor groups were detected ($p > 0.062$, Scheffe post-hoc). This is shown in Fig. 3-9. The level (L2-L3 or L4-L5) had no significant effect on vertebral capacity ($p = 0.221$).

Tab. 3-4 Vertebral Capacity – the AREA refers to the two endplates attached to the disc (e.g., the inferior endplate of L2 and the superior endplate of L3 for L2-L3).

	LWS	FSU	upper AREA	lower AREA	Mean AREA	upper BMD	lower BMD	Mean BMD	VC
			cm^2	cm^2	cm^2	$\frac{mgK_2HPO_4}{ml}$	$\frac{mgK_2HPO_4}{ml}$	$\frac{mgK_2HPO_4}{ml}$	$cm^2 \cdot \frac{mgK_2HPO_4}{ml}$
Young Male	3001	L2-L3	15.76	15.42	15.59	165.1	161.6	163.4	2547
		L4-L5	15.12	14.85	14.99	166.9	176.5	171.7	2573
	3005	L2-L3	14.39	14.32	14.36	157.2	150.0	153.6	2205
		L4-L5[4]	15.08	15.47	15.28	150.5	159.0	154.7	2364
	3007	L2-L3[4]	14.53	16.17	15.35	146.4	161.6	154.0	2363
		L4-L5	14.76	14.20	14.48	153.6	160.7	157.2	2276
	3012	L2-L3	16.94	16.90	16.92	107.0	110.2	108.6	1837
		L4-L5[4]	17.22	17.25	17.23	99.4	135.8	117.6	2027
	3013	L2-L3[4]	18.11	18.74	18.42	92.5	97.1	94.8	1747
		L4-L5	18.25	18.23	18.24	92.6	109.8	101.2	1845
	3019	L2-L3	13.20	13.16	13.18	140.9	141.1	141.0	1858
		L4-L5[4]	12.74	13.10	12.92	153.0	170.7	161.5	2086
	3021	L2-L3[4]	16.49	17.05	16.77	177.5	168.4	172.9	2901
		L4-L5	15.96	15.65	15.81	178.1	189.0	183.6	2901
	3031	L2-L3	16.17	16.96	16.57	131.8	125.2	128.5	2129
		L4-L5	18.16	19.70	18.93	124.7	121.1	122.9	2327
	3032	L2-L3	14.25	14.53	14.39	170.5	162.8	166.6	2398
		L4-L5	14.68	14.77	14.73	171.2	178.3	174.7	2573
Midlife Male	3006	L2-L3	14.52	13.96	14.24	136.4	136.2	136.3	1941
		L4-L5	15.63	15.60	15.62	134.4	155.8	145.1	2266
	3009	L2-L3[5]	15.91	17.18	16.55	93.2	74.6	83.9	1388
	3016	L2-L3	16.12	16.76	16.44	122.8	119.1	121.0	1989
		L4-L5	17.42	17.68	17.55	119.2	134.4	126.8	2225
	3023	L2-L3	14.19	14.66	14.43	130.3	118.6	124.5	1795
		L4-L5	15.60	15.56	15.58	111.9	142.5	127.2	1982
	3025	L4-L5[5]	16.04	16.62	16.33	98.4	88.7	93.5	1527
	3028	L2-L3	13.07	11.56	12.32	132.6	127.5	130.1	1602
		L4-L5	17.94	17.24	17.59	127.2	143.0	135.1	2376
	3030	L2-L3	16.52	16.17	16.35	136.0	124.2	130.1	2126
		L4-L5	16.47	15.82	16.15	129.3	150.4	139.9	2259

[4] FSU were used for testing the ultimate strength
[5] Only one FSU of the respective lumbar spine is included in this study

	LWS	FSU	upper AREA	lower AREA	Mean AREA	upper BMD	lower BMD	Mean BMD	VC
			cm2	cm2	cm2	$\frac{mgK_2HPO_4}{ml}$	$\frac{mgK_2HPO_4}{ml}$	$\frac{mgK_2HPO_4}{ml}$	$cm^2 \cdot \frac{mgK_2HPO_4}{ml}$
Midlife Female	3004	L2-L3	13.76	13.59	13.68	88.3	94.2	91.3	1248
		L4-L5	13.15	12.98	13.07	104.6	116.7	110.7	1446
	3011	L2-L3	11.34	11.21	11.28	116.6	119.3	117.9	1330
		L4-L5	11.84	11.44	11.64	103.5	125.7	114.6	1334
	3014	L2-L3	15.96	15.11	15.54	102.3	99.4	100.9	1567
		L4-L5	15.37	13.87	14.62	102.0	115.1	108.6	1587
	3017	L2-L3	12.23	13.17	12.70	184.6	186.9	185.8	2359
		L4-L5	11.83	12.73	12.28	187.9	194.4	191.2	2347
	3018	L2-L3[5]	11.39	11.80	11.60	162.6	153.8	158.2	1834
	3026	L2-L3	13.36	13.75	13.56	124.6	110.2	117.4	1591
		L4-L5	15.36	15.30	15.33	108.2	133.3	120.8	1851
	3027	L4-L5[5]	13.69	10.76	12.23	111.8	112.4	112.1	1371

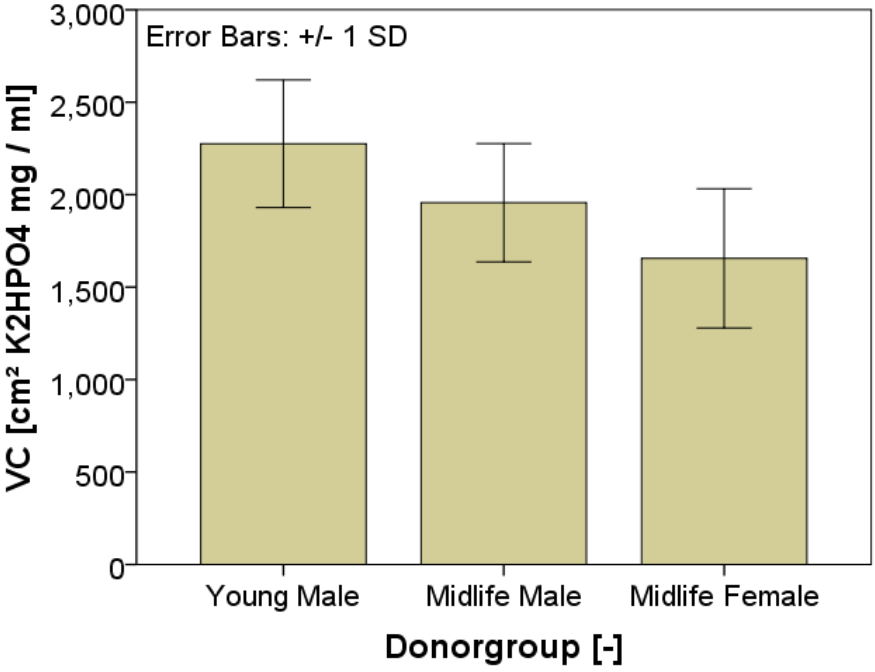

Fig. 3-9 Mean VC of the three donor groups (each n = 12); VC of the Young male group is significantly larger than that of the Midlife Females donors.

3.1.5 Intervertebral Disc Height – Frobin Classification

Based on the spinal lateral projections made out of the CT scans, the corrected relative intervertebral disc (IVD) height was determined by two observers. The value gives the ratio between vertebral distance (disc height) and mean depth of the cranial vertebra.

The outcome might depend on slight differences between the vertebra corners selected by the observers. Nevertheless, the regression of the results including the outliers showed a satisfying regression slope of 0.88 (R^2 = 0.75, Fig. 3-10). The slope does not differ significantly from 1 ($p = 0.133$). The underlying statistical test has been described in chapter 2.1.

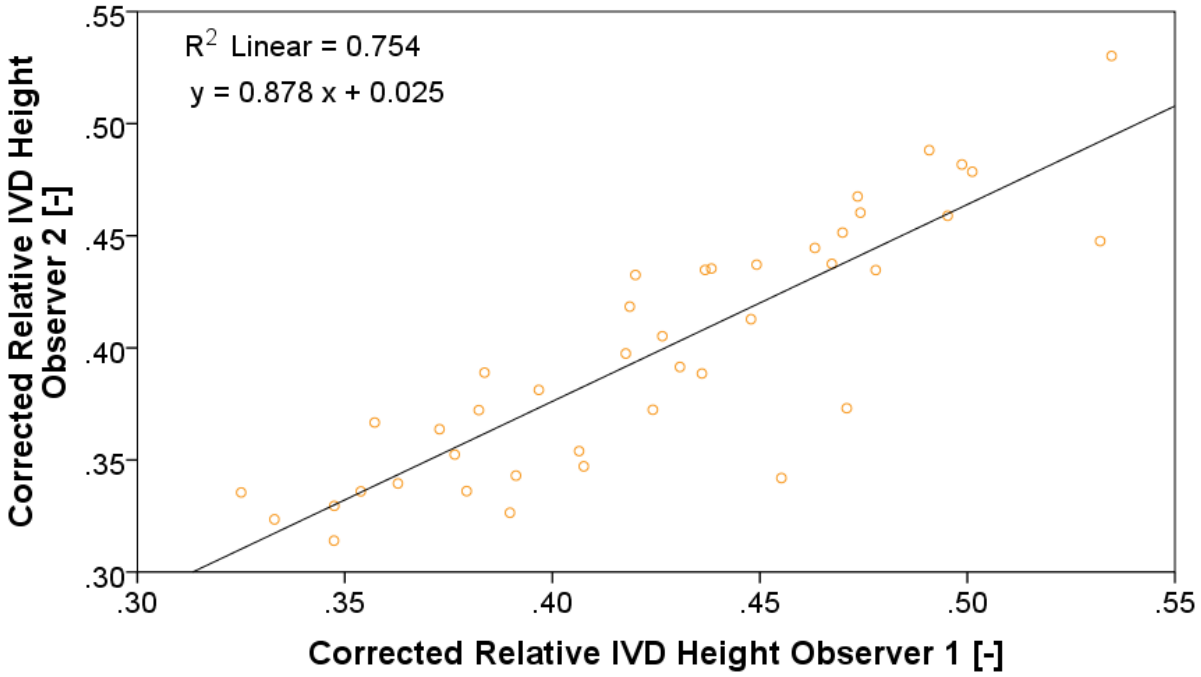

Fig. 3-10 Linear regression of corrected IVD height estimation of observer 1 and observer 2.

In the following, the values are the mean value of the findings of both observers. The corrected relative disc heights of the L2-L3 and L4-L5 functional spinal units of the male and female donors are shown in detail in Fig. 3-11 and Fig. 3-12. In comparison to the reference values of the corresponding age groups published by Frobin et al. (1997), the averaged mean IVD height for male and female L2-L3 FSUs is 10% and 8% greater, respectively; and for male and female L4-L5 FSUs, it is 5% and 4% (Tab. 3-5), respectively. Deviations in the mean IVD heights compared to norm values were similar to those determined in the previous projects (F1899 and F2069).

The two-way ANOVA did not detect a significant difference between male and female IVD height ($p = 0.059$), however, the height for L4-L5 segments was 16% greater than that for L2-L3 ($p < 0.001$). The individual data for IVD height is listed in Tab. 3-6.

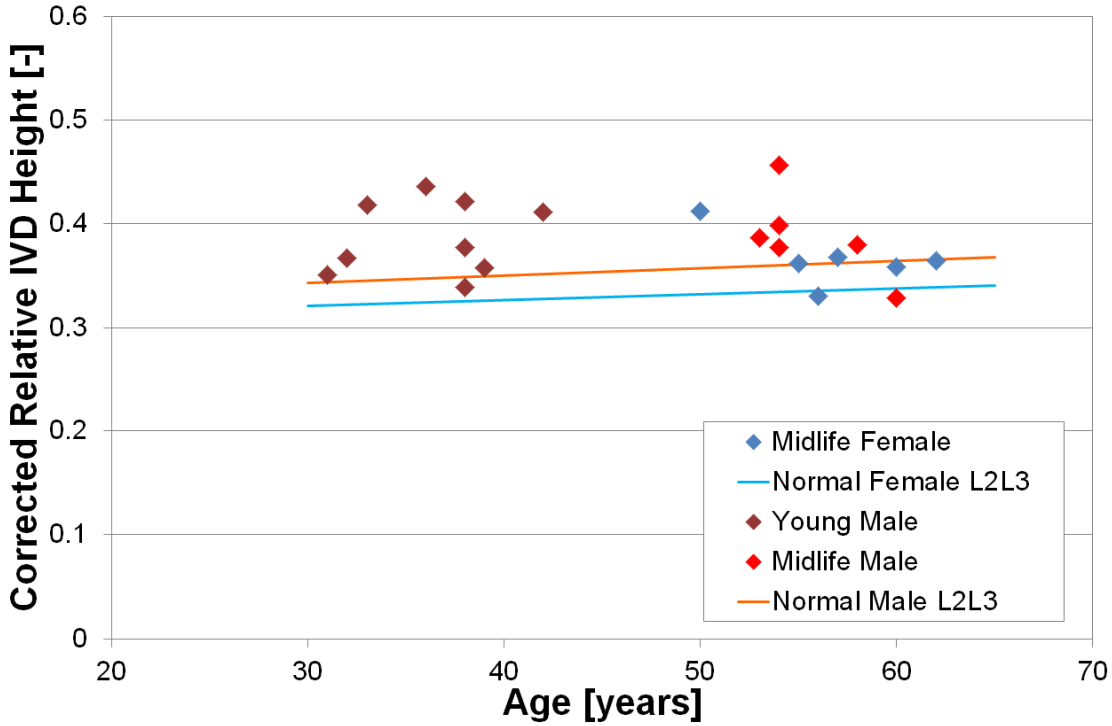

Fig. 3-11 Age dependence of corrected relative disc height of L2-L3 motion segments (reference values for the normal population were calculated based on Frobin et al., 1997).

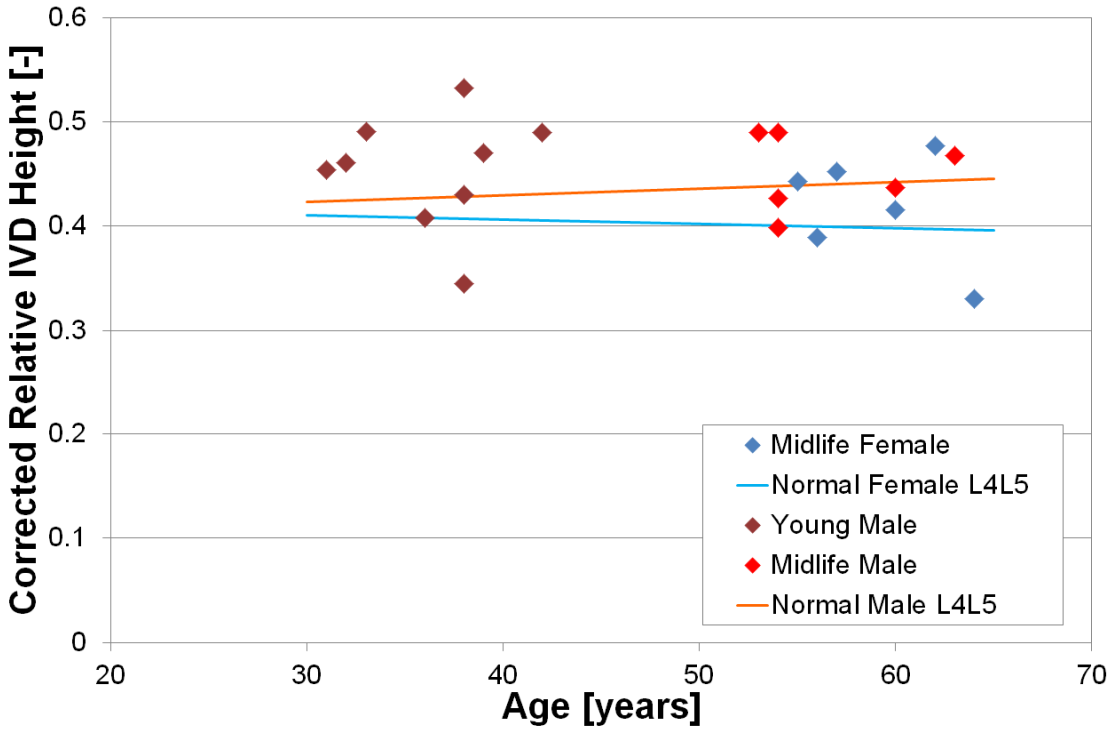

Fig. 3-12 Age dependence of corrected relative disc height of L4-L5 motion segments (reference values for the normal population were calculated based on Frobin et al., 1997).

Tab. 3-5 Comparison of determined disc height and calculated norm values (according to Frobin et al., 1997).

Gender	Level	Minimum value in comparison to norm [%]	Maximum value in comparison to norm [%]	Mean value in comparison to norm [%]
male	**L2-L3**	-10	27	10
	L4-L5	-20	24	5
female	**L2-L3**	-1	20	8
	L4-L5	-17	20	4

Tab. 3-6 Corrected relative disc height of FSU used in this study (gender: m = male, f = female, hyphens indicate FSUs excluded from this study).

LWS	gender	Corrected relative IVD height	
		L2-L3	L4-L5
3001	m	0.42	0.53
3004	f	0.33	0.39
3005	m	0.35	0.45
3006	m	0.40	0.43
3007	m	0.36	0.47
3009	m	0.38	-
3011	f	0.36	0.44
3012	m	0.38	0.34
3013	m	0.34	0.43
3014	f	0.36	0.42
3016	m	0.33	0.44
3017	f	0.36	0.48
3018	f	0.41	-
3019	m	0.42	0.49
3021	m	0.44	0.41
3023	m	0.38	0.49
3025	m	-	0.47
3026	f	0.37	0.45
3027	f	-	0.33
3028	m	0.46	0.40
3030	m	0.39	0.49
3031	m	0.41	0.49
3032	m	0.37	0.46

3.1.6 Thompson Classification

The morphological Thompson grading was carried out for the dynamic compression load groups, dynamic shear load and ultimate strength specimens. Photographs of the transversal section were evaluated by two observers. Three datasets were removed from the overall data because the test results appeared to be implausible or not evaluable (ultimate strength: 3005 L4-L5 Young Male, see 3.4; dynamic compression: FSU 3005 L2-L3 HIGH Young Male and FSU 3025 L4-L5, OFFSET Midlife Male, see chapter 0.) The results for all specimens tested by the two observers differed in at least one aspect (nucleus, annulus fibrosus, endplates or vertebral body).

In Fig. 3-13, box plots of the overall grade of degeneration for the five different load groups are shown. There was a significant difference between the group means of the NORM and SHEAR FSUs ($p = 0.047$, Scheffe post-hoc). NORM experiments were done with the FSUs of midlife donors while SHEAR experiments were carried out with the donations of young objects. The FSUs in dynamic compression ranged between an average (two observers) grade of 2.5 and 4.1. The ultimate strength specimens ranged between 2.9 and 5.0 and those for dynamic shear ranged between 2.0 and 3.3. It is important to take into account that prior to this morphological Thompson grading, the specimens already underwent high cycle loading (NORM, OFFSET, HIGH, SHEAR or overload breakage (ULTIMATE), respectively.

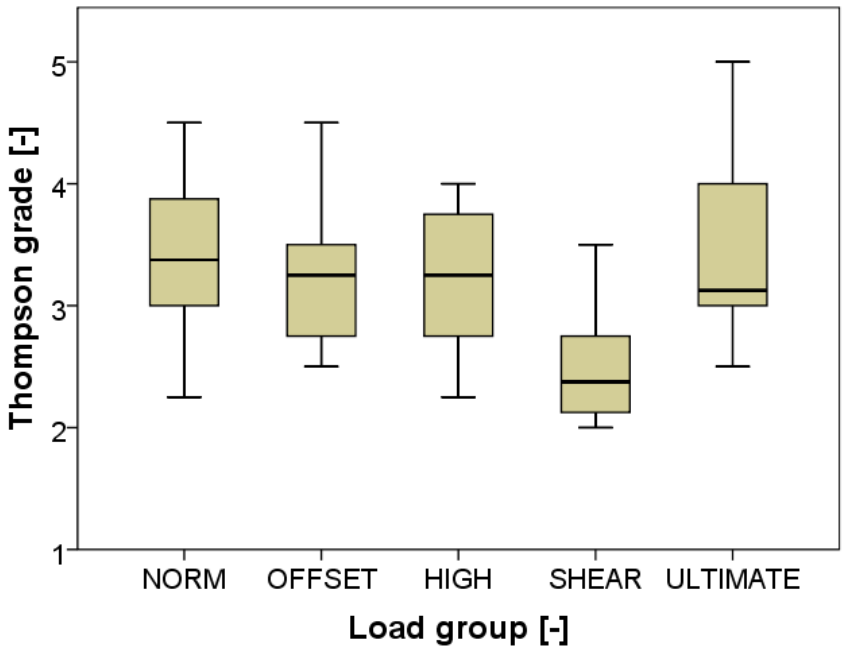

Fig. 3-13 Box plots of the average grade of disc degeneration for the different load groups (NORM n = 8, OFFSET n = 7, HIGH n = 13, SHEAR n = 6, ULTIMATE n = 5).

The grade of degeneration differs within the load groups. In Fig. 3-14 to Fig. 3-16, representative photographs of the different states of degeneration of the separated FSUs are shown.

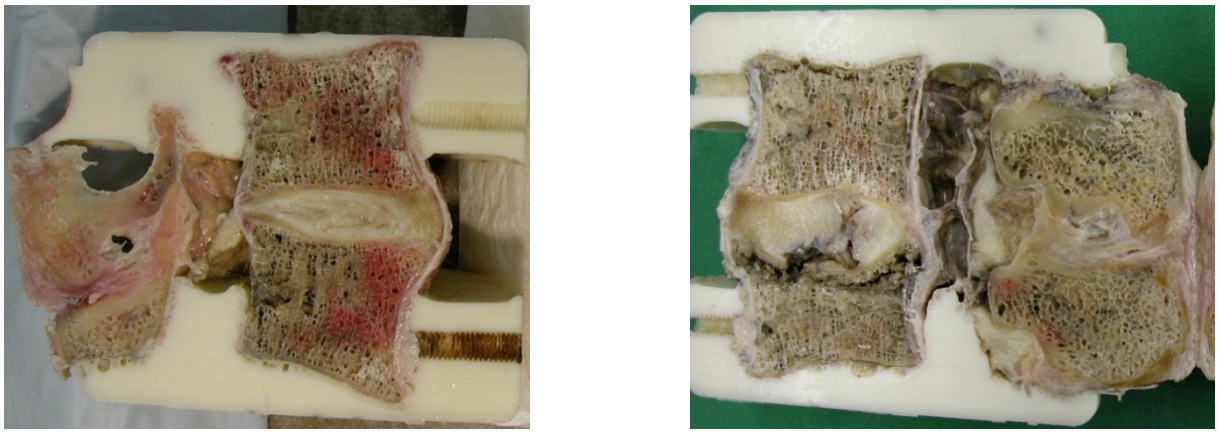

Fig. 3-14 FSUs tested in compression fatigue mode (LWS 3023 L4-L5, LWS 3014 L2-L3); left: low grade of degeneration, right: high grade of degeneration.

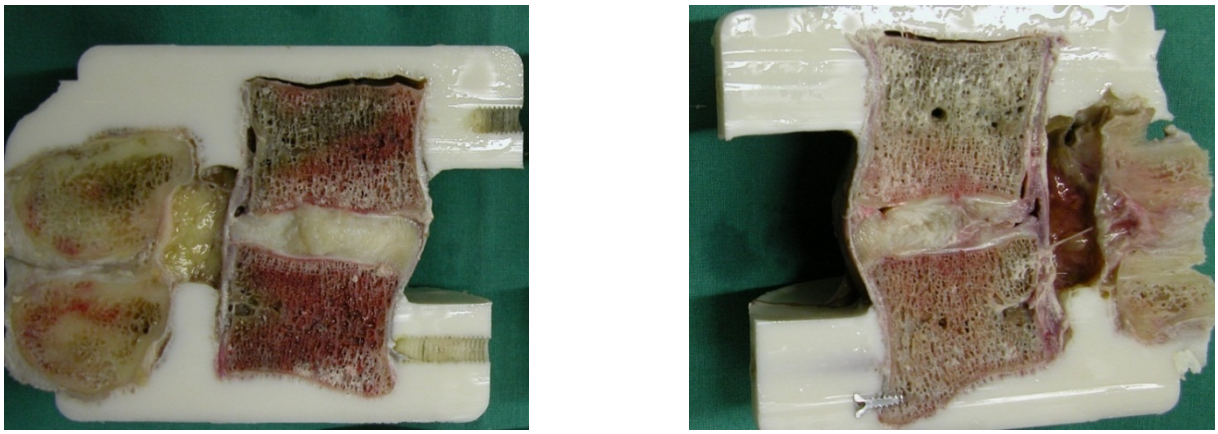

Fig. 3-15 FSUs tested in shear fatigue mode (LWS 3007 L4-L5, LWS 3021 L4-L5); left: low grade of degeneration, right: high grade of degeneration.

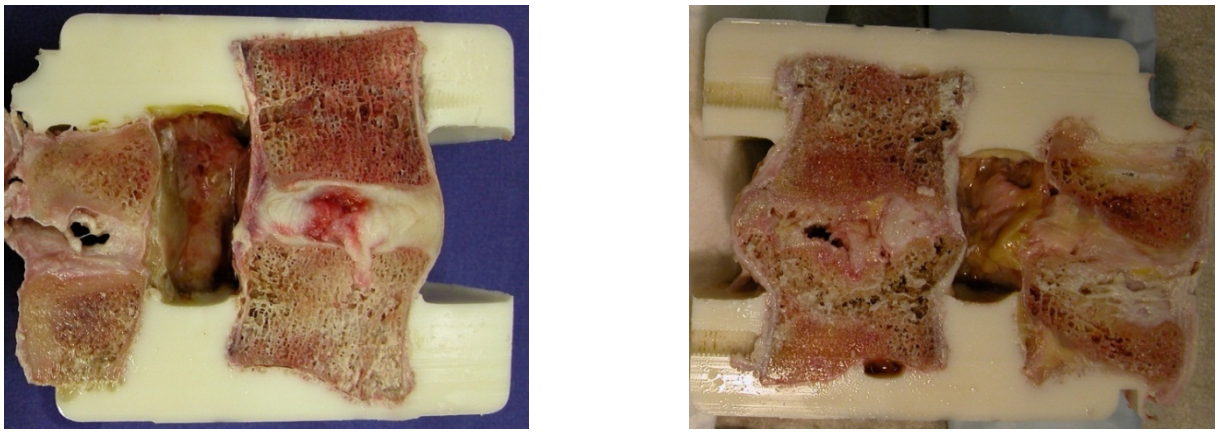

Fig. 3-16 FSUs tested for ultimate strength (LWS 3019 L4-L5, LWS 3013 L2-L3); left: low grade of degeneration, right: high grade of degeneration.

The results of the observers for the FSUs tested in NORM fatigue load are displayed in Tab. 3-7. The maximum difference between the observers with regard to the individual aspects (nucleus, annulus, endplate and vertebral body) is 2 grades. With

respect to the mean for each FSU, the results of the observers differ by 0.2 to 1 grades. The overall group mean grade was 3.49.

The Thompson grades determined by the two observers for the FSUs tested under OFFSET fatigue load are listed in Tab. **3-8**. The difference in the mean grades for the FSUs ranged from 0.2 to 1. The overall group mean grade was 3.27. The Thompson grades determined for the FSUs tested under HIGH fatigue load are displayed in Tab. **3-9**. The maximum difference between the two observers is 1 grade. The Thompson grade for one specimen was consistent in all four aspects. The overall group mean grade was 3.27.

The Thompson grades for the FSUs tested in SHEAR mode are displayed in Tab. 3-10. The maximum difference between two observers for an FSU was 0.5 grades. The means for two FSUs were equal. The overall group mean grade was 2.52.

The Thompson grades of the FSUs tested for ultimate strength determined by two observers are shown in Tab. 3-11. The maximum difference with regard to the means for the FSUs is 0.8 grades. The grade determined by the two observers for two of the FSUs was consistent in all four aspects. The overall group mean grade was 3.54.

Tab. 3-7 Grade of degeneration of FSUs tested in dynamic compression mode with NORM load according to Thompson et al. (1990) (NU: nucleus, AN: annulus fibrosus, EP: endplates, VB: vertebral body).

LWS	Level	Observer 1					Observer 2					Overall Mean
		NU	AN	EP	VB	Mean	NU	AN	EP	VB	Mean	
3006	**L4-L5**	3	4	2	3	3.0	3	4	4	5	4.0	3.5
3009	**L2-L3**	5	5	4	3	4.3	4	3	4	3	3.5	3.9
3011	**L4-L5**	3	3	4	3	3.3	3	3	4	4	3.5	3.4
3014	**L2-L3**	5	5	4	4	4.5	4	4	3	4	3.8	4.1
3017	**L2-L3**	3	3	3	3	3.0	3	3	3	4	3.3	3.1
3023	**L4-L5**	2	2	2	3	2.3	3	3	2	3	2.8	2.5
3026	**L4-L5**	3	3	3	2	2.8	3	3	4	3	3.3	3.0
3028	**L2-L3**	4	4	3	3	3.5	4	4	4	5	4.3	3.9

Tab. 3-8 Grade of degeneration of FSUs tested in dynamic compression mode with OFFSET load according to Thompson et al. (1990) (NU: nucleus, AN: annulus fibrosus, EP: endplates, VB: vertebral body).

LWS	Level	Observer 1					Observer 2					Overall Mean
		NU	AN	EP	VB	Mean	NU	AN	EP	VB	Mean	
3004	**L2-L3**	5	5	4	4	4.5	4	4	3	3	3.5	4.0
3006	**L2-L3**	3	2	3	3	2.8	3	4	4	3	3.5	3.1
3014	**L4-L5**	4	3	3	3	3.3	4	4	3	3	3.5	3.4
3016	**L4-L5**	4	3	2	2	2.8	4	4	3	4	3.8	3.3
3026	**L2-L3**	3	3	2	2	2.5	3	3	3	3	3.0	2.8
3027	**L4-L5**	4	4	2	3	3.3	4	4	4	3	3.8	3.5
3030	**L2-L3**	3	3	2	2	2.5	3	3	3	3	3.0	2.8

Tab. 3-9 Grade of degeneration of FSUs tested in dynamic compression mode with HIGH load, according to Thompson et al. (1990) (NU: nucleus, AN: annulus fibrosus, EP: endplates, VB: vertebral body).

LWS	Level	Observer 1					Observer 2					Overall Mean
		NU	AN	EP	VB	Mean	NU	AN	EP	VB	Mean	
3001	**L4-L5**	3	3	3	2	2.8	2	2	3	2	2.3	2.5
3004	**L4-L5**	3	3	3	2	2.8	3	3	3	2	2.8	2.8
3011	**L2-L3**	4	3	3	2	3.0	3	3	4	3	3.3	3.1
3013	**L4-L5**	3	3	4	4	3.5	4	3	4	5	4.0	3.8
3016	**L2-L3**	4	4	4	2	3.5	4	4	4	3	3.8	3.6
3017	**L4-L5**	3	3	2	3	2.8	3	4	4	4	3.8	3.3
3018	**L2-L3**	4	4	4	4	4.0	4	4	3	4	3.8	3.9
3019	**L2-L3**	3	3	3	3	3.0	3	4	4	4	3.8	3.4
3023	**L2-L3**	4	4	4	3	3.8	4	4	2	3	3.3	3.5
3028	**L4-L5**	4	4	3	3	3.5	4	3	4	5	4.0	3.8
3030	**L4-L5**	3	3	3	2	2.8	3	3	4	3	3.3	3.0
3031	**L4-L5**	3	3	2	2	2.5	3	3	3	4	3.3	2.9
3032	**L2-L3**	4	3	3	2	3.0	3	3	2	3	2.8	2.9

Tab. 3-10 Grade of degeneration grading of FSUs tested in SHEAR mode, according to Thompson et al. (1990) (NU: nucleus, AN: annulus fibrosus, EP: endplates, VB: vertebral body).

LWS	Level	Observer 1					Observer 2					Overall Mean
		NU	AN	EP	VB	Mean	NU	AN	EP	VB	Mean	
3001	**L2-L3**	3	2	3	2	2.5	1	2	2	3	2.0	2.3
3007	**L4-L5**	3	2	2	1	2.0	2	2	2	2	2.0	2.0
3012	**L2-L3**	3	3	2	1	2.3	2	2	2	3	2.3	2.3
3021	**L4-L5**	3	4	2	3	3.0	3	4	3	4	3.5	3.3
3031	**L2-L3**	3	3	2	2	2.5	3	3	3	3	3.0	2.8
3032	**L4-L5**	3	2	2	2	2.3	2	3	2	3	2.5	2.4

Tab. 3-11 Grade of degeneration of FSUs tested for ultimate strength, according to Thompson et al. (1990) (NU: nucleus, AN: annulus fibrosus, EP: endplates, VB: vertebral body).

LWS	Level	Observer 1					Observer 2					Overall Mean
		NU	AN	EP	VB	Mean	NU	AN	EP	VB	Mean	
3007	**L2-L3**	3	3	3	3	3.0	3	3	3	3	3.0	3.0
3012	**L4-L5**	4	4	4	3	3.8	4	4	4	4	4.0	3.9
3013	**L2-L3**	5	5	5	5	5.0	5	5	5	5	5.0	5.0
3019	**L4-L5**	3	3	2	3	2.8	3	3	3	3	3.0	2.9
3021	**L2-L3**	4	3	3	3	3.3	2	2	3	3	2.5	2.9

3.2 Parameter Measurements

Each of the 36 specimens from the three donor groups underwent reference measurements, quasistatic and dynamic parameter testing and fatigue testing. The mean ages for Midlife Male and Midlife Female only differed by two years with a standard deviation of 3.4 to 3.9 years, therefore the groups could be treated as one age group. The Young Male group was about 20 years younger than the Midlife groups. The data of the specimen sets for dynamic testing are displayed in Tab. 3-12.

Three FSUs were excluded from the parameter evaluation. One of the FSUs had already failed within the load exposure during initial parameter testing (FSU 3025 L4-L5). Compared to the other specimens, the second one exhibited distinctively higher peak-to-peak displacement during fatigue testing (FSU 3005 L2-L3), which was most probably caused by some kind of loosening. Furthermore, the parameter testing results of FSU 3023 L4-L5 could not be evaluated due to errors during data acquisition.

Tab. 3-12 Subsumption of FSUs used for dynamic testing (the crossed out FSUs in grey were excluded from the group statistics below).

		Young Male	Midlife Male	Midlife Female
LWS Level L2-L3		3001, ~~3005~~, 3012, 3019, 3031, 3032	3006, 3009, 3016, 3023, 3028, 3030	3004, 3011, 3014, 3017, 3018, 3026
LWS Level L4-L5		3001, 3007, 3013, 3021, 3031, 3032	3006, 3016, ~~3023~~, ~~3025~~, 3028, 3030	3004, 3011, 3014, 3017, 3026, 3027
Age [years]	Range	32 - 42	53 - 60	50 - 64
	Mean ± SD	37.1 ± 3.5	55.4 ± 2.8	57.83 ± 3.9
Body Height [cm]	Range	173 - 185	170 - 180	152 - 172
	Mean (SD)	178.7 ± 4.6	174.6 ± 3.4	163.4 ± 6.8
Body Mass [kg]	Range	66.8 - 117.4	49.1 - 112.6	46.6 - 117.5
	Mean (SD)	79.1 ± 15.1	90.7 ± 17.6	93.4 ± 26.2

The results reflect slight creeping over the testing period. Severe creeping could only be observed during the first quasistatic cycles applied. Stiffness of the FSUs is non-linear, therefore initial stiffness for the small loads and peak stiffness for the high loads or displacements differed strongly from each other. This non-linearity was of major interest for shear stiffness when analysing the posterior and anterior displacements and also for interpreting the stiffness at different offsets and amplitudes in compression. The initial stiffness and peak stiffness for the different load levels did not correspond to the same absolute displacement position and were therefore only comparable to a limited extent.

The statistical analysis of the results was done using parametrical tests (PASW 18, SPSS Inc./IBM Corporation, Armonk, NY, US). Unless noted otherwise, the statistical analyses were done at a significance level of $\alpha = 0.05$. The percentage values describing a decrease or an increase are based on the estimated means obtained using a factorial ANCOVA. Data were not always normally distributed; consequently the validity of the statistical results may be limited in some cases. This should be

especially considered with regard to significant p values that are close to an α level of 0.05.

3.2.1 Quasistatic Measurements

A two-way ANCOVA with the load pattern and donor group as factors and with AREA as a covariate was applied. The load IDs were compared by means of Bonferroni post-hoc testing of the estimated group means. The estimated mean values for stiffness of the Young and Midlife males, as well as Midlife Female and Male were compared using the contrasts provided by the statistics software.

3.2.1.1 Quasistatic Compression Loading

Three load patterns were applied in quasistatic compression loading (Tab. 2-4). All of them covered a compression offset of -1000 N and amplitude of -1000 N (ramp mode). They differed with regard to the simultaneously applied shear pre-load: no shear load (ID01), anterior shear load (ID02) and posterior shear load (ID03). In order to rate the creep proportion that might be inherent in the determined differences between the load patterns, the first reference measurement after quasistatic testing (ID01ref2, see Table 2-3) was included in the analysis. It covers the same load pattern as ID01.

In Fig. 3-17, the apparent stiffness c_{app} is displayed. A significant difference was detected between the subset groups ($p < 0.001$). The covariate AREA had no significant effect on stiffness ($p = 0.976$). Shear pre-load reduces compression stiffness significantly ($p < 0.001$). Anterior shear pre-load reduces stiffness by 29% while posterior shear load decreases stiffness by 39%. The difference between the anterior and posterior shear load was not significant ($p = 0.09$). The stiffness mean of the three donor groups was different. Midlife Female stiffness was significantly smaller (23%) compared to stiffness for the Midlife Male group ($p < 0.001$). There was no significant difference between the two male donor groups ($p = 0.202$).

Reference stiffness after quasistatic testing did not differ significantly from stiffness without shear pre-load ($p = 0.237$). The differences observed for the load patterns were not due to creeping but to the effects of shear pre-load and the donor groups. In Fig. 3-18, the initial stiffness $c_{initial}$ measured during quasistatic loading with different constant shear loads is shown. The validity of the statistical analysis is limited since the data of the subset Midlife Female under ID01 load were not normally distributed (Kolomogorov-Smirnov Test, $p = 0.002$) and the equality of error variance was not given (Levene's Test, $p = 0.036$).

In addition, the difference between the subset groups was significant ($p < 0.001$) for this initial stiffness; AREA had no significant effect on the stiffness ($p = 0.692$). $C_{initial}$ without shear load was significantly higher than the stiffness with additional shear load ($p < 0.001$). An anterior shear pre-load results in a decreases stiffness by 56 % while a posterior shear load decreases stiffness by 60 %. There was no difference detected between the effect of a posterior shear load and an anterior shear load ($p > 0.999$). The stiffness mean of the donor groups was 27 % higher for Midlife Male than for Midlife Female ($p = 0.002$). However, no difference was detected between Midlife and Young Male ($p = 0.337$).

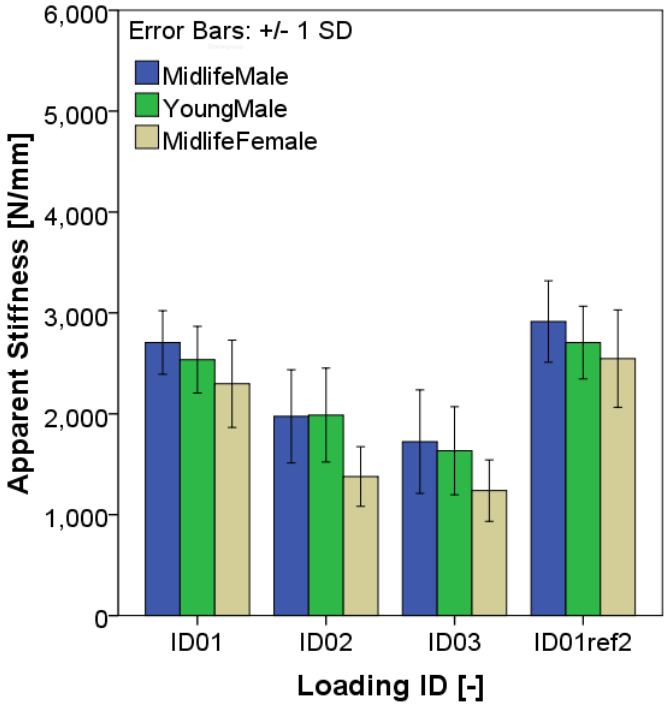

Fig. 3-17 Apparent stiffness under axial quasistatic load (ID01: without shear, ID 02: with anterior shear, ID 03: with posterior shear, ID01ref2: without shear and after testing) for the three donor groups (Young Male, Midlife Male and Midlife Female).

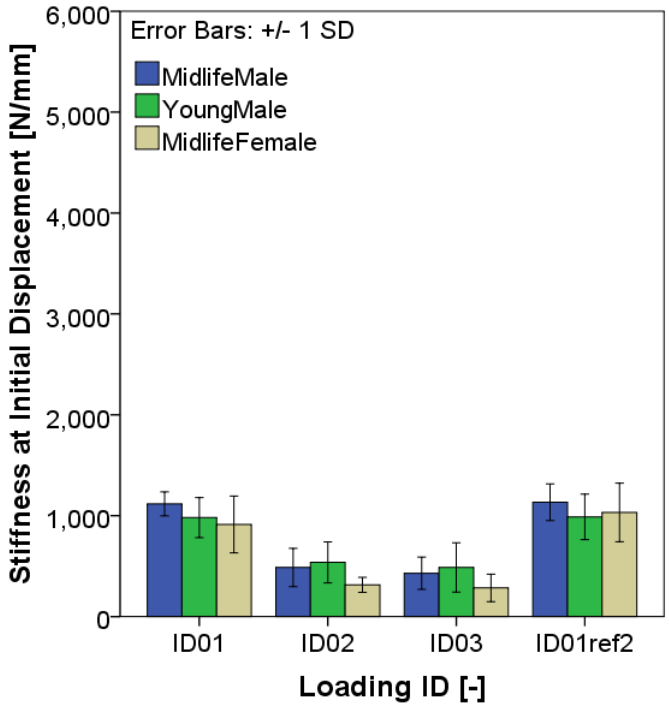

Fig. 3-18 Initial stiffness if specimens are exposed to axial quasistatic load (ID01: without shear, ID02: with anterior shear, ID03: with posterior shear, ID01ref2: without shear and after testing) for the three donor groups (Young Male, Midlife Male and Midlife Female).

Fig. 3-19 displays the stiffness at high displacement c_{peak} determined from the results of quasistatic loading with different constant shear loads. Analogous to c_{app} and $c_{initial}$, the stiffness at high compressive displacement c_{peak} for the subset groups was significantly different ($p < 0.001$); AREA had no significant effect on stiffness ($p = 0.840$). C_{peak} without shear load was significantly larger than the stiffness with additional shear load in the posterior direction ($p < 0.001$). However, no significant difference was found between shear load in the anterior direction and no shear load ($p = 0.069$) or between the anterior and posterior shear load ($p = 0.025$). The analyses did not reveal a significant difference between the two male donor groups ($p = 0.371$); the stiffness of the Midlife Female specimens was 17% smaller than the stiffness of the Midlife Male group ($p < 0.001$).

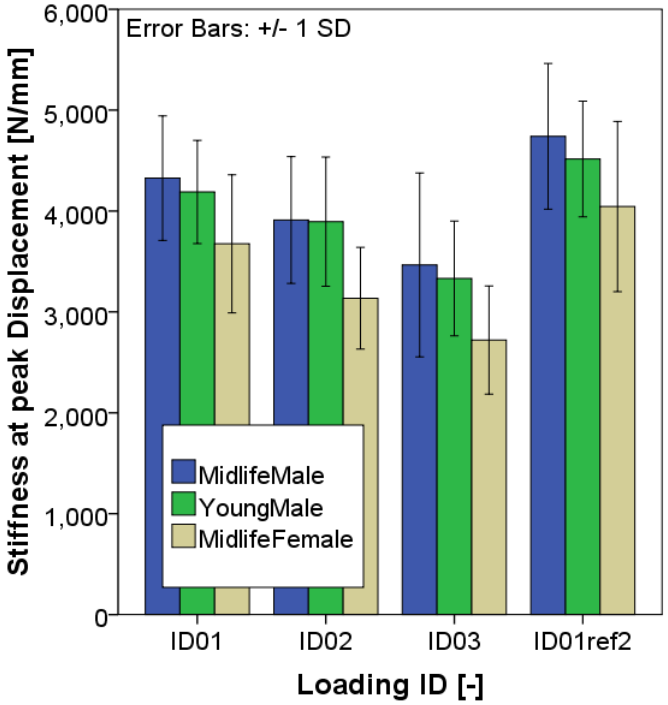

Fig. 3-19 Peak stiffness under quasistatic load (ID01: without shear, ID 02: with anterior shear, ID 03: with posterior shear, ID01ref2: without shear and after testing) for Young Male, Midlife Male and Midlife Female.

3.2.1.2 Quasistatic Shear Loading

The load of the two quasistatic shear load IDs is applied as ramp around offset mode, but they differed with respect to pre-load - ID04 covers a shear load alternating around an offset of 0 N, while ID05 covers an anterior shear load alternating around an offset of 100 N (Tab. 2-4). Stiffness in the shear direction was analysed.

In Fig. 3-20, the apparent stiffness c_{app} in the shear direction measured under quasistatic load is displayed. The data of subset Midlife Male under ID05 load were not normally distributed (Kolmogorov-Smirnov Test, $p = 0.041$) and the equality of error variance was not given (Levene's Test, $p = 0.028$); hence, the validity of the statistical analysis is limited.

The subset groups differed significantly ($p < 0.001$): AREA had no effect ($p = 0.993$). The apparent stiffness was significantly larger for anterior pulsatile loading (ID 05, $p = 0.005$). The stiffness of the Young Male specimens was significantly larger than the stiffness of the Midlife Male specimens ($p = 0.005$). The difference between the Midlife Male and Midlife Female group was not significant ($p = 0.175$).

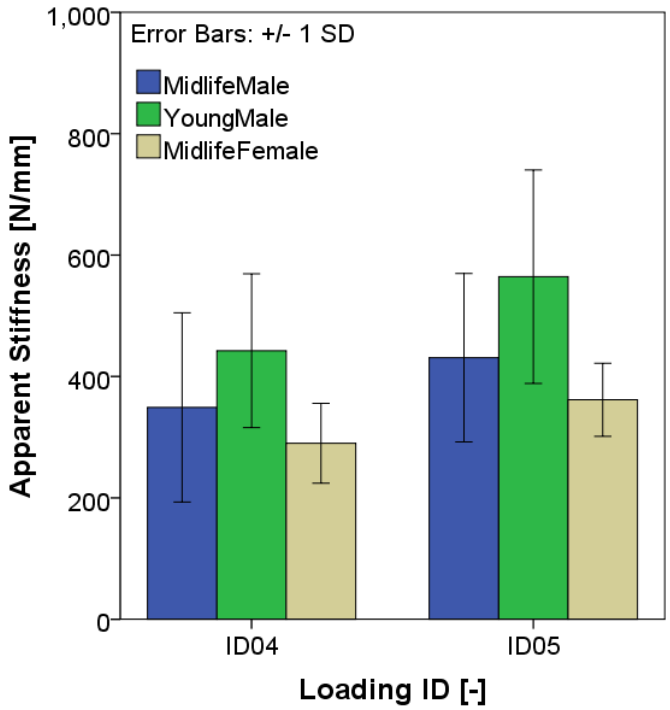

Fig. 3-20 Apparent shear stiffness during quasistatic shear loading (ID04 and 05) of Young Male, Midlife Male and Midlife Female.

In Fig. 3-21, the stiffness at high displacement in the anterior direction c_{ant} during quasistatic shear loading is displayed. The data of the subsets of Midlife Male under ID04 and ID05 were not normally distributed (Kolmogorov-Smirnov Test, $p < 0.036$) and the homogeneity of variance was also not given (Levene's Test, $p = 0.037$); hence, the validity of the statistical analysis is limited.

The data subsets were significantly different ($p < 0.001$). Again, the covariate AREA had no significant effect ($p = 0.868$). C_{ant} was significantly larger for pulsatile anterior loading (ID 05, $p = 0.001$). The difference between the two Male groups was significant and the stiffness of the Young Male group was larger ($p = 0.001$). The stiffness of the Midlife Female group was smaller than the stiffness of the Midlife Male group ($p = 0.049$).

Fig. 3-22 displays the stiffness at high displacement in the posterior shear direction c_{post}. Again, the subset groups differed significantly ($p = 0.034$) and likewise the effect of the covariate AREA ($p = 0.774$). Stiffness under anterior loading (ID05) did not differ significantly from an alternating load of around zero (ID04, $p = 0.075$). There was no significant difference between Young and Midlife Male ($p = 0.095$) and the same applies for Midlife Male and Midlife Female ($p = 0.413$).

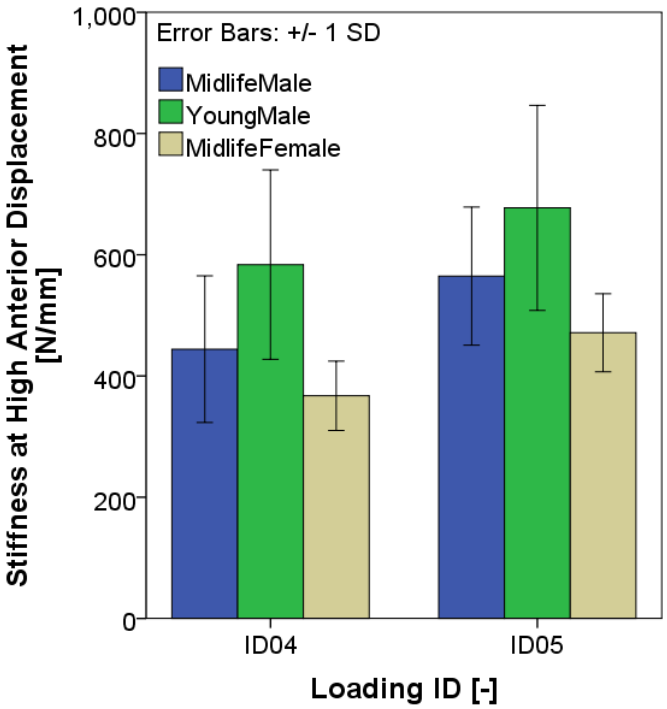

Fig. 3-21 Stiffness at maximum anterior displacement during quasistatic shear loading (ID 04 and 05) of Young Male, Midlife Male and Midlife Female.

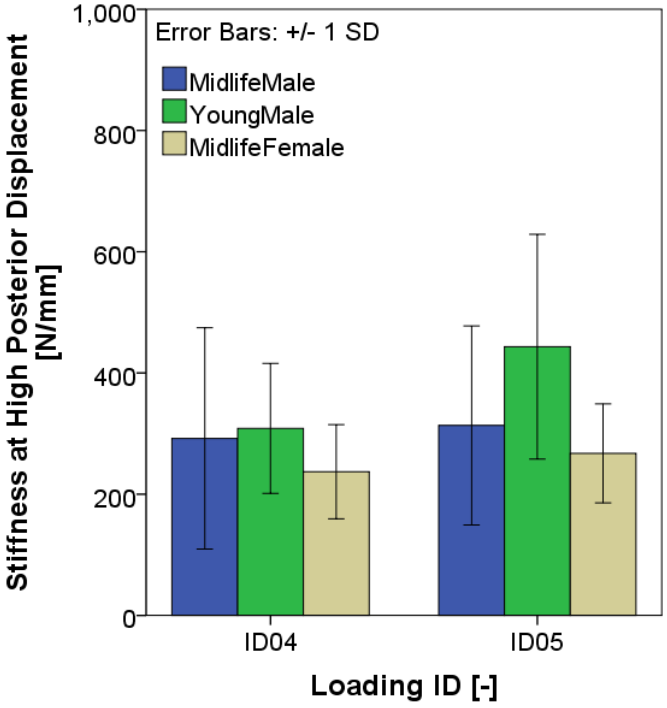

Fig. 3-22 Stiffness at maximum posterior displacement during quasistatic shear loading (ID 04 and 05) of Young Male, Midlife Male and Midlife Female.

3.2.2 Frequency-Dependent Measurements

Frequency-dependent measurements in preconditioning covered compression and shear load patterns. The following analysis concentrates on changes in stiffness over a frequency range of 0.02 to 10 Hz and on changes due to the varying amplitudes and offsets (mean of sinusoidal signal) of dynamic loading.

The test frequencies 3, 7 and 12 Hz were excluded to achieve logarithmically equidistant measuring points for statistical analysis (0.02, 0.05, 0.1, 0.2, 0.5, 1, 2, 5, 10 Hz). A statistical analysis was done by applying a repeated measures two-way ANCOVA with AREA as covariate for compression testing. AREA was not assumed to have an effect in shear direction, therefore it was not included in the analysis (repeated measures two-way ANOVA).

Some subset data were not normally distributed and the covariance matrices were heterogenic, therefore the validity of the statistical analysis is limited. The sphericity for the repeated measures ANCOVA was not given, therefore the Greenhouse-Geisser corrected values are reported for the frequency analysis.

3.2.2.1 Dynamic Compression

The two different compression offsets 800 N and 1000 N (ID12 and ID16, respectively, see Tab. 2-5) were compared using simple contrasts provided by the statistics software. Contrasts were also used to compare the three different amplitudes ±200 N, ±550 N and ±1000 N (ID14, ID16 and ID18, respectively, Tab. 2-5).

Apart from the data for the largest amplitude, all of the curves showed a clear positive linear relationship between frequency and the determined stiffness. Analogous to the quasistatic loading, the apparent stiffness c_{app} was generally smaller than the stiffness at high compression displacement c_{peak} and generally larger than the stiffness at low compression displacement $c_{initial}$. This was due to the strong non-linear deformation behaviour of the specimens in the compression direction. However, all three stiffness parameters were analysed.

In Fig. 3-23, c_{app} for different load patterns is shown depending on the frequency; AREA had no significant effect on the stiffness ($p = 0.231$). The stiffness level increased significantly with the increasing frequency ($p < 0.001$). The increase over frequency range was 19%. Apparent stiffness was significantly larger (by 21%) for 1000 N offset compared with 800 N offset ($p < 0.001$). Stiffness at 550 N amplitude was significantly smaller than at 200 N (by 9 %, $p = 0.045$) and again smaller at 1000 N amplitude by 30% ($p < 0.001$).

Fig. 3-24 shows the results for c_{peak} for different load patterns depending on the frequency. C_{peak} increased significantly with the increasing frequency ($p < 0.001$). The increase over frequency range was 17%. c_{peak} was significantly larger for an offset of 1000 N (by 11%) compared with an offset of 800 N ($p = 0.038$). Stiffness at 550 N amplitude did not differ significantly from 200 N ($p = 0.513$) or 1000 N amplitude ($p = 0.847$). AREA had no significant effect ($p = 0.122$).

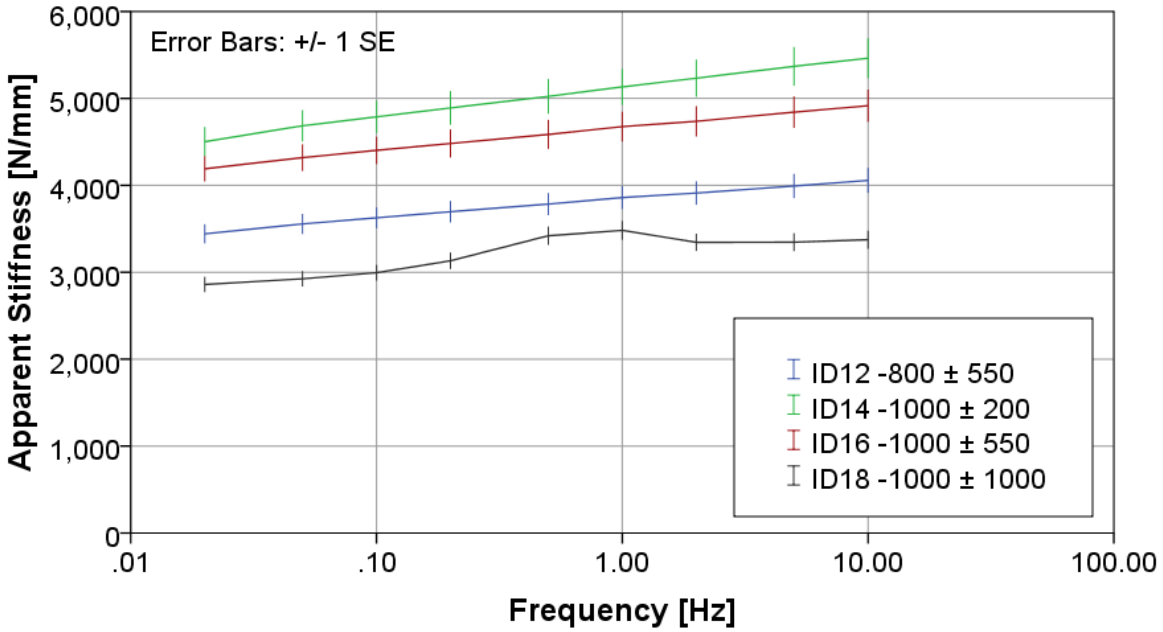

Fig. 3-23 Apparent stiffness depending on frequency and axial load pattern.

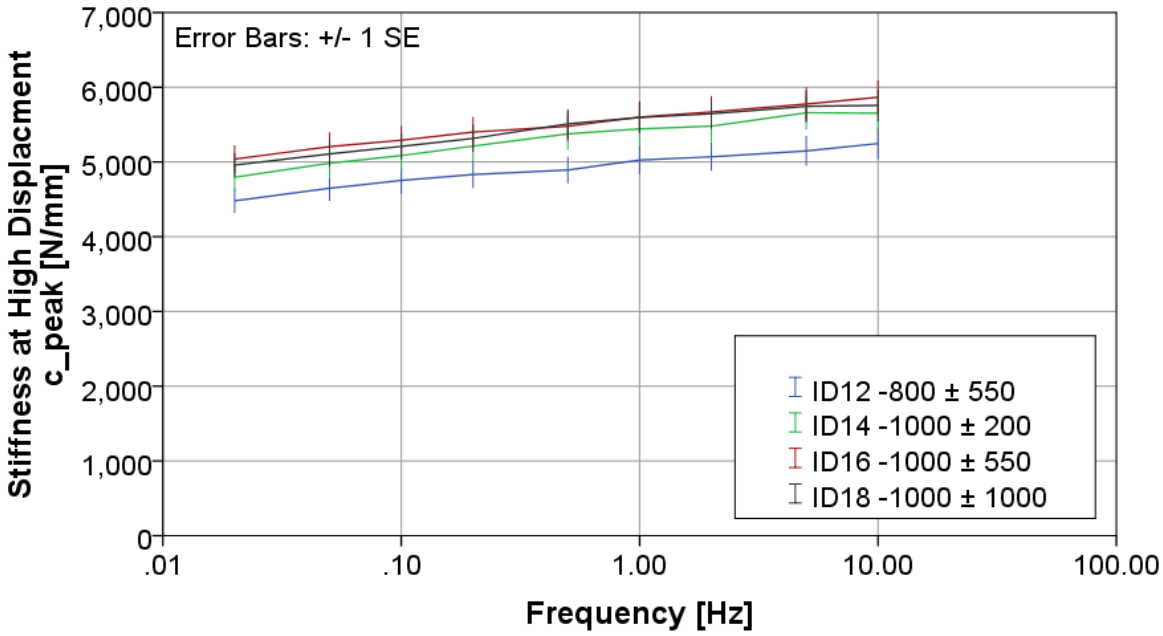

Fig. 3-24 Stiffness at high compression displacement c_{peak} depending on frequency and load pattern.

Fig. 3-25 shows the results for $c_{initial}$ for different load patterns depending on the frequency. $C_{initial}$ increased significantly with the increasing frequency ($p < 0.001$). The increase over frequency range was 16%. $c_{initial}$ was significantly larger (by 38%) for an offset of 1000 N compared with an offset of 800 N ($p < 0.001$). Stiffness at 550 N amplitude was significantly smaller than 200 N (by 22%, $p < 0.001$) and again smaller at 1000 N amplitude by 68% ($p < 0.001$). AREA had no significant effect ($p = 0.45$).

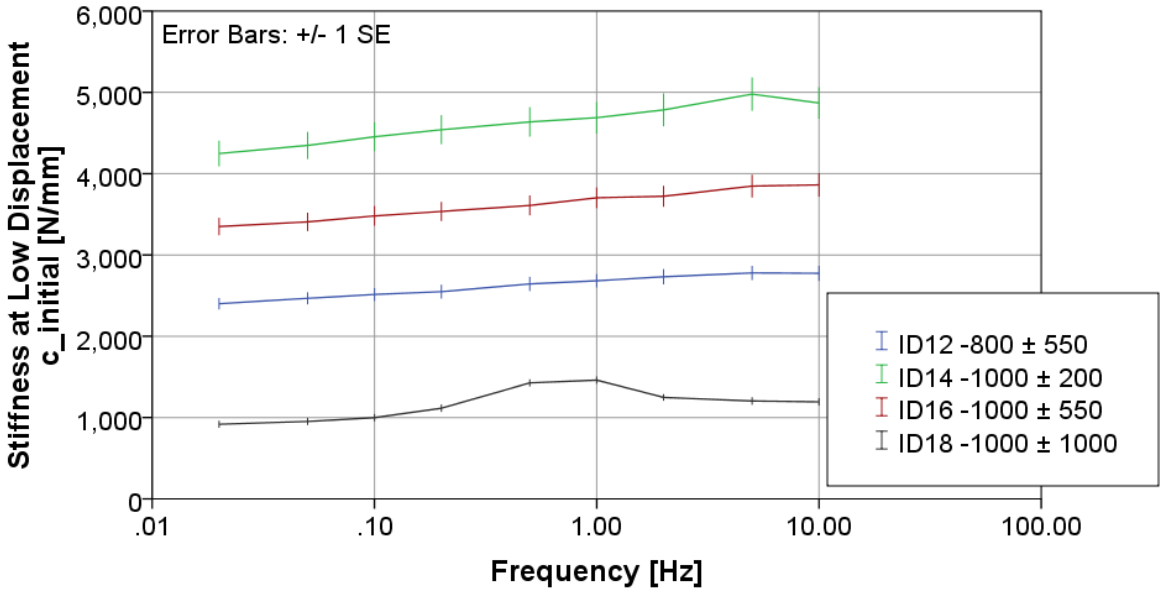

Fig. 3-25 Stiffness at low compression displacement depending on frequency and load pattern.

3.2.2.2 Dynamic Shear

Shear load patterns covered 0 N, 100 N (anterior) and -100 N (posterior) offsets (ID21, ID24 and ID30, see Tab. 2-5). Analogous to the compression direction, predefined contrasts of the statistical software were used for the analysis. The two amplitudes 50 N and 200 N (ID28 and ID30, see Tab. 2-5) were analysed in the same way.

All the data curves showed a clear positive linear relationship between frequency and the determined stiffness in the shear direction. Analogous to the quasistatic loading, the apparent stiffness c_{app} is generally larger than the stiffness at posterior shear displacement c_{post} and generally smaller than the stiffness at anterior shear displacement c_{ant}. As in the compression direction, this was due to the strong non-linear deformation behaviour of the specimens in the shear direction. However, all three stiffness parameters were analysed.

In Fig. 3-26, c_{app} for different load patterns is shown depending on the frequency. The stiffness level increased significantly with the increasing frequency ($p < 0.001$). The increase over frequency range was 25%. The difference between the two amplitudes at posterior offset was not significant ($p = 0.092$). Stiffness at posterior offset was 17% smaller than around 0 N, however, this difference was not significant ($p = 0.09$). Stiffness at anterior offset was significantly larger by 28% than stiffness of around 0 N ($p < 0.007$).

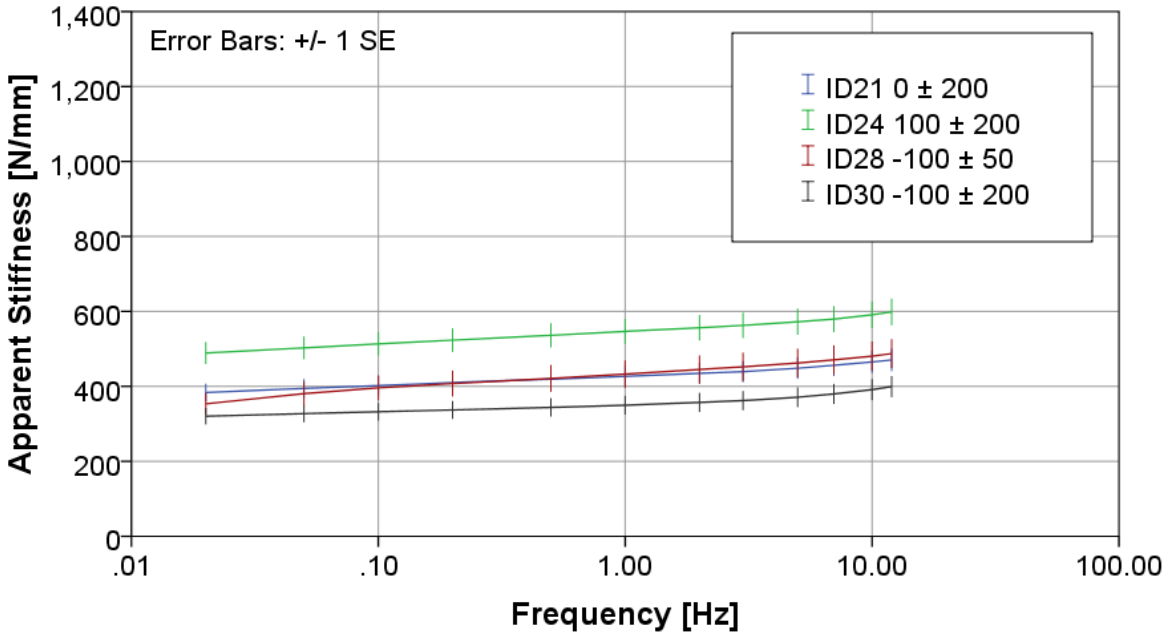

Fig. 3-26 Apparent stiffness depending on frequency and shear load pattern.

Fig. 3-27 shows c_{ant} for different load patterns depending on the frequency. The stiffness level increased significantly with the increasing frequency ($p < 0.001$). The increase over frequency range was 23%. A larger amplitude at posterior offset had no detectable effect on the posterior stiffness ($p = 0.945$). Stiffness at posterior offset was smaller by 22% than at around 0 N ($p = 0.006$). Stiffness at anterior offset was significantly larger by 21% than stiffness of around 0 N ($p = 0.009$).

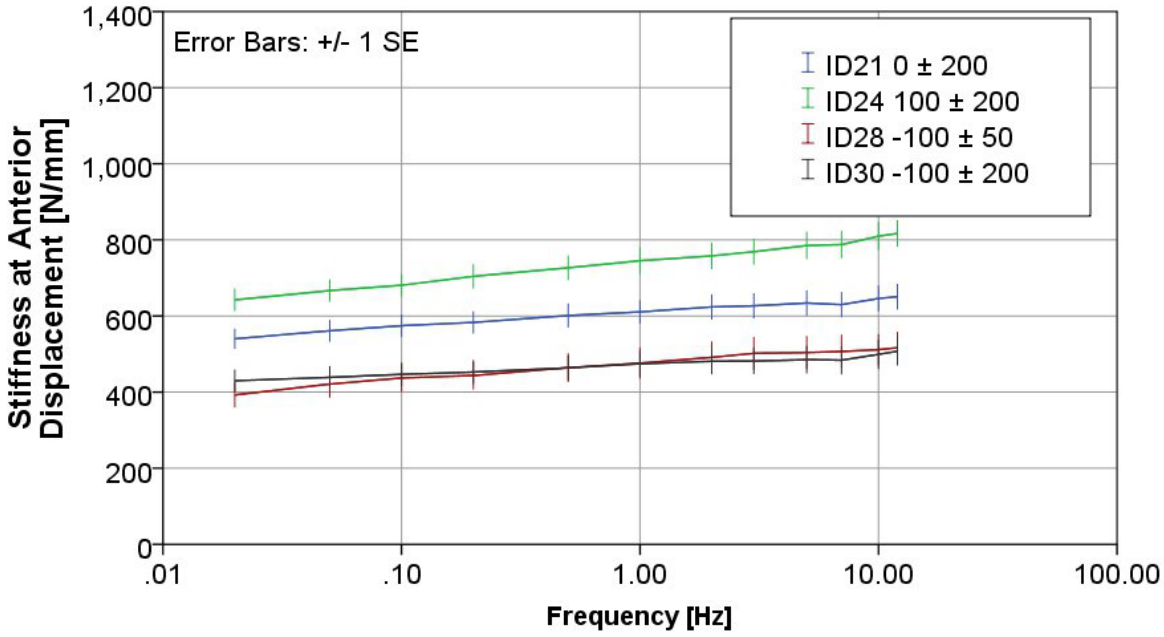

Fig. 3-27 Stiffness at anterior displacement depending on frequency and load pattern.

Fig. 3-28 shows c_{post} for different load patterns depending on the frequency. The stiffness level increased significantly with the increasing frequency ($p < 0.001$). The increase over the frequency range was 27%. A larger amplitude at posterior offset

resulted in a 20% smaller stiffness, however, this was not significant (p = 0.073). Stiffness at posterior offset was in the same range as around 0 N (p = 0.963). Stiffness at anterior offset was significantly larger by 29% than stiffness of around 0 N (p = 0.031).

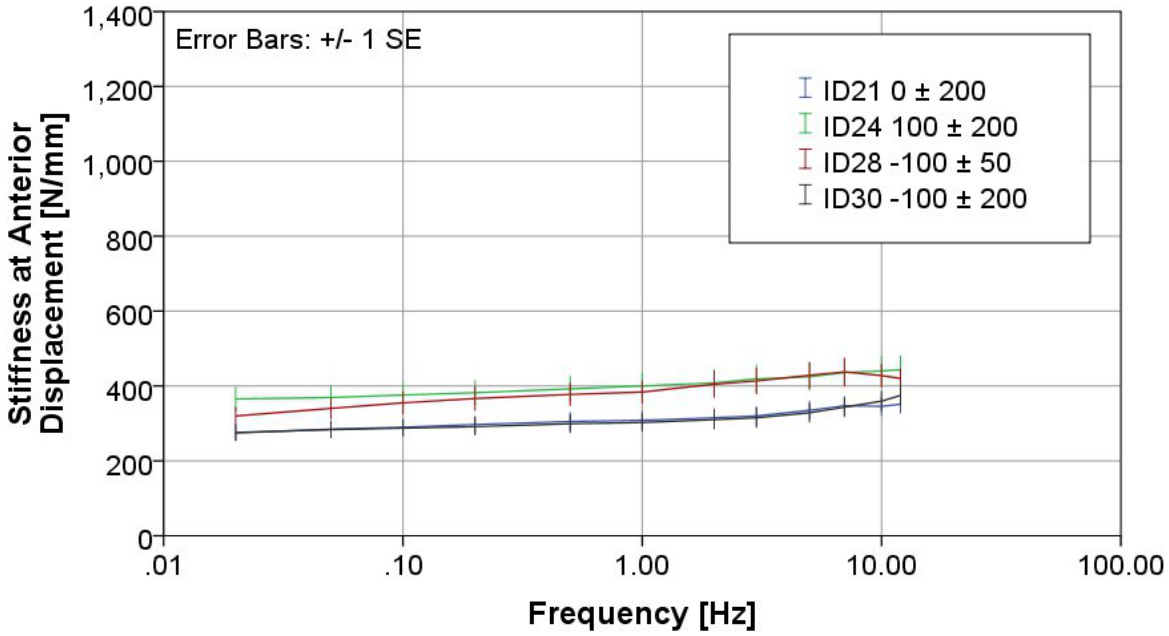

Fig. 3-28 Stiffness at posterior displacement depending on frequency and load pattern.

3.2.3 Reference During Parameter Measurements

Quasistatic reference measurements covered ramp compression load with an offset of -1000 N and an amplitude of ±1000 N at a frequency of 0.005 Hz. The analysis of this focuses on the apparent stiffness (c_{app}). The two-way ANCOVA with the donor group and load ID as factors and AREA as a covariate were used. The load IDs before testing (ID01ref1), after quasistatic testing (ID01ref2) and after preconditioning (ID33), were compared by using repeated contrasts.

In Fig. 3-29, the apparent stiffness at three different stages during parameter measurements is displayed. A significant effect was detected for both load ID and donor group (p < 0.012). The covariate AREA had no significant effect on thestiffness (p = 0.985). Stiffness after quasistatic preconditioning was significantly larger by 14% than stiffness before testing (p = 0.005). After the parameter measurements (quasistatic and dynamic) were completed, the stiffness was again increased by 6%, however, this was not significant (p = 0.092). There was no significant difference between the two male donor groups (p = 0.103). However, the stiffness of the female specimens was significantly smaller by 13% than the stiffness of the Midlife Male group (p = 0.003).

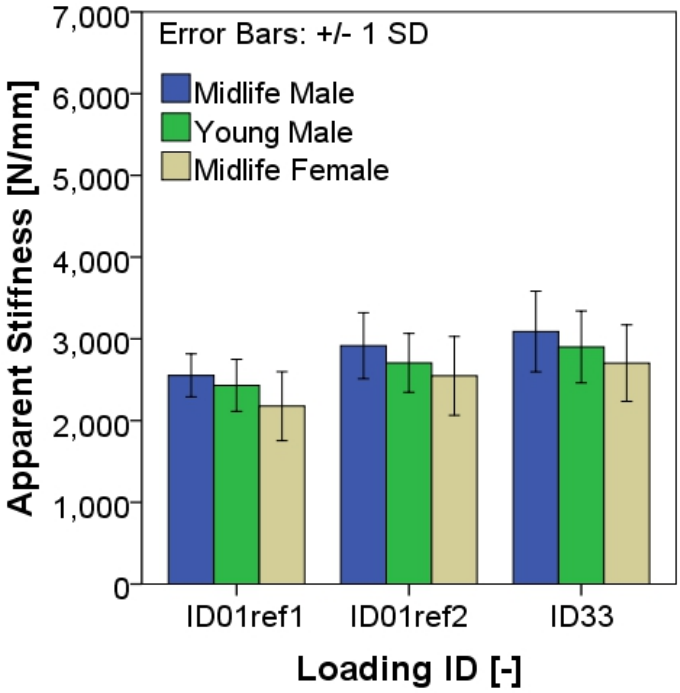

Fig. 3-29 Apparent stiffness during compressive quasistatic load at the beginning of testing (ID01ref1), after quasistatic testing (ID01ref2) and after preconditioning (ID33) for the three donor groups (Midlife Male, Young Male and Midlife Female).

The dynamic reference measurements covered a sinusoidal compression load of -800±550 N. The analysis of the dynamic reference measurements was done by a Repeated measure three-way ANCOVA. Besides donor group and load ID as factors and AREA as a covariate, the loading frequency is included as an additional repeated factor. The following analysis concentrates on changes in stiffness over a frequency range of 0.02 to 10 Hz. Test frequencies 3, 7, and 12 Hz were excluded to achieve logarithmically almost equidistant measuring points for the statistical analysis (0.02, 0.05, 0.1, 0.2, 0.5, 1, 2, 5, 10 Hz). The load IDs before testing (ID12ref1), after quasistatic testing (ID12ref2) and after parameter measurements (ID34) were compared by using repeated contrasts provided by the statistics software.

In Fig. 3-30, the apparent stiffness c_{app} measured during dynamic loading at three different preconditioning stages is displayed over the frequency. A significant effect was detected for the load ID ($p < 0.001$). However, the effect of the donor group was not significant here ($p = 0.076$) and neither was the covariate AREA ($p = 0.778$). Dynamic stiffness after quasistatic preconditioning was significantly larger by 15% than stiffness before testing ($p = 0.005$). After completed preconditioning (quasistatic and dynamic), stiffness was again increased by 6%, however, this was not significant ($p = 0.161$). There was no significant difference between the two male donor groups ($p = 0.059$) or between the Midlife Female specimens and the Midlife Male ones ($p = 0.051$).

The pooled stiffness level increased significantly with the increasing frequency ($p < 0.001$). The increase over the frequency range was 18%.

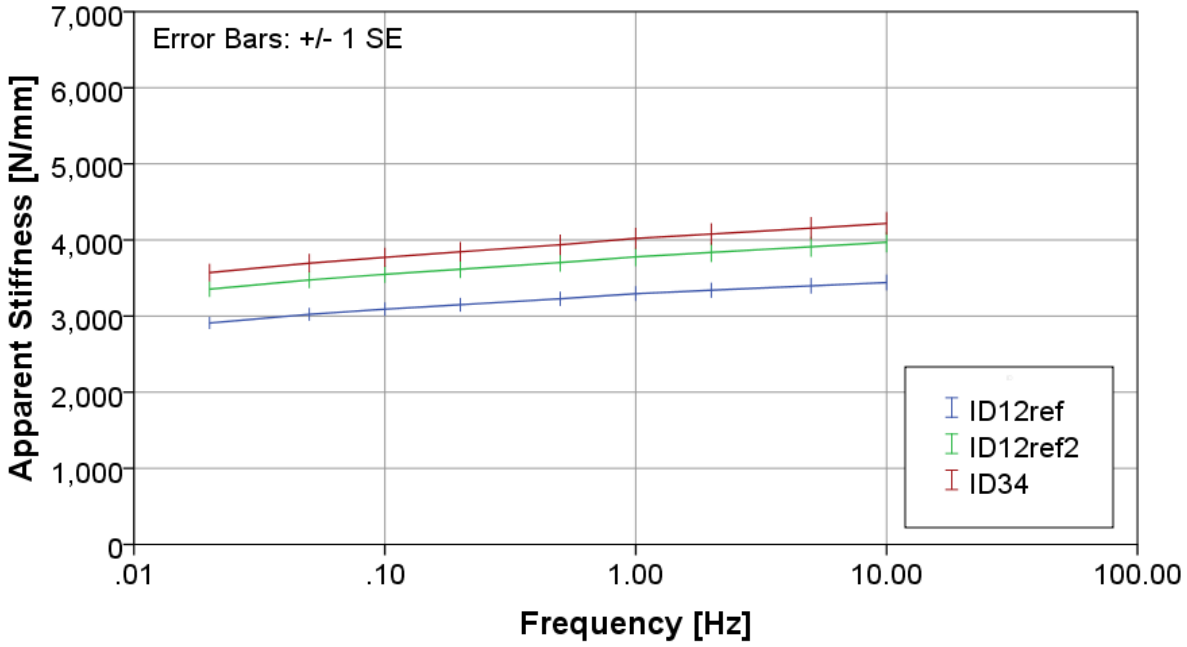

Fig. 3-30 Dynamic apparent stiffness during compressive dynamic load before testing (ID12ref1), after quasistatic testing (ID12ref2) and after preconditioning (ID34) over frequency.

3.2.4 Influence of Preparation Procedure

The long testing time, including preparation, made it necessary to test two FSUs from one spine on two subsequent days. The second FSUs had to be kept refrigerated for 24 hours. To verify that no alteration of the mechanical behaviour of the FSUs occurred during storage, a one-way ANOVA was carried out by analysing the quasistatic and dynamic stiffness at initial compression displacement ($c_{initial,stat}$ at 0.005 Hz; $c_{initial,dyn}$ at 5 Hz) of the first reference measurement. No significant difference was detected between the stored FSU and the one that was embedded and tested immediately after thawing ($c_{initial,stat}$: $p = 0.428$, $c_{initial,dyn}$: $p = 0.844$).

During preparation, minor superficial cuts were observed at the anterior longitudinal ligament of most of the specimens (Fig. 3-31). These cuts occurred during explantation. It turned out that withdrawal of the abdominal vessels is difficult to achieve without touching the anterior side of the lumbar spine with the dissection instrument.

After mechanical testing, all but one ligament exhibited conspicuous deformations or failure. Specimen FSU 3028 L2-L3 exhibited an undefined anterior longitudinal ligament after testing. However, it is assumed that the cuts did not influence the mechanical behaviour.

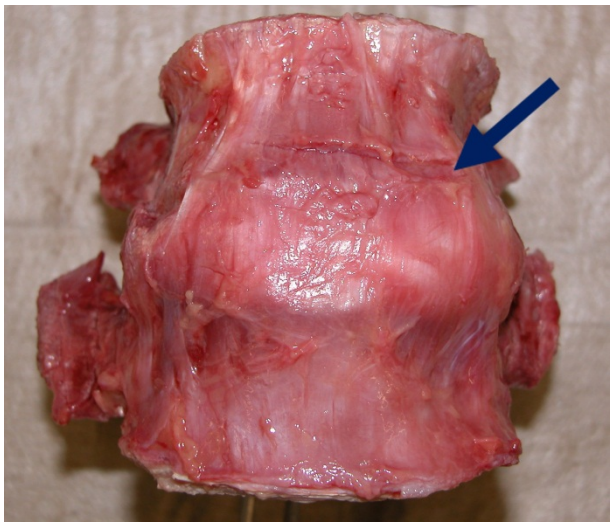

Fig. 3-31 Anterior superficial cut caused by explantation at FSU 3026 L4-L5 (arrow indicates cut).

3.3 Fatigue Measurements

In total, 36 fatigue measurements were performed. Two FSUs were excluded from the fatigue evaluation (as well as from parameter testing - as stated in chapter 0). Additionally, the fatigue results of 3001 L2-L3 (SHEAR) were excluded from the evaluation since the machine's displacement limit was set considerably lower than for the rest of the load group. The fact that this specimen did not fail could therefore not be included in the results.

The group characteristics for the different load groups result in the values shown in Tab. 3-13. The load group HIGH comprises the age groups Young and Midlife and is therefore referred to as HIGH (young) and HIGH (midlife). In Fig. 3-32, the mean Vertebral Capacity (VC) of the five load groups is also displayed. The groups HIGH (young) and SHEAR appear to have a higher mean value than the other groups. However, there was no significant difference between the mean AREA or the mean BMD of the five groups ($p > 0.38$, one-way ANOVA) and the same applied for the VC. Although a weak difference was detected by a one-way ANOVA ($p = 0.047$), direct comparison using a Scheffe post-hoc test did not show a significant difference ($p > 0.14$).

Tab. 3-13 Load group characteristics for the specimens included in the fatigue load experiments (mean ± standard deviation).

Load group	n	Age [years]	VC [$cm^2 \cdot mg\ K_2HPO_4$ / ml]
NORM	8	56.8 ± 3.1	1793.7 ± 386.5
OFFSET	7	57.7 ± 3.9	1727.0 ± 375.9
HIGH (young)	5	36.6 ± 4.1	2200.4 ± 330.3
HIGH (midlife)	8	55.5 ± 3.9	1922.1 ± 397.5
SHEAR	5	37.4 ± 3.7	2342.9 ± 409.3

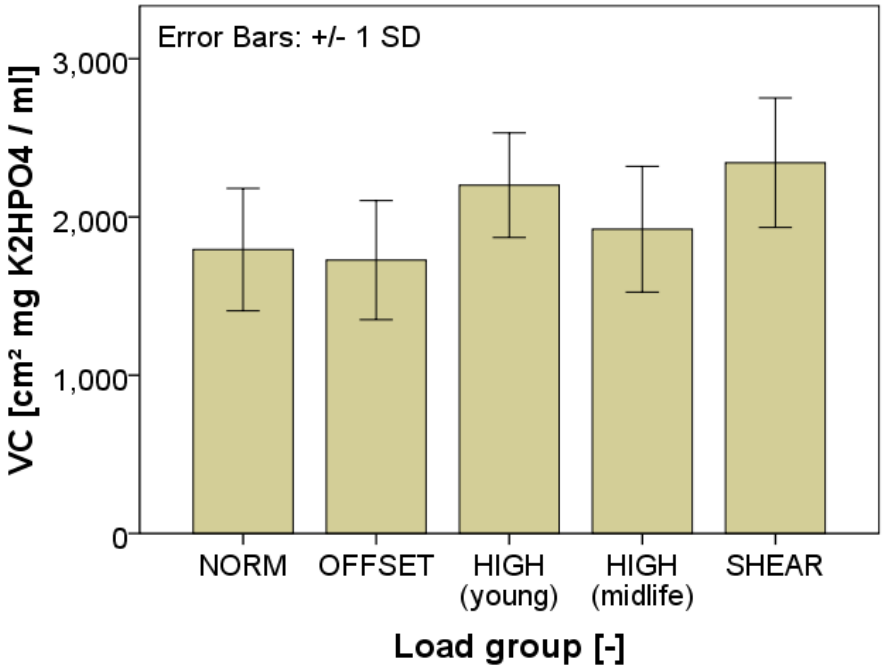

Fig. 3-32 Overview of the mean Vertebral Capacity (VC) of the five load groups involved in the fatigue experiments. The statistical analysis did not exhibit significant differences between the groups (n_{NORM} = 8, n_{OFFSET} = 7, $n_{HIGH,Young}$ = 5, $n_{HIGH,Midlife}$ = 8, n_{SHEAR} = 5).

3.3.1 Axial Compression

During axial fatigue testing, the cyclic sinusoidal compression (f = 5 Hz) was overlaid by the on-going creep of the FSUs. Severe change of the creep curve indicates the failure of a specimen. In Fig. 3-33, an exemplary creep (time displacement) curve of a specimen that failed after a few loading cycles is shown. Note that the gaps in the diagram result from the intermediate reference measurements.

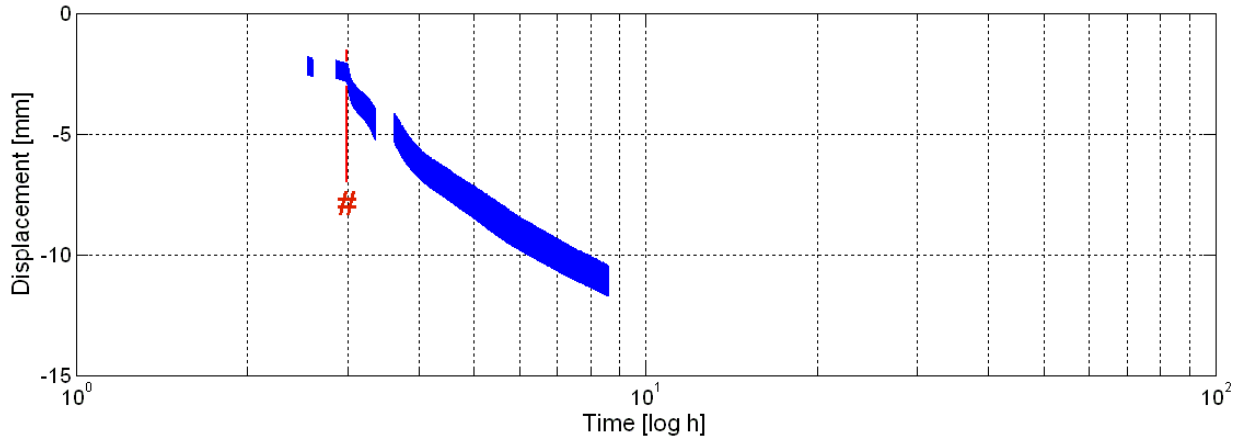

Fig. 3-33 Typical creep curve of failed specimen FSU 3013 L4-L5; failure at 3,286 cycles (# indicates failure).

Cycles to failure (N) were determined by two independent observers. Cases with a deviation of more than 10 % were reviewed. Linear regression showed high

reproducibility for failure cycle detection ($R^2 > 0.99$). The slope was not significantly different from 1 ($p > 0.634$, Fig. 3-34).

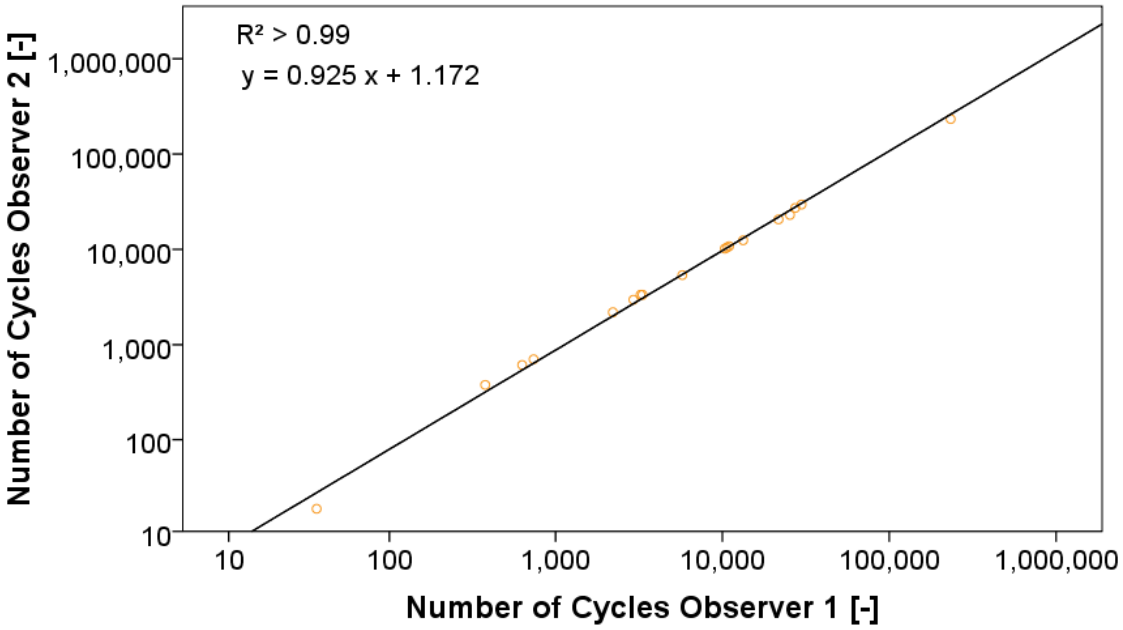

Fig. 3-34 Cycles to failure, linear regression between Observer 1 and Observer 2.

All apparently unfailed specimens were dissected to determine the extent of soft tissue impairment. They exhibited clefts in the disc and delamination of the annulus in most cases. Reversible indentation of the endplates of specimen 3017 L2-L3 was easier to achieve; this was most probably due to the underlying damage of the cancellous bone. The creep curve showed no pronounced failure. Therefore, the damage was classified as impairment primary to failure. With regard to specimen FSU 3001 L4-L5, the nucleus penetrated the cranial endplate locally. Again, no pronounced failure was observed in the creep curve; therefore, the specimen was classified as unfailed.

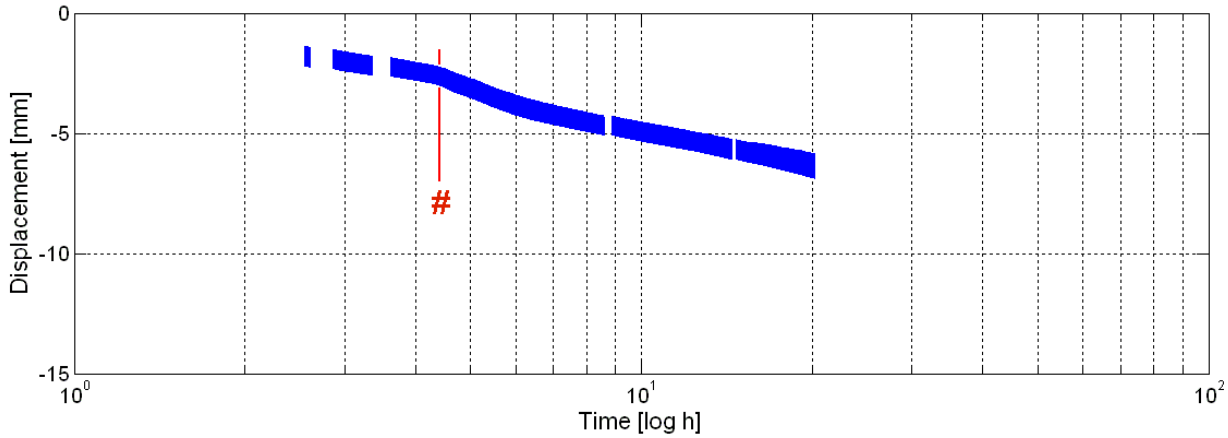

Fig. 3-35 Creep curve of FSU 3030 L4-L5 showing indistinct failure at 24,202 load cycles (# indicates failure).

In addition, one specimen with indistinct failure event in the creep curve was dissected (FSU 3030 L4-L5, Fig. 3-35), as well as one specimen with peculiarly late and relatively slow failure (FSU 3023 L4-L5, Fig. 3-36).

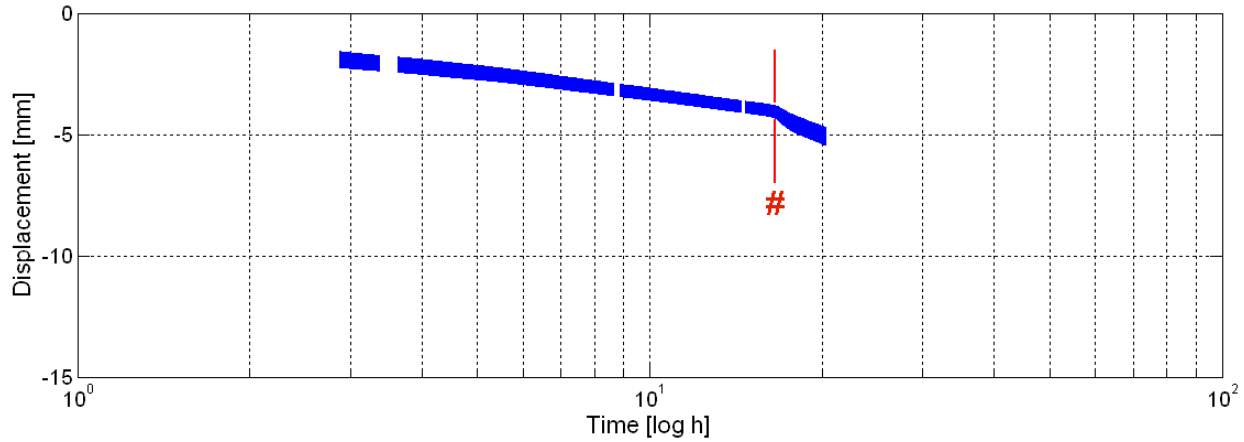

Fig. 3-36 Creep curve of FSU 3023 L4-L5 that failed at 233,120 load cycles (# indicates failure).

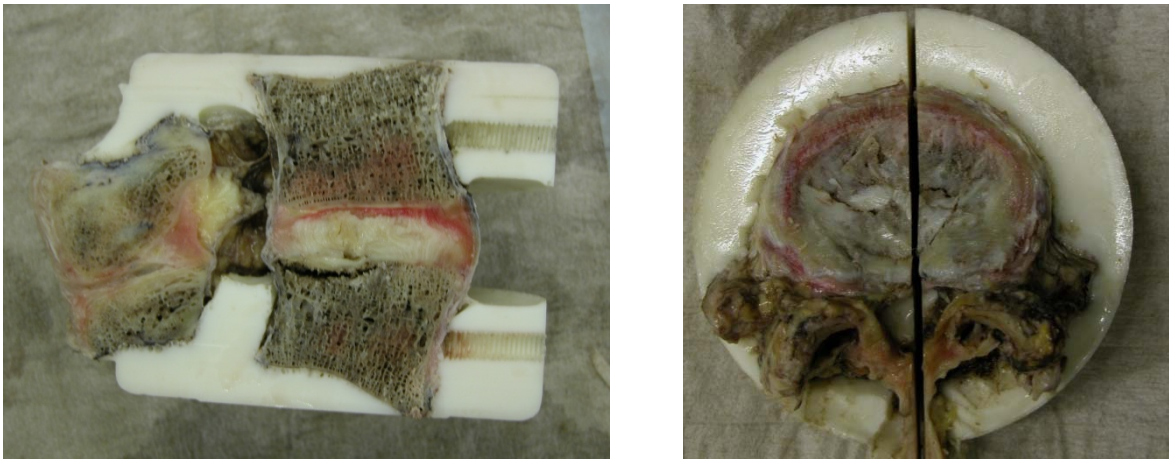

Fig. 3-37 Fractured endplate of FSU 3030 L4-L5: the left picture shows the transection along the mid-sagittal plane made for the Thompson grading; the right picture shows obvious clefts within the cranial endplate of the caudal vertebra.

With regard to the two dissected failed specimens, a fractured caudal endplate was found for FSU 3030 L4-L5 (Fig. 3-37), therefore the specimen was finally considered as failed.

In the case of FSU 3023 L4-L5, no distinct endplate fracture was found. Manual compression of the specimen revealed failure of the cancellous bone directly below the caudal endplate (Fig. 3-38). The cranial endplate showed poor resistance if indented. Although both endplates appeared to be intact (Fig. 3-39), the specimen was considered as failed due to the distinct failure event detected in the creep curve. This is the only specimen for which the creep curve failure criterion was fulfilled, although clear failure of the endplates has not been observed.

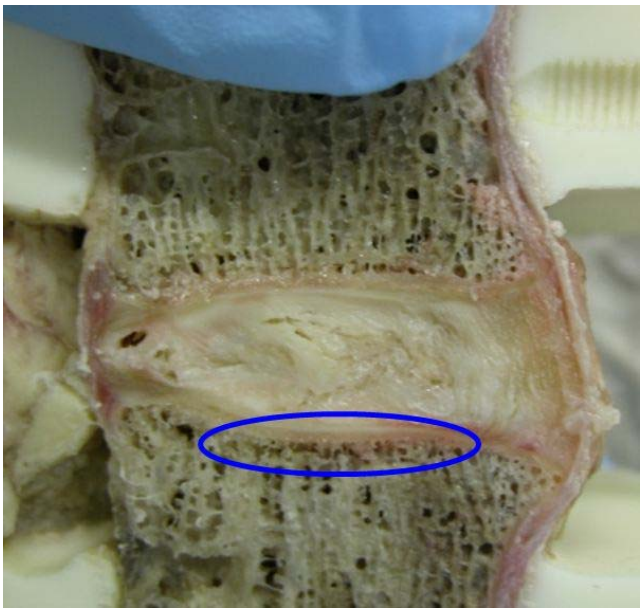

Fig. 3-38 Lateral view of sectioned specimen FSU 3023 L4-L5 under bending. The area with failure of the cancellous bone is marked.

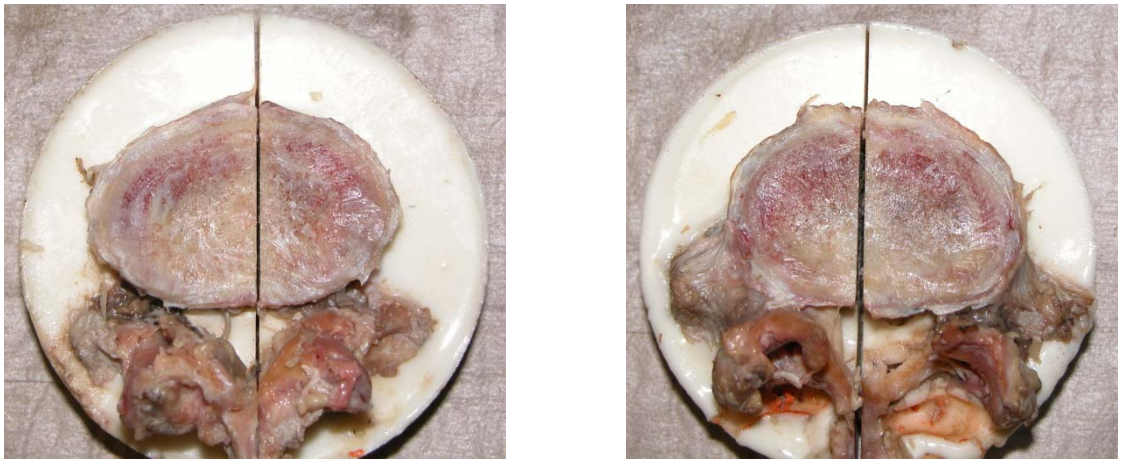

Fig. 3-39 Top view of the endplates of specimen FSU 3023 L4-L5: left: caudal endplate of L4; right: cranial endplate of L5.

The soft tissue of three additional specimens with clear discontinuity of the creep curve was completely dissected because the failing structure could not be identified from the mid-sagittal images of the Thompson grading (FSU 3004 L4-L5, FSU 3011 L2-L3 and FSU 3026 L2-L3). All three specimens showed failure of the endplate and cancellous bone.

One creep curve could not be clearly classified as a failure event (FSU 3031 L4-L5), but showed a small shift in the creep curve (Fig. 3-40). The specimen was carefully examined after the testing. Besides clefts within the disc (Fig. 3-41), no signs of failure could be detected and the specimen was therefore classified as a survivor – at least with respect to the bony structure.

In Fig. 3-42 to Fig. 3-44, the measured and expected failure cycles are displayed together with the expected failure line according to the model of Brinckmann et al. (1989) and Seidel et al. (2008). Generally, the measured values tend to be larger than the calculated values. The overall shape of the model's curves appears to be

appropriate. Actually, the prediction might be a conservative limit, even though the experimental uncertainties and limitations are still huge.

For alternative dependencies, like prediction of the number of cycles to failure depending on the corrected relative IVD height (Fig. 3-45), no obvious correlation could be found.

All of the specimens that underwent compression fatigue are listed in Tab. 3-14 with their corresponding failure cycles and mechanisms. Only the most obvious failures are listed. Endplate failure implies failure of the vertebral body and cancellous bone. Failure of the vertebral body refers to a clear fracture of the cortical bone.

The linear black box model to predict the logarithmised cycles to failure resulted in the following equation (p = 0.003, R^2 = 0.54):

$$\log(N_k) = 3.125 + VC \cdot 0.002 \cdot \frac{ml}{mgK2HPO4 \cdot cm^2} - F_{Amplitude} \cdot 0.002 \cdot \frac{1}{KN} \qquad \textbf{(3-1)}$$

R^2 is satisfying for the sample. Peak force (maximum absolute value out of offset and amplitude) does not contribute to the model

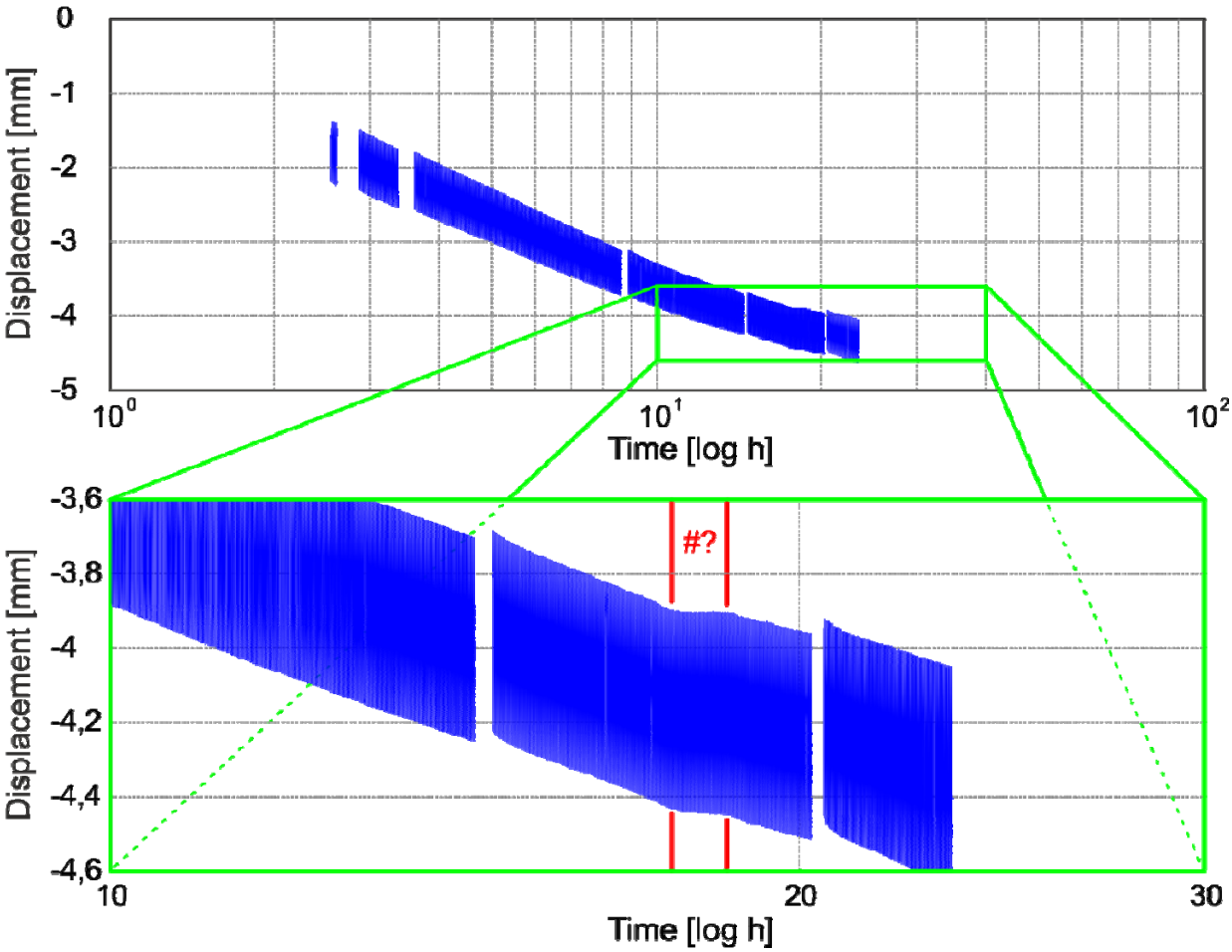

Fig. 3-40 Creep curve of specimen FSU 3031 L4-L5. A minor shift in the creep curve can be seen in the complete overview (top). Some discontinuities are visible in the magnification (bottom).

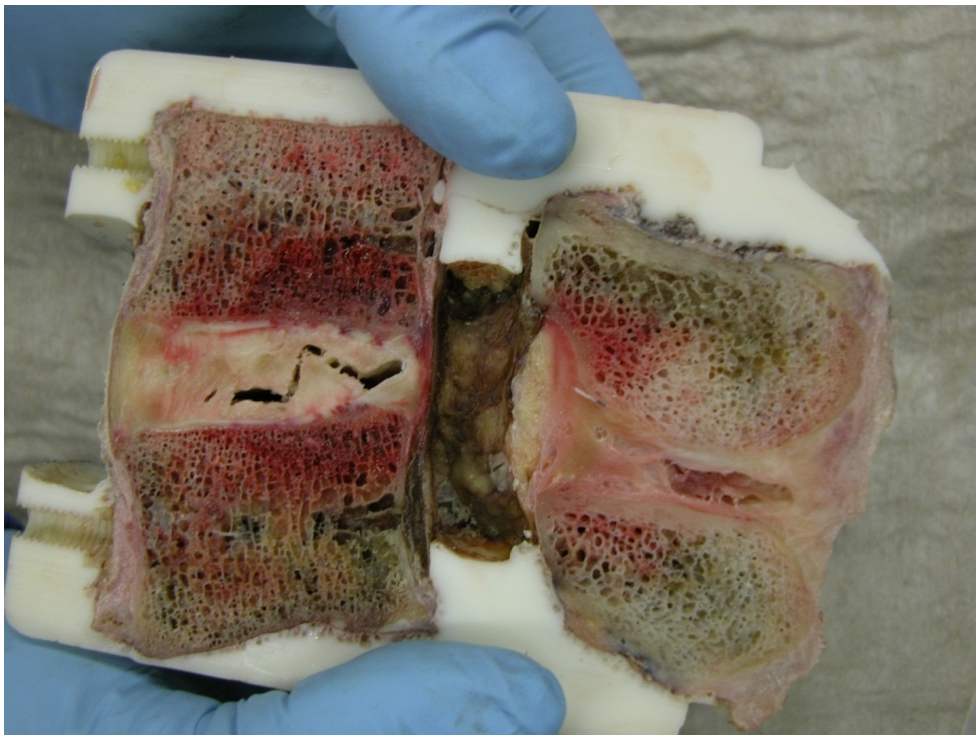

Fig. 3-41 Clefts visible within the disc of FSU 3031 L4-L5 if the separated specimen is bent.

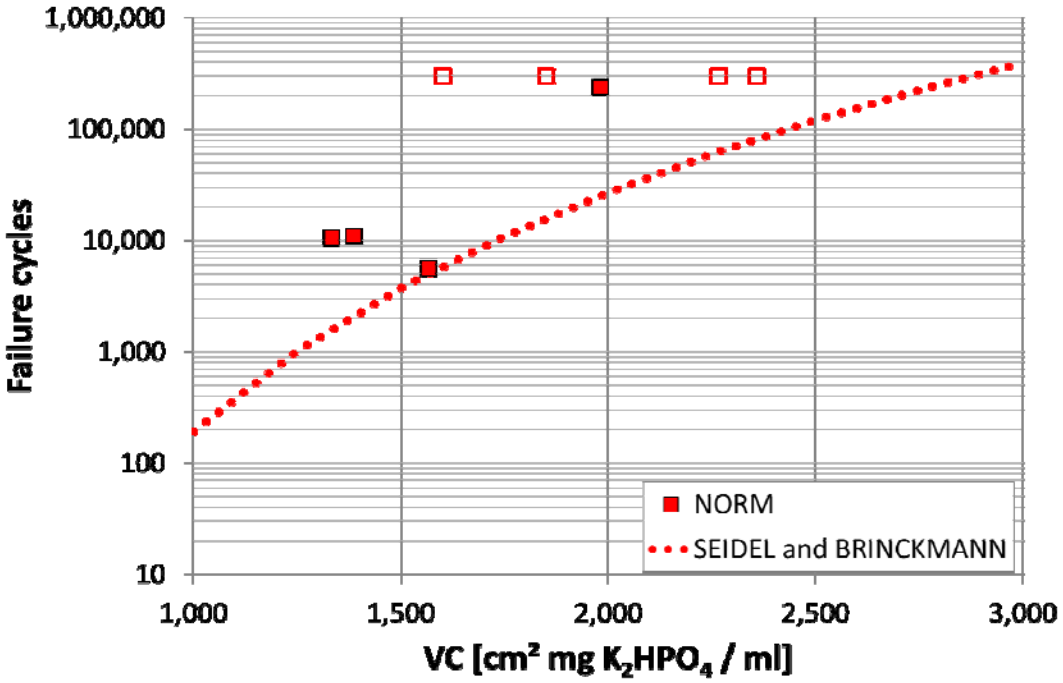

Fig. 3-42 Number of cycles to failure depending on the vertebral capacity of NORM loaded specimens. Unfilled markers represent specimens that did not fail within the number of cycles displayed; the dotted line represents the predicted failure cycles according to Seidel et al. (2008) and Brinckmann et al. (1989).

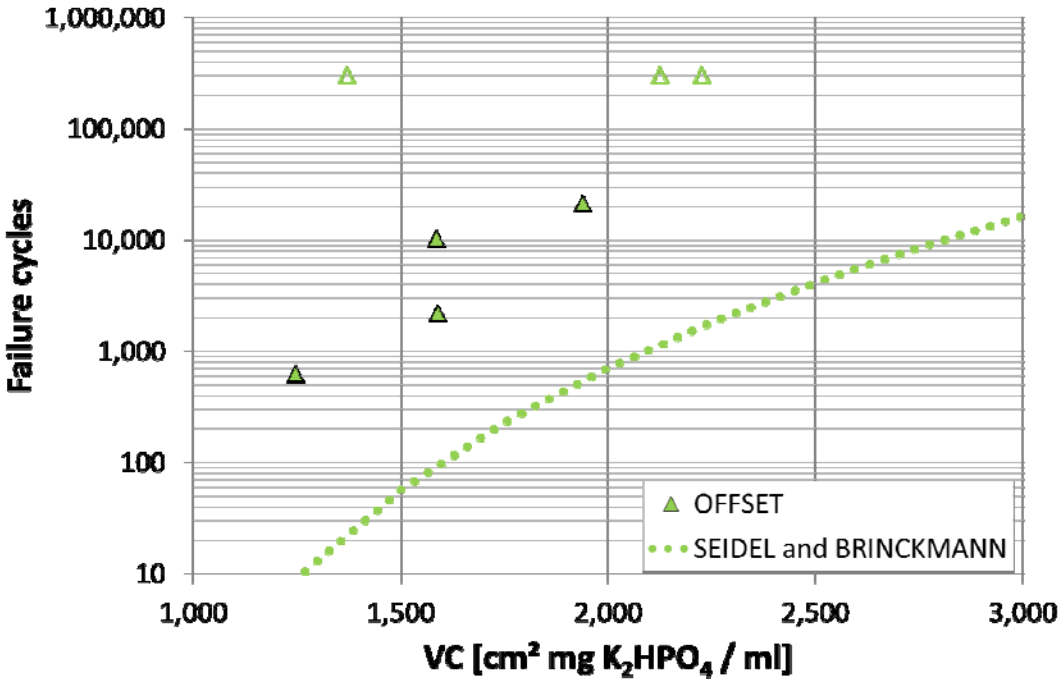

Fig. 3-43 Number of cycles to failure depending on the vertebral capacity of OFFSET loaded specimens. Unfilled markers represent specimens that did not fail within the number of cycles displayed; the dotted line represents the predicted failure cycles according to Seidel et al. (2008) and Brinckmann et al. (1989).

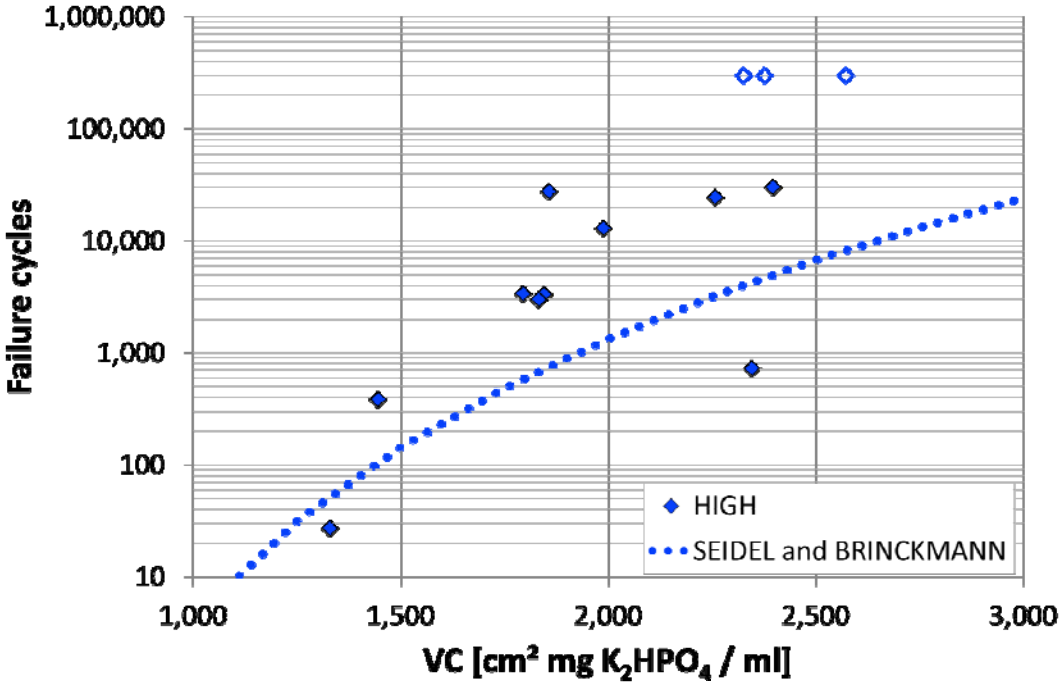

Fig. 3-44 Number of cycles to failure depending on the vertebral capacity of HIGH loaded specimens. Unfilled markers represent specimens that did not fail within the number of cycles displaced; the dotted line represents the predicted failure cycles according to Seidel et al. (2008) and Brinckmann et al. (1989).

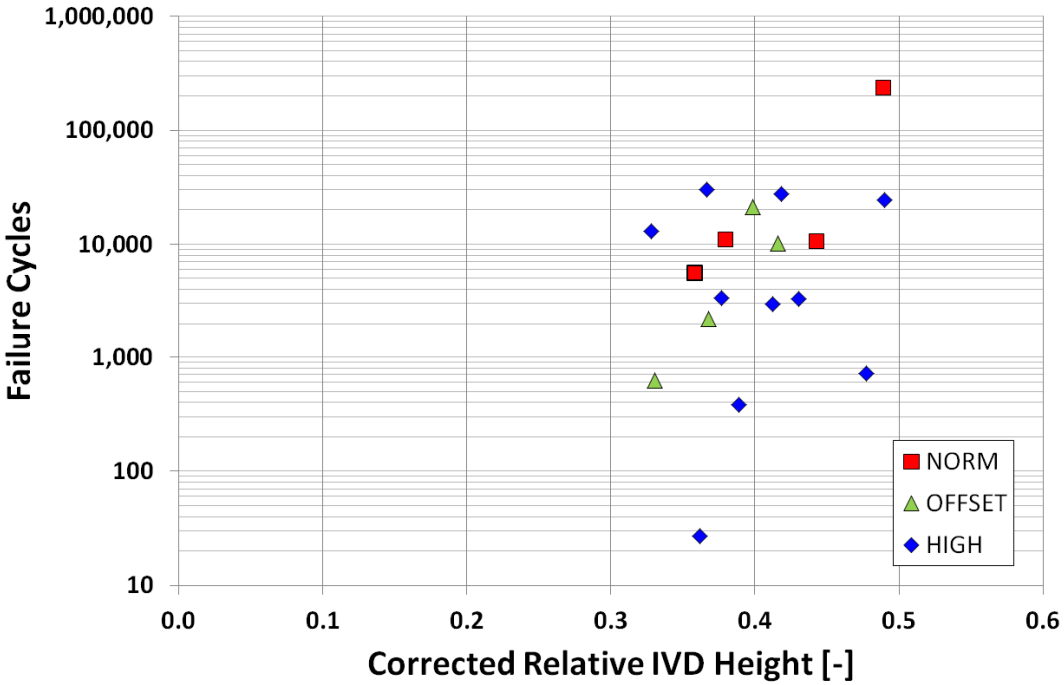

Fig. 3-45 For compressive fatigue loading, the number of cycles to failure shows poor dependency on the corrected relative IVD height for all failed specimens of the three groups.

Tab. 3-14 FSUs that underwent compression fatigue loading with cycles to failure and failure mechanism (Donor group: YM = Young Male, MM = Midlife Male, MF = Midlife Female).

Load group	ID	Level	Donor group	Failure cycles	Failure mechanism
NORM	3006	L4-L5	MM	-	-
	3009	L2-L3	MM	10,891	caudal endplate, cranial vertebral body
	3023	L4-L5	MM	233,120	sub-endplate cancellous bone
	3028	L2-L3	MM	-	-
	3011	L4-L5	MF	10,558	vertebral bodies
	3014	L2-L3	MF	5,563	caudal endplate, cranial vertebral body, penetration of cranial endplate by nucleus
	3017	L2-L3	MF	-	-
	3026	L4-L5	MF	-	-
OFFSET	3006	L2-L3	MM	21,151	cranial endplate
	3016	L4-L5	MM	-	-
	3030	L2-L3	MM	-	-
	3004	L2-L3	MF	621	caudal endplate and vertebral body
	3014	L4-L5	MF	10,261	caudal endplate and vertebral body
	3026	L2-L3	MF	2,197	cranial endplate
	3027	L4-L5	MF	-	-
HIGH	3001	L4-L5	YM	-	-
	3013	L4-L5	YM	3,286	caudal endplate, penetration of cranial endplate by nucleus, vertebral body
	3019	L2-L3	YM	27,253	caudal endplate, cranial vertebral body
	3031	L4-L5	YM	-	-
	3032	L2-L3	YM	29,710	penetration of caudal endplate by nucleus, vertebral body caudal
	3016	L2-L3	MM	12,889	caudal endplate
	3023	L2-L3	MM	3,331	caudal endplate, cranial vertebral body
	3028	L4-L5	MM	-	-
	3030	L4-L5	MM	24,202	caudal endplate
	3004	L4-L5	MF	378	caudal endplate, cranial cancellous bone
	3011	L2-L3	MF	27	caudal endplate, cranial cancellous bone
	3017	L4-L5	MF	720	caudal vertebral body, sub-endplate caudal and cranial cancellous bone
	3018	L2-L3	MF	2,944	caudal endplate, cranial vertebral body

3.3.2 Shear

Five out of six specimens tested in the shear mode failed according to the failure criteria (discontinuity of creep curve). In the case of unfailed FSU 3001 L2-L3, the displacement limit was initially set to 10 mm for technical reasons and was therefore reached before failure occurred. After analysing this first fatigue curve, the test setup was changed to enable a limit of 18 mm. Therefore, FSU 3001 L2-L3 was excluded from the statistical analysis, but was analysed with regard to the failure mechanism.

The peak-to-peak displacement value at the beginning of the fatigue loading was between 2 mm and 3 mm. In some cases, failure was accompanied by an increase in anterior displacement. Either there was an increase in peak-to-peak displacement (minor event: discontinuity of peak-to-peak displacement) or an increase in the level of displacement (major event: discontinuity of creep curve). The displacement diagrams of the failed specimens (Appendix 5.3) showed two or more changes of this kind. In Fig. 3-46, a typical shear failure curve with the failures marked as 1, 2 and 3 is displayed.

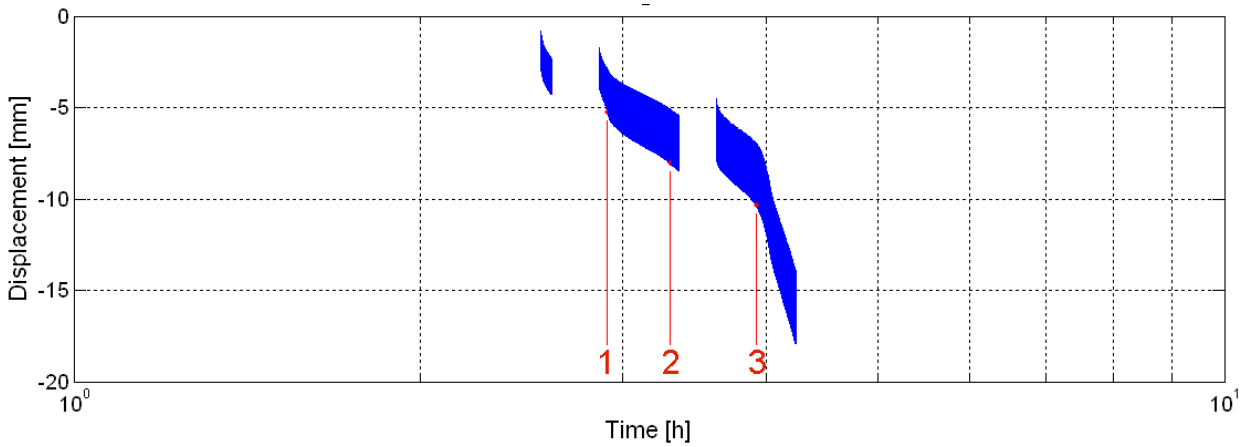

Fig. 3-46 Fatigue displacement (FSU 3032 L4-L5): marks 1 and 2 indicate minor failures; mark 3 indicates the major and final failure.

Post-test X-rays, CTs and dissection revealed a separation of the annulus from the endplates (delamination) in all the cases of failure (Fig. 3-47 and Fig. 3-48). For FSU 3001 L2-L3, disc delamination was revealed during post-test preparation.

While the anterior longitudinal ligament appears intact in all cases, the posterior ligament was partly detached in four cases. Detachment was defined as a visible or exposed gap between the vertebral bodies and ligaments (Fig. 3-49).

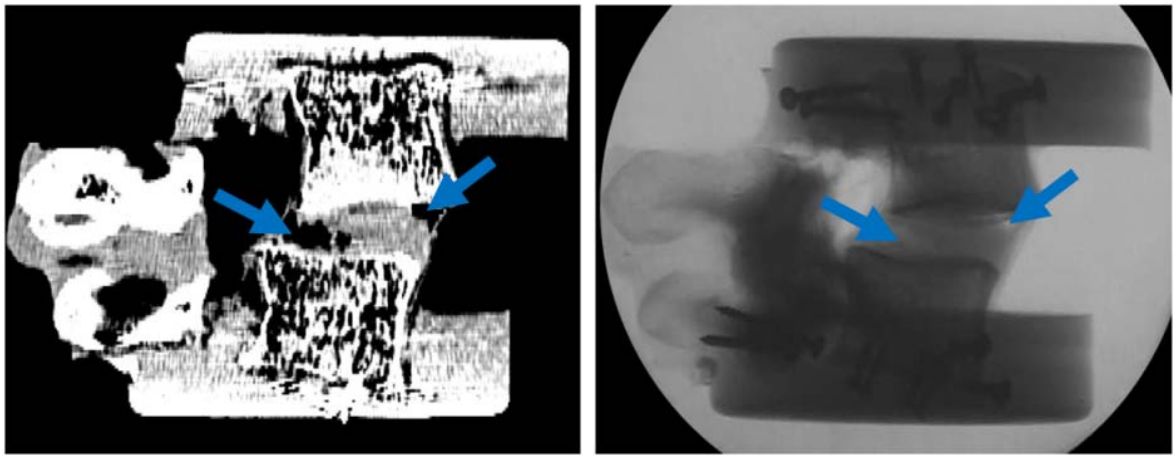

Fig. 3-47 Example of X-ray (left) and CT scan (right) showing disc luxation at FSU 3021 L4-L5 (arrows indicate detachment).

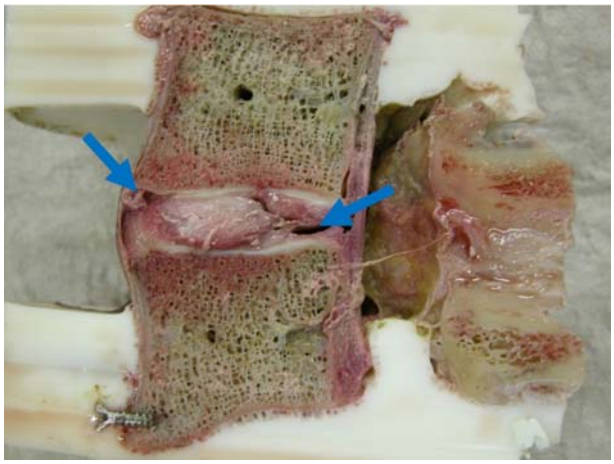

Fig. 3-48 Visible disc luxation at FSU 3021 L4-L5 (the arrows indicate detachment). This is one of the photos taken during dissection.

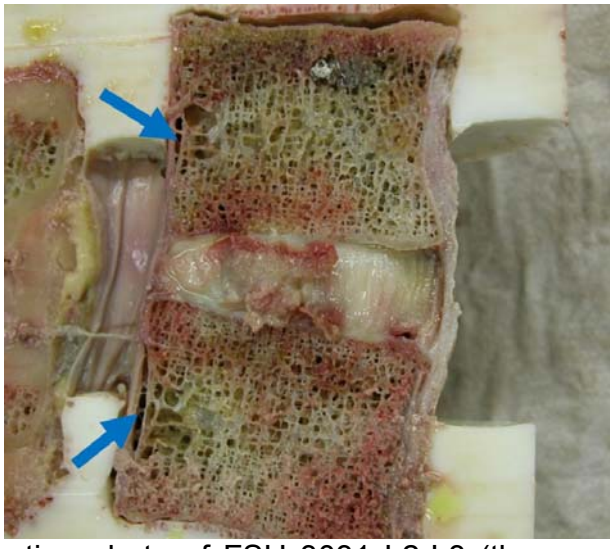

Fig. 3-49 Dissection photo of FSU 3031 L2-L3 (the arrows indicate detached posterior longitudinal ligament). The cranial vertebra was disconnected from the embedding resin.

Failure of the bony posterior elements was exclusively apparent for FSUs with a major failure event in the creep curve. Fractures were rather indistinct in the X-rays due to the superimposing complex structure. The CT scans were used to reconstruct the 3D models. The fractures were clearly visible (Fig. 3-50), however, the fracture edges in the 3D model were distorted by segmenting and smoothing during numerical processing. In the end, only an examination of the facet joints and pedicles during dissection gave clear results of participation of the facet joint bearing area (Fig. 3-51).

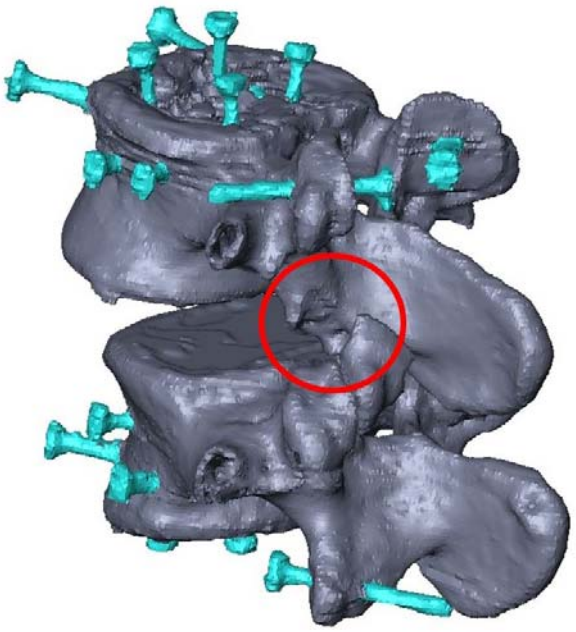

Fig. 3-50 3D model of FSU 3007 L4-L5 with marked fracture of the posterior elements. In addition, the positions of the screws to improve potting are visible.

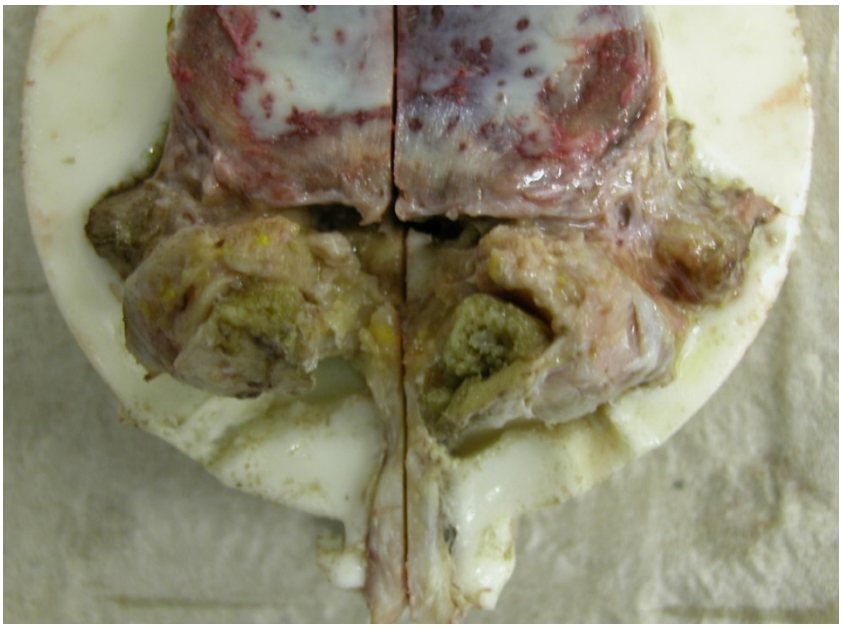

Fig. 3-51 Fracture of the posterior elements of FSU 3007 L4-L5. Top view of L5 shows participation of the joint bearing area.

Another occurrence detectable in the displacement diagrams is loosening of the fixation. All but one specimen were slightly moved out of the fixation because the fixation screws were pulled out of the bone. Loosening of the fixation can be seen on the CT scans during post-test preparation (Fig. 3-53 and Fig. 3-53).The latter gives a better understanding of the possible secondary damages because the specimen can be manually stressed. In one case, the vertebral body was slightly damaged at the edge of the embedding material (FSU 3032 L4-L5). In Tab. 3-15, all six specimens for which failure was observed are listed in detail.

Fig. 3-52 CT scan displaying successful fixation (FSU 3021 L4-L5).

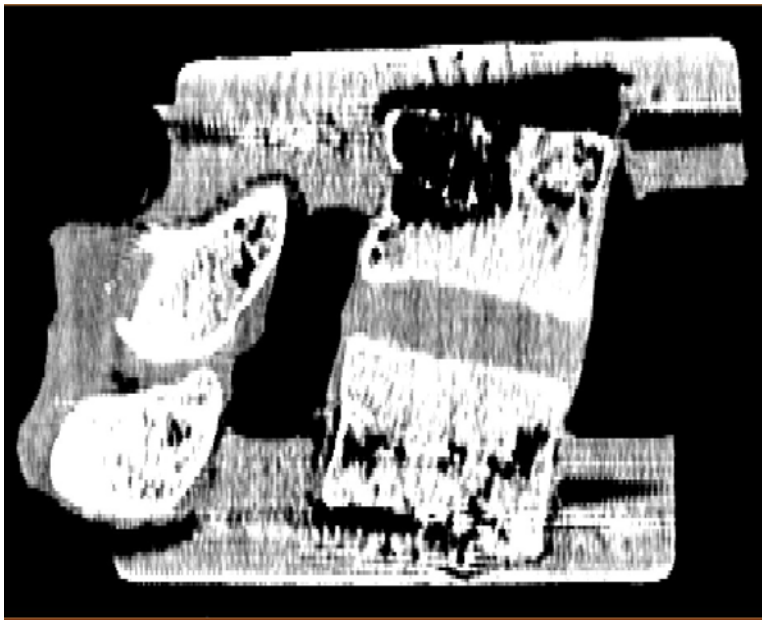

Fig. 3-53 CT scan showing fixation pull-out (FSU 3032 L4-L5).

Tab. 3-15 Observed failure of shear loaded specimens ('loose fixation' corresponds to apparent relative movement between resin and vertebral body).

FSU	Failure criterion	Disc	Posterior longitudinal ligament	Posterior bony elements	Fixation
3001 L2-L3	not failed	detached	intact	intact	loose
3007 L4-L5	failed	delamination	partly detached	fractured	loose
3012 L2-L3	failed	delamination	partly detached	fractured	loose
3021 L4-L5	failed	delamination	partly detached	fractured	intact
3031 L2-L3	failed	delamination	partly detached	fractured	loose
3032 L4-L5	failed	delamination	intact	fractured	loose

In Fig. 3-54, the failure cycles of the first major failure of all the specimens failed in anterior shear fatigue is displayed over the VC. Linear regression resulted in R^2 = 0.003 and was not significant ($p = 0.93$, $\alpha = 0.05$). An exponential regression with the corrected relative IVD height was likewise also not significant, however, it indicated a relation ($p = 0.131$, $R^2 = 0.59$, Fig. 3-55).

In Tab. 3-16, the number of cycles at which the failure events occurred is given. The corresponding creep diagrams can be found in Appendix 5.3.

Tab. 3-16 Averaged shear failure cycles of the FSUs tested in SHEAR mode; numbers in bold indicate major failures (discontinuity of creep curve); numbers in normal letters indicate minor failures (discontinuity of peak-to-peak displacement).

FSU	1st event	2nd event	3rd event	4th event	5th event
3001 L2-L3	3,887	-	-	-	-
3007 L4-L5	**30,137**	35,349	**38,091**	-	-
3012 L2-L3	**798**	1,306	1,812	-	-
3021 L4-L5	4,725	5,261	5,736	**6,566**	**7,139**
3031 L2-L3	20,209	24,906	**27,556**	-	-
3032 L4-L5	1,863	8,818	**15,347**	-	-

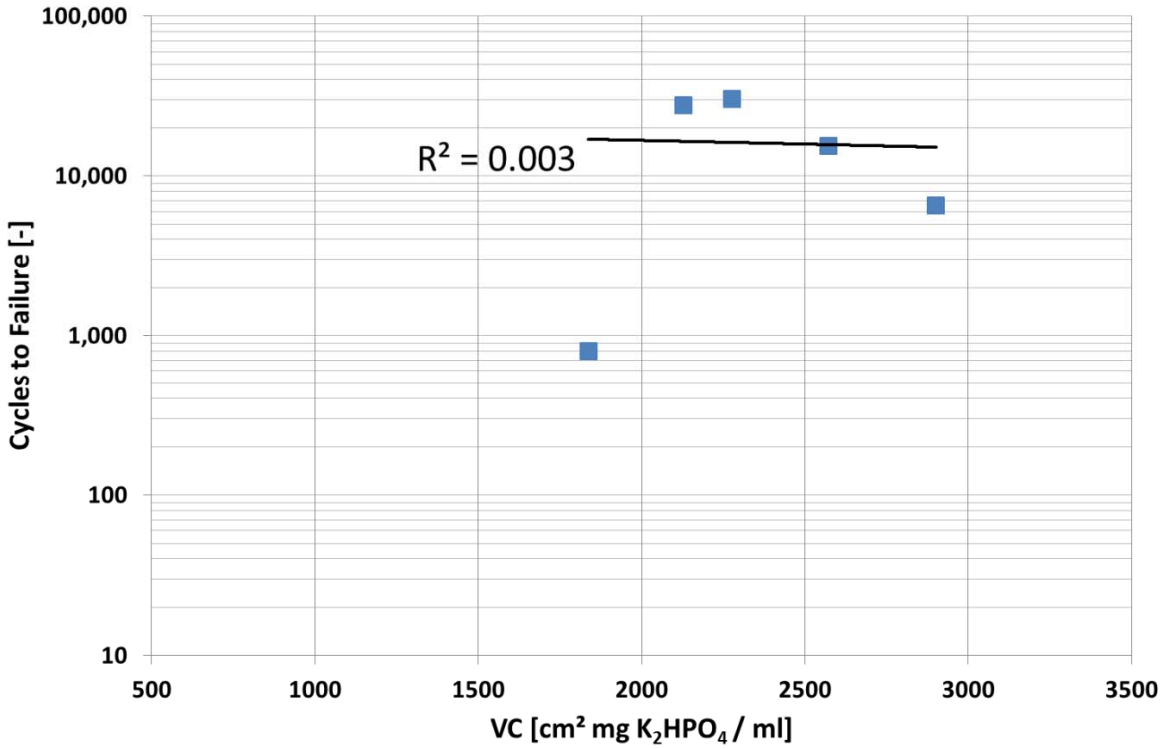

Fig. 3-54 Failure cycles of the first major failure of all specimens failed in anterior shear fatigue displayed over the VC (regression curve p = 0.93).

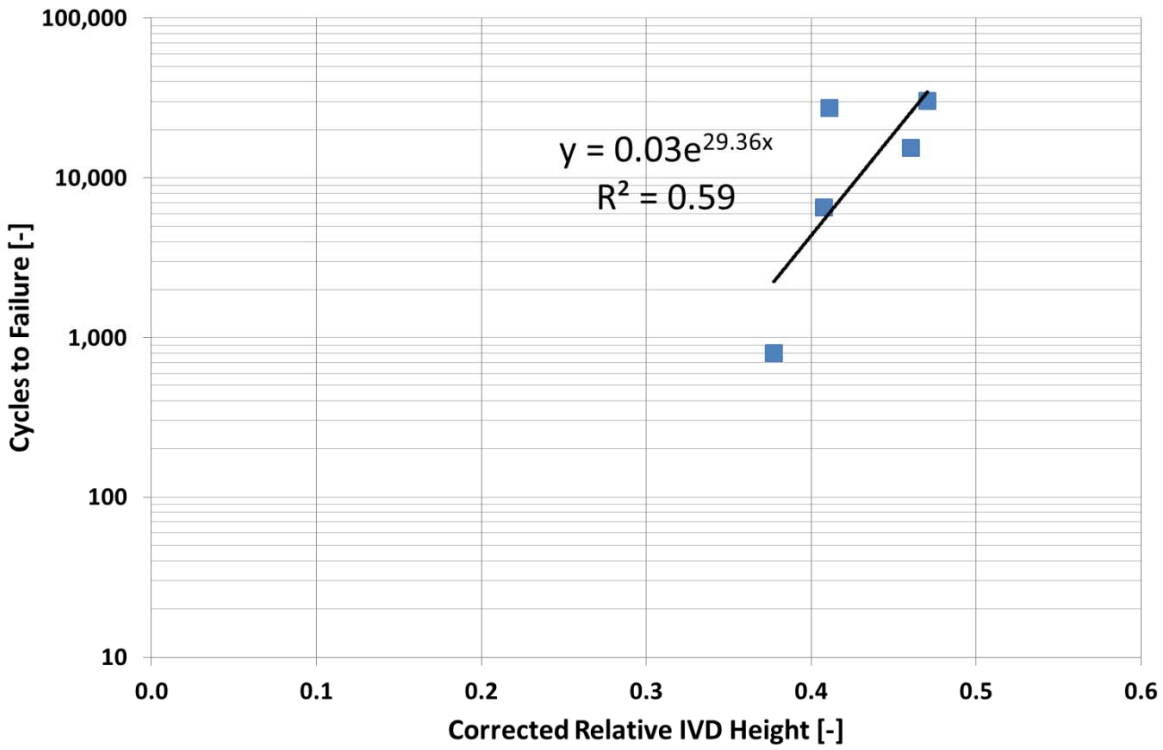

Fig. 3-55 Failure cycles of the first major failure of all specimens failed in anterior shear fatigue displayed over the IVD height (exponential regression curve p = 0.131).

In Tab. 3-17, the results from the shear force verification via the internal bending moment are displayed (chapter 2.2.2.2). The relative height of the zero point of bending moment was larger than 0 and smaller than 1 for most of the specimens tested. FSU 3021 L4-L5 started slightly below the disc and FSU 3032 L4-L5 ended slightly above the assumed disc. At no stage was the zero point within the embedded region for any of the specimens.

The absolute shift was within a range of 3.0 mm to 6.7 mm and therefore rated as small. The smallest shift of zero point of bending moment was determined for the FSU 3001 L2-L3 where no major failure was detected. The largest shift was determined for FSU 3012 L2-L3. This specimen showed a single major failure at a very low number of cycles with two minor failures following. All other specimens failed later and, apart from FSU 3001 L2-L3, showed a major failure as the last failure event. The verification of shear stress therefore showed a sufficiently stable load pattern.

Tab. 3-17 Determined absolute shift, as well as relative height of zero point of bending moment at the beginning of fatigue loading and after the last failure.

FSU	Relative height – start [mm/mm]	Relative height – after failure [mm/mm]	Absolute shift [mm]
3001 L2-L3	0.20	0.53	3.0
3007 L4-L5	0.37	0.91	4.8
3012 L2-L3	0.11	0.85	6.7
3021 L4-L5	-0.29	0.15	3.9
3031 L2-L3	0.20	0.86	5.9
3032 L4-L5	0.50	1.13	5.7

3.3.3 Reference During Fatigue

After 0 cyc (ID33), 1,000 cyc (ID38), 10,000 cyc (ID43), 100,000 cyc (ID48), 200,000 cyc (ID53) and 300,000 cyc, quasistatic reference measurements consisting of ramp compression load with an offset of -1000 N and an amplitude of -1000 N at a frequency of 0.005 Hz were performed. The apparent stiffness (c_{app}) of those cycles was analysed by a two-way ANCOVA with donor group and load ID as factors and AREA as a covariate. At every time-point, only reference values from un-failed specimens were included into analysis.

Both factors had a significant effect ($p < 0.023$) on the stiffness; AREA had no significant effect ($p = 0.248$). The stiffness did not show any significant changes to 100,000 cycles (ID48) ($p > 0.581$). After another 100,000 cycles (ID53), the stiffness increased significantly ($p = 0.004$). Subsequently, a drop in stiffness was observed (ID58), however, this was not significant ($p = 0.342$). The quasistatic stiffness during fatigue testing was significantly larger by 18% for Midlife Males compared to Young Males ($p = 0.006$). No difference was detected between Midlife Female and Midlife Male ($p = 0.517$). Quasistatic c_{app} during fatigue testing is shown in Fig. 3-56.

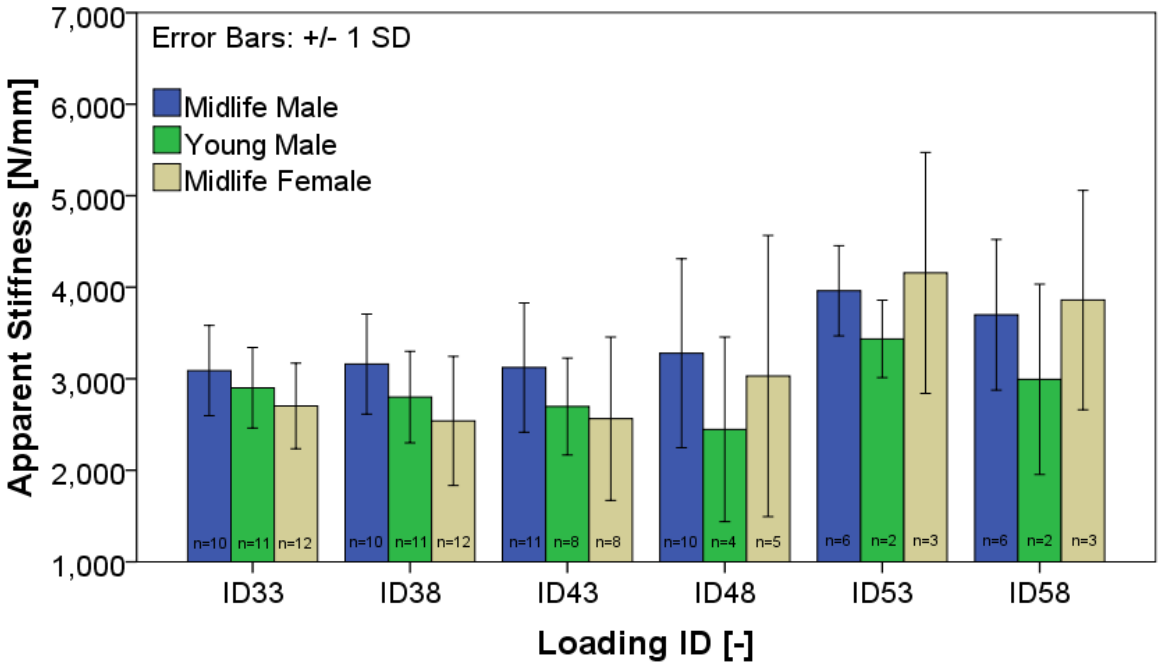

Fig. 3-56 Quasistatic apparent stiffness during fatigue testing (ID33: 0 cyc, ID38: 1,000 cyc, ID43: 10,000cycles, ID48: 100,000 cycles, ID53: 200,000 cycles, ID58: 300,000 cycles).

The dynamic reference measurements were also investigated after 0 cyc (ID34), 1,000 cyc (ID39), 10,000 cyc (ID44), 100,000 cyc (ID49), 200,000 cyc (ID54) and 300,000 cyc (ID59). The statistical methods were comparable to those used during the reference measurements of the parameter section (repeated measures three-way ANCOVA, see chapter 3.2.3). The apparent stiffness of the specimens exposed to a sinusoidal compression load of -800±1000 N was investigated over a frequency range of 0.02 to 10 Hz. The test frequencies 3, 7, and 12 Hz were again excluded to achieve logarithmically equidistant measuring points for the statistical analysis (0.02, 0.05, 0.1, 0.2, 0.5, 1, 2, 5, 10 Hz). The data obtained after failure of the respective specimen were excluded. The load IDs were compared by using repeated contrasts. Some subset data were not normally distributed and the covariance matrices were heterogenic, therefore the validity of the statistical analysis is limited. Sphericity for the repeated measures ANCOVA was not given, therefore the Greenhouse-Geisser corrected values were reported for the frequency analysis.

Dynamic c_{app} during fatigue testing pooled over frequency is shown in Fig. 3-57. Both the load ID and donor group had a significant effect ($p < 0.003$); AREA again had no significant effect ($p = 0.684$). The stiffness did not show any significant changes to 10,000 cycles (ID44) ($p > 0.941$). After 100,000 cycles (ID49), the stiffness increased by 15 %, however, this was not significant ($p = 0.062$). After 200,000 cycles (ID54), the stiffness increased significantly ($p = 0.005$) and stayed at that level for the next 100,000 cycles (ID59, $p = 0.871$). The dynamic stiffness during fatigue testing was significantly larger by 19 % for Midlife Males compared to Young Males ($p = 0.002$). No difference was detected between Midlife Female and Midlife Male ($p = 0.611$). Again, the pooled stiffness increased by 25 % over the frequency range ($p < 0.001$).

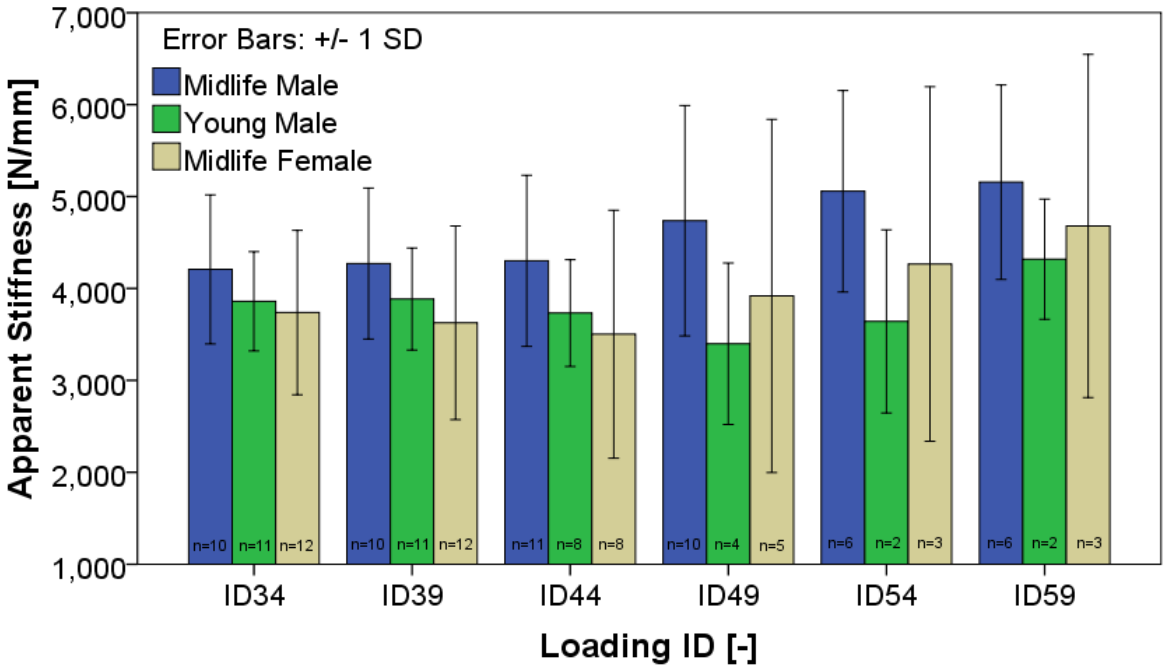

Fig. 3-57 Dynamic apparent stiffness during fatigue testing pooled over frequency (ID34: 0 cyc, ID39: 1,000 cyc, ID44: 10,000cycles, ID49: 100,000 cycles, ID54: 200,000 cycles, ID59: 300,000 cycles).

3.3.4 Equivalent Fatigue Load Cycles

Modification of the preconditioning measurement protocol with regard to project F2069 was mainly carried out to allow full creeping of the disc and to cover the transition zone between quasistatic and dynamic loading. The modifications pertained to the load pattern, the number of cycles and the frequency range. Since preconditioning covered a notable part of the test in both projects, the impact on the fatigue strength of the test object was to be illustrated in terms of equivalent fatigue load cycles $n_{equivalent}$. Those were calculated by applying the prediction of the maximal numbers of cycles to failure according to Seidel et al. (2008). The method is described in 2.2.2.3.

The whole set of compression parameter testing accounts for less than 152 equivalent loading cycles ($n_{equivalent}$) in terms of the NORM load pattern for this study. Together with all the reference measurements performed before fatigue loading this add up to 167 to 169 load cycles (Tab. 3-18) for the failed specimens. With regard to the protocol of the previous project (F 2069), the parameter testing and the intermediate reference measurements accounts for 610 to 626 NORM fatigue cycles for the failed specimens. If the contribution of these initial cycles is calculated with respect to the HIGH and OFFSET fatigue load, the equivalent loading cycles are rather low. For failed specimens it is 6 to 9 and 17 to 48, respectively.

The influence on fatigue caused by parameter and reference testing in this study is negligible, because the accuracy of determining the point of failure is in the same range. For the data of project 2069 this might not be the case and correcting the numbers of cycles to fatigue failure might be reasonable. The shear load in the parameter measurements is also negligible if compared to the applied shear fatigue

load ($n_{equivalent}$ = 7) and the eight reference measurements performed in between the fatigue testing cycles have a minor influence as well (each $n_{equivalent}$ < 7). Fig. 3-58 shows the influence of $n_{equivalent}$ on the measured cycles to failure. A visually detectable difference exists for only three specimens and even here the influence is small.

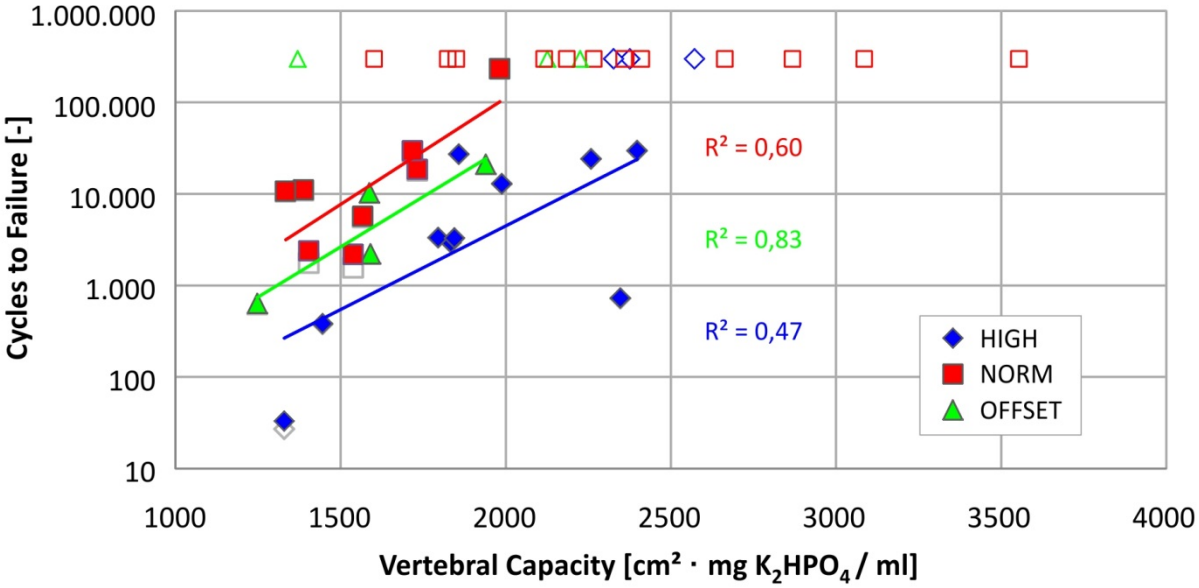

Fig. 3-58 Number of cycles to failure depending on the vertebral capacity for the compression fatigue measurements. The grey unfilled markers represent cycles to failure without the addition of the equivalent load cycles. The coloured unfilled markers represent specimens that did not fail within the number of cycles displayed.

Tab. 3-18 Summary of the measured load cycles and the corrected load cycles based on the VC of the specimens.

LWS	Level	VC [cm² mgK_2HPO_4/ml]	Fatigue load group	Measured fatigue cycles	Equivalent cycles parameter testing	Corrected total cycles
3001	L4-L5	2572	HIGH	>300000	10	>300000
3004	L4-L5	1446	HIGH	378	6	384
3005	L2-L3	2204	HIGH	56584	9	56593
3011	L2-L3	1330	HIGH	27	6	33
3013	L4-L5	1845	HIGH	3286	8	3294
3016	L2-L3	1989	HIGH	12889	8	12897
3017	L4-L5	2348	HIGH	720	9	729
3018	L2-L3	1834	HIGH	2944	8	2952
3019	L2-L3	1859	HIGH	27253	8	27261
3023	L2-L3	1796	HIGH	3331	8	3339
3028	L4-L5	2376	HIGH	>300000	9	>300000
3030	L4-L5	2259	HIGH	24202	9	24211
3031	L4-L5	2327	HIGH	>300000	9	>300000
3032	L2-L3	2398	HIGH	29710	9	29719
3006	L4-L5	2266	NORM	>300000	169	>300000
3009	L2-L3	1388	NORM	10891	168	11059
3011	L4-L5	1334	NORM	10558	167	10725
3014	L2-L3	1567	NORM	5563	168	5731
3017	L2-L3	2359	NORM	>300000	169	>300000
3023	L4-L5	1982	NORM	233120	169	233289
3026	L4-L5	1851	NORM	>300000	169	>300000
3028	L2-L3	1602	NORM	>300000	168	>300000
3004	L2-L3	1248	OFFSET	621	17	638
3006	L2-L3	1940	OFFSET	21151	48	21199
3014	L4-L5	1587	OFFSET	10261	33	10294
3016	L4-L5	2226	OFFSET	>300000	59	>300000
3025	L4-L5	1527	OFFSET		30	
3026	L2-L3	1591	OFFSET	2197	33	2230
3027	L4-L5	1371	OFFSET	>300000	23	>300000
3030	L2-L3	2126	OFFSET	>300000	55	>300000
1101	L4-L5	1733	NORM F2069	17960	610	18570
1104	L4-L5	1719	NORM F2069	28929	611	29540
1131	L4-L5	1539	NORM F2069	1562	618	2180
1136	L4-L5	1405	NORM F2069	1759	626	2385
1106	L4-L5	2185	NORM F2069	>300000	598	>300000
1107	L4-L5	1824	NORM F2069	>300000	607	>300000
1108	L4-L5	2869	NORM F2069	>300000	588	>300000
1110	L4-L5	3554	NORM F2069	>300000	583	>300000
1124	L4-L5	2117	NORM F2069	>300000	600	>300000
1126	L4-L5	3086	NORM F2069	>300000	586	>300000
1133	L4-L5	2664	NORM F2069	>300000	591	>300000
1135	L4-L5	2411	NORM F2069	>300000	594	>300000

3.4 Ultimate Strength Measurements

All six specimens failed. However, one dataset was excluded due to the limitation of the measuring technique (FSU 3005 L4-L5). The sensor range was saturated immediately after the failure event and important fracture data were collected at the outer end of the measuring range. The measuring results were therefore not reliable. In Fig. 3-59, a typical force displacement diagram is displayed.

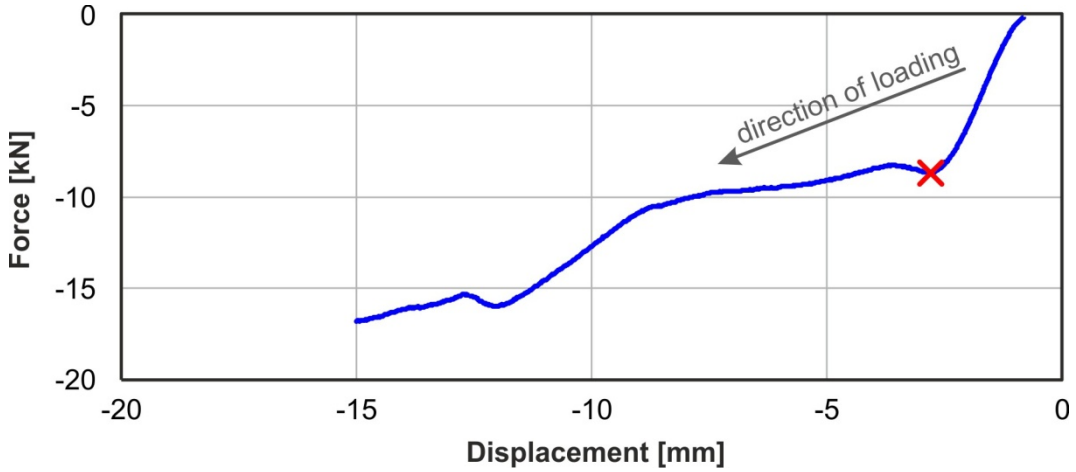

Fig. 3-59 Typical force displacement diagram of axial ultimate strength experiments (FSU 3012 L4-L5, red mark indicates point of fracture).

Force displacement curves exhibited an almost linear increase in force and a first force peak with subsequent force drop as reported by Brinckmann et al. (1989). They also reported that some specimens showed no force drop after fracture. However, all of the specimens used to determine the fracture force in this study showed a clear force drop after fracture. Tab. 3-19 displays the determined ultimate strength and corresponding VC.

Tab. 3-19 Determined ultimate strength in comparison to calculated ultimate strength according to Brinckmann et al. (1989).

LWS	Level	Vertebral Capacity [cm² mg K_2HPO_4/ ml]	Ultimate Strength	
			Measured [kN]	Brinckmann [kN]
3007	L2-L3	2,363	9.223	7.598
3012	L4-L5	2,027	8.685	6.563
3013	L2-L3	1,747	6.378	5.701
3019	L4-L5	2,086	8.848	6.745
3021	L2-L3	2,901	11.554	9.255

In Fig. 3-60, the results of ultimate strength testing and the calculated ultimate strength that have been expected according to Brinckmann et al. (1989) are displayed (chapter 2.1.6). The regression slope of measured fracture force ($R^2 = 0.93$, $p = 0.009$, $\alpha = 0.05$) was parallel to the expected values, but the measured values were larger than estimated by Brinckmann's regression by about 2 kN.

In Fig. 3-61, the axial ultimate strength in the axial direction measured in this study is displayed together with the ultimate strength measured by Skrzypiec et al. (2012) in the anterior shear direction. Analogous to shear fatigue strength, no significant relation was found between shear ultimate strength and VC ($p = 0.817$, linear regression, $\alpha = 0.05$).

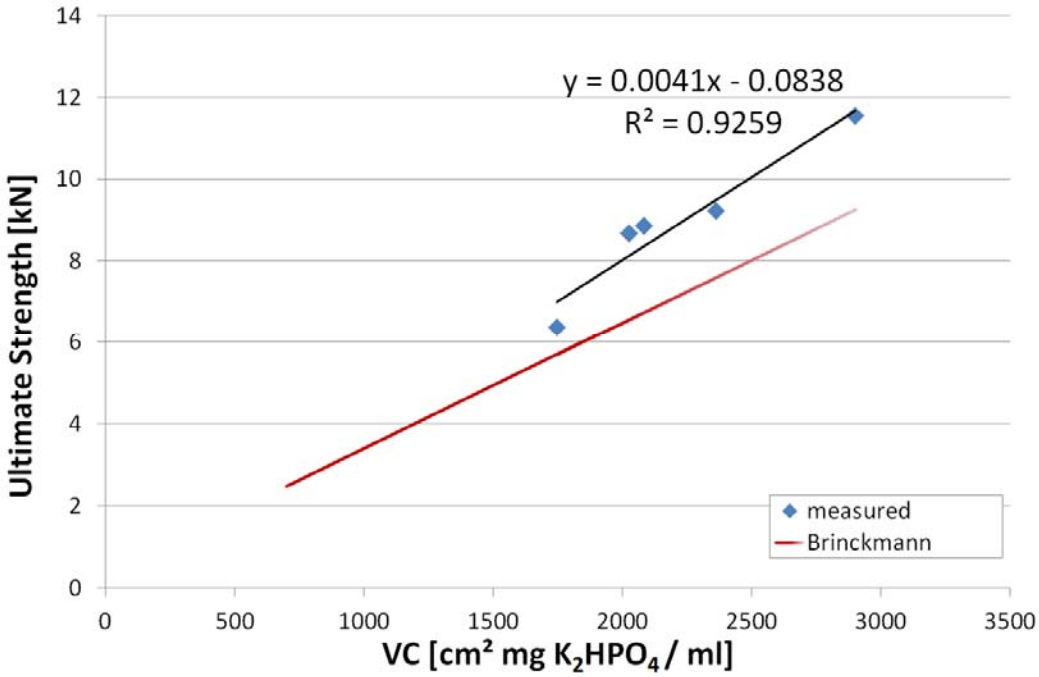

Fig. 3-60 Measured fracture force and its dependence on vertebral capacity in comparison to expected fracture force according to Brinckmann et al. (1989).

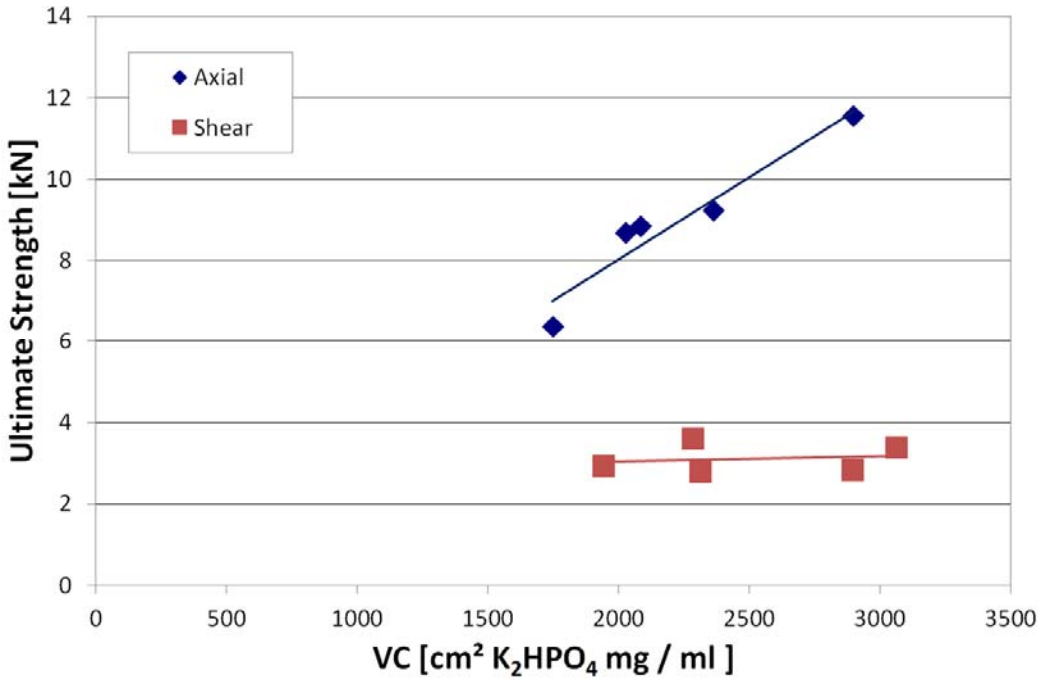

Fig. 3-61 Ultimate strength in the axial (this study) and anterior shear direction (Skrzypiec et al., 2012) displayed over VC.

3.5 Test Environment

The temperature of the Ringer solution surrounding the specimens during testing could be kept between 36 °C and 38 °C.

Microscopic analysis of the Ringer solution showed viable germs. The indication for spore-forming bacteria was observed in some test-end micrographs (Fig. 3-62). A qualitative comparison of the start micrographs of consecutive experiments did not show a serious increase of germs (Fig. 3-63). A comparison between test-end micrographs also did not show any major qualitative differences regarding the number of bacteria.

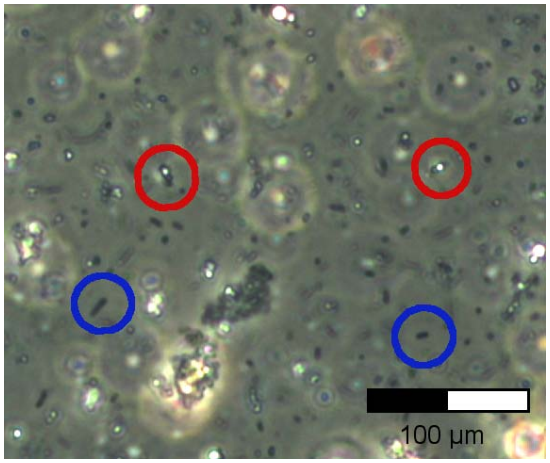

Fig. 3-62 Ringer solution micrograph taken at the end of an experiment (FSU 3028 L4-L5). Red marks indicate spore-forming organisms; blue marks indicate examples for non-spore-forming organisms.

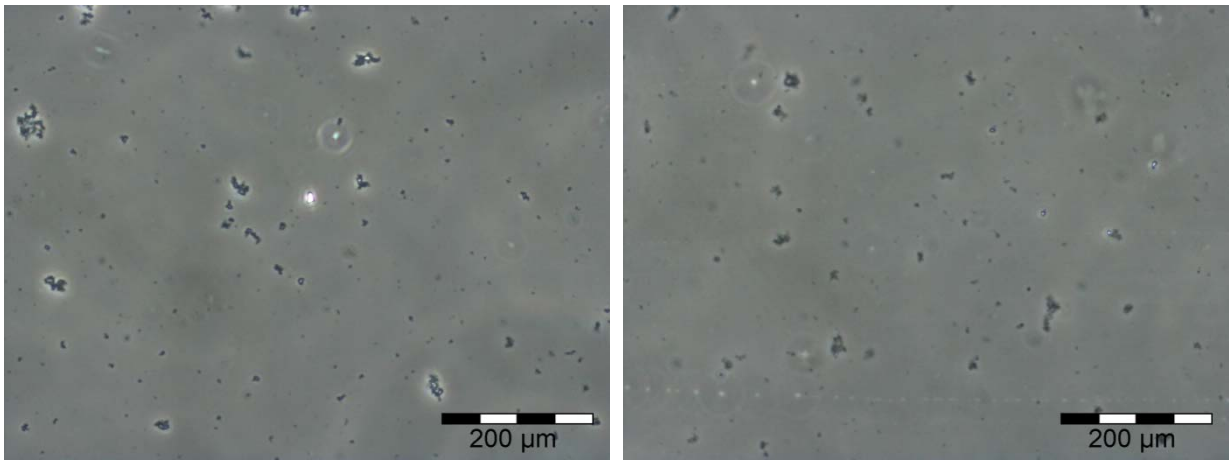

Fig. 3-63 Micrographs taken at the beginning of two consecutive measurements showing only a low number of bacteria (left: FSU 3028 L2-L3; right: FSU 3028 L4-L5).

In comparing the test-start with the test-end micrographs, an increase of germs was observed (Fig. 3-64). Since there were still areas of fluid that appeared clean, the number of germs after 26 h of bacterial exposure was considered to be low. This indicated that no reasonable bacteria-driven degeneration had taken place.

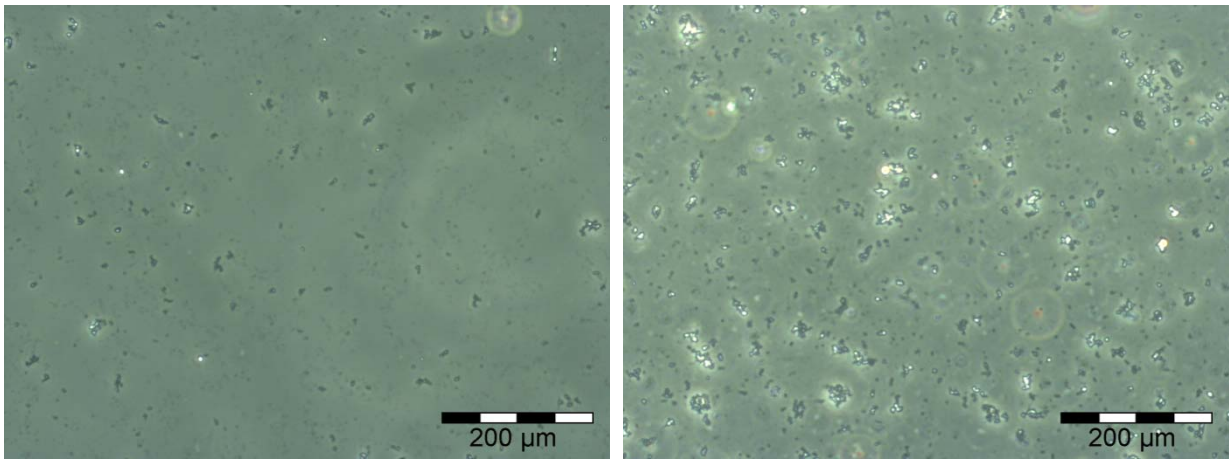

Fig. 3-64 Micrographs taken at the beginning and end of a measurement showing the increase in the number of bacteria (left: FSU 3030 L2-L3 test start; right: FSU 3030 L2-L3 test end).

4 Discussion and Conclusions

The specimens from 32 donors (three different groups) exhibited a large inner-group and intra-group variation with respect to the VC. Therefore, it appears to be meaningful using VC as a predictor variable. Considered from a mechanical point of view, AREA serves as a scaling for converting axial compressive force to stress. BMD is known to be related to Young's modulus of the vertebral bony structure. The product of the two (area times Young's modulus, which are commonly used as the characteristic values of metal structures), has a certain similarity to the longitudinal axial stiffness.

The in vitro experiments in this study do not refer to voluntarily performed active spinal movements of living subjects (as commonly done in in vitro testing by performing extension-flexion movements). The loading in the dynamic parameter measurements and in the fatigue testing is assigned to represent dynamic whole body vibrations as occurring in the workplace. The actual in vivo knowledge about these loading is scarce.

The most promising step would be the usage of these in vitro results in combination with numerical dynamic whole body models. The parameter testing could be used to define the properties of the numerical discs. In combination with measured external loading of living subjects, the model could exhibit whether fatigue loads on FSUs are similar to those used in these experiments. This model-experiment interaction demands several loops. The values in this study have already been chosen based on actual finite element models predicting axial amplitudes of around 1000N for some extreme exposure conditions, e.g. in forwarders and harvesters (Seidel 2008). The offsets for the axial compression fatigue testing (-1000 N to -2000 N) were chosen slightly above the model predicted values for very massive subjects. However, pressure measurements in a presiding in vitro project (F1899) exhibited physiological disc pressures (14 bar) for these loading (Huber 2005).

There is some evidence that the shear load is smaller in subjects exposed to vibration at the workplace than the applied fatigue load in the present study (750 N ± 750 N) (Seidel 2008, Schust 2013). The value has been chosen based on the small amount of knowledge concerning the anterior fracture strength of specimens, but exhibited rather small cycles to failure in these experiments.

The presented parameter tests covered a wide range of frequencies (0.005 Hz to 12 Hz), offsets and amplitudes (both up to 1000 N). Therefore, the results of these experiments might also be used in models designed for the prediction of spinal loading caused by quasi-static movements as carrying heavy weights at the workplace.

One influencing factor, not addressed in this study might be the posture of the subjects. The specimens in these in vitro experiments were potted in their present orientation. The angle between the two vertebrae represents the in situ cadaver orientation. It is not known how far this orientation differs from the on in the workplace, but it is likely that further flexion will decrease the resistible cycles to failure (F2069).

4.1 Parameter Measurements

The different amplitudes, offsets and preloads resulted in a wide range of response behaviours in both the quasistatic and dynamic testing. This study is another step to gain more confidence about spinal stiffness. In looking at the stiffness of FSUs, one has to consider that the meaning of the stiffness magnitude is not straightforward. On the one hand, high stiffness means less deformation of tissue, which can indicate that the respective load pattern is less stressful for these elements. On the other hand, large stiffness can be a result of restricted compliance. Up to now, it has not been determined whether stiffness is associated with physiological advantages or disadvantages.

There was a reduction in quasistatic compression stiffness when additional shear load was applied. That means that the overall deformation of the FSU was increased when shear load was applied. This deformation consists mainly of the deformation of soft tissue elements like the disc and facet joint capsular, which means that they are more stressed in situations with shear load. Shear preload in work situations can occur when the body is exposed to load in bent (forward or backward) positions. Posterior shear preload tends to have a lower stiffness, which is due to the fact that the joint bearing areas are pulled apart from each other, which might allow more axial movement. Under anterior displacement, the facet joint surfaces are pressed against each other and restrict movement. For the same reason, quasistatic shear stiffness is larger in the anterior direction than when alternating around zero.

The specimens of the different groups of donors behave differently in compression than in shear. It appears that there are different influencing properties for each direction. For axial compression, Midlife Females showed lower stiffness (larger compliance) than males in the same age range. One reason could be that the discs of the males had less degeneration, even though no difference in IVD height was found. In shear mode, Young Male stiffness was larger than Midlife Male, but Midlife Male and Female were on the same level. This could indicate a relationship between apparent stiffness and bony capacity – BMD was larger for the Young Male group. Even though this parameter was measured for the centre of the vertebrae, it could also be regarded as an indicator of overall bone quality.

In dynamic compression and shear testing, the stiffness increased as the frequency increased for all load cases. At higher frequencies, the amount of fluid that can be pushed through the porous structure of the disc, endplate and vertebrae is smaller, which increases the overall stiffness. This stiffness depends on the fluid content inside the respective structures.

A higher offset in dynamic compression testing resulted in a higher stiffness, whereas a larger amplitude resulted in a smaller stiffness (see Fig. 3-23). This can be partly explained by the non-linear stiffness. Increasing the offset of the axial compressive force moves the work point in the direction of the peak stiffness (c_{peak}), which used to be higher than the initial stiffness ($c_{initial}$). However, by increasing the amplitude of the cyclic loading, the cyclic loading stroke increases not only to areas with high stiffness but also in the unloaded direction close to 0 N. This effect overlays the effect of the decreased stiffness at maximum compression. The stiffness is mainly determined by

the progressive stiffness at the peak values, while amplitude and offset represent indirect descriptions of the same (Fig. 4-1).

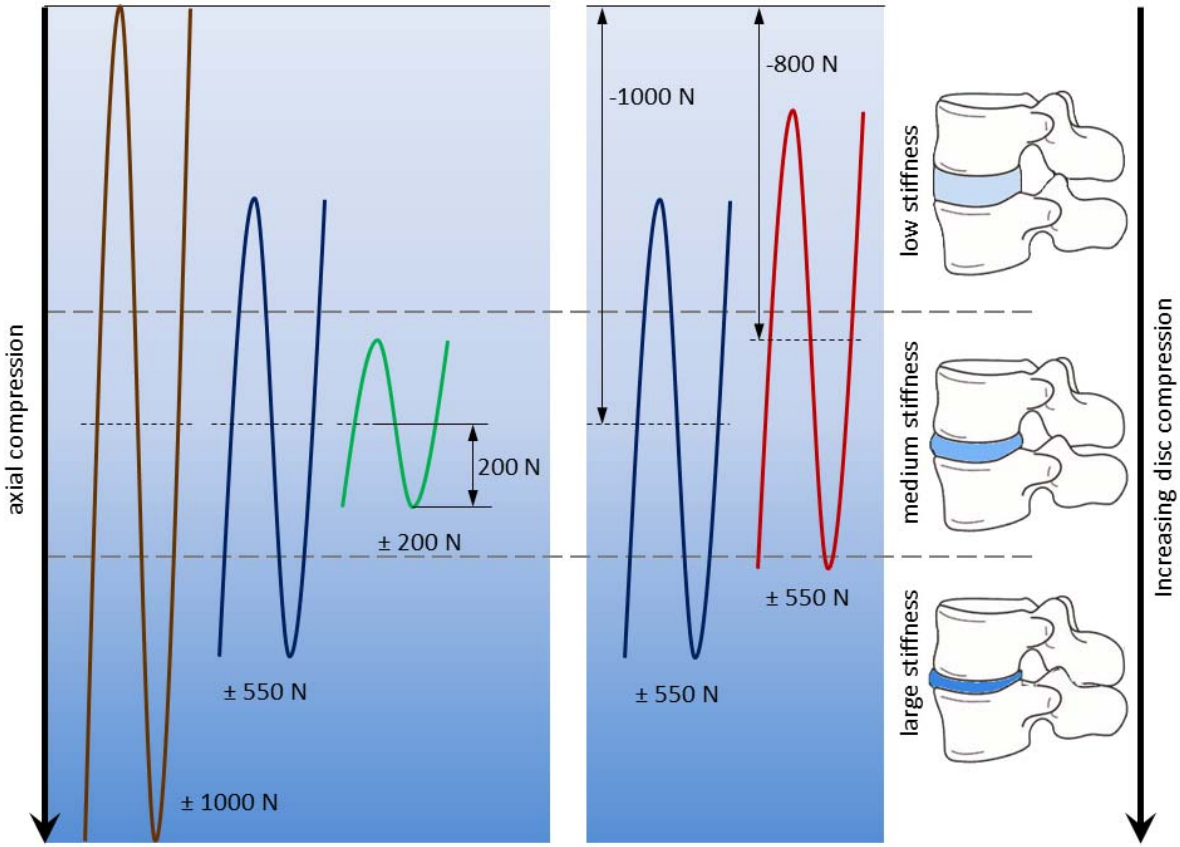

Fig. 4-1 Applied load patterns in dynamic compression; Stiffness magnitude due to disc compression is represented by three areas and indicated by different color intensity, on the left side the different amplitudes and on the right side the different offsets are displayed. The position of peak values is decisive for determined apparent stiffness.

For shear loading, the amplitude had no effect on the stiffness, but this was only tested for a posterior offset load of -100 N. In contrast to the small amplitude of 50 N, the larger amplitude of 200 N also produced an anterior shear load for a certain part of the load cycle. The orientation of the facet joint leads to a mechanism, in which anterior displacement of the upper vertebra reduces the distances between the surfaces of the facet joints and might also result in a slight upward movement of the vertebra. This is restricted by the disc, which is in axial tension if only shear is applied. Displacement of the upper vertebra in the posterior direction results in a downward movement, which axially compresses the disc. Considering that the disc is made for absorbing compression rather than tensile load, it seems reasonable that the capability of tensile deformation is less than the compression displacement. This might explain the larger stiffness in the anterior direction compared to the posterior direction. It is obviously questionable whether the two different amplitudes are comparable since they cover different mechanical phenomena. If offset shear load occurs due to anteriorly displaced superior vertebrae, the dynamic shear stiffness is larger than for specimens without offset load - as also observed in the quasistatic shear testing. The stiffness for posteriorly displaced vertebrae is again smaller than

in anterior direction. The anterior peak force is lower than for the other two offsets and therefore the work range covers less of the area where the facet joints are pressed together and the upper vertebra is shifted upwards. Again, the peak forces are more decisive for the stiffness than amplitude and offset (Fig. 4-2).

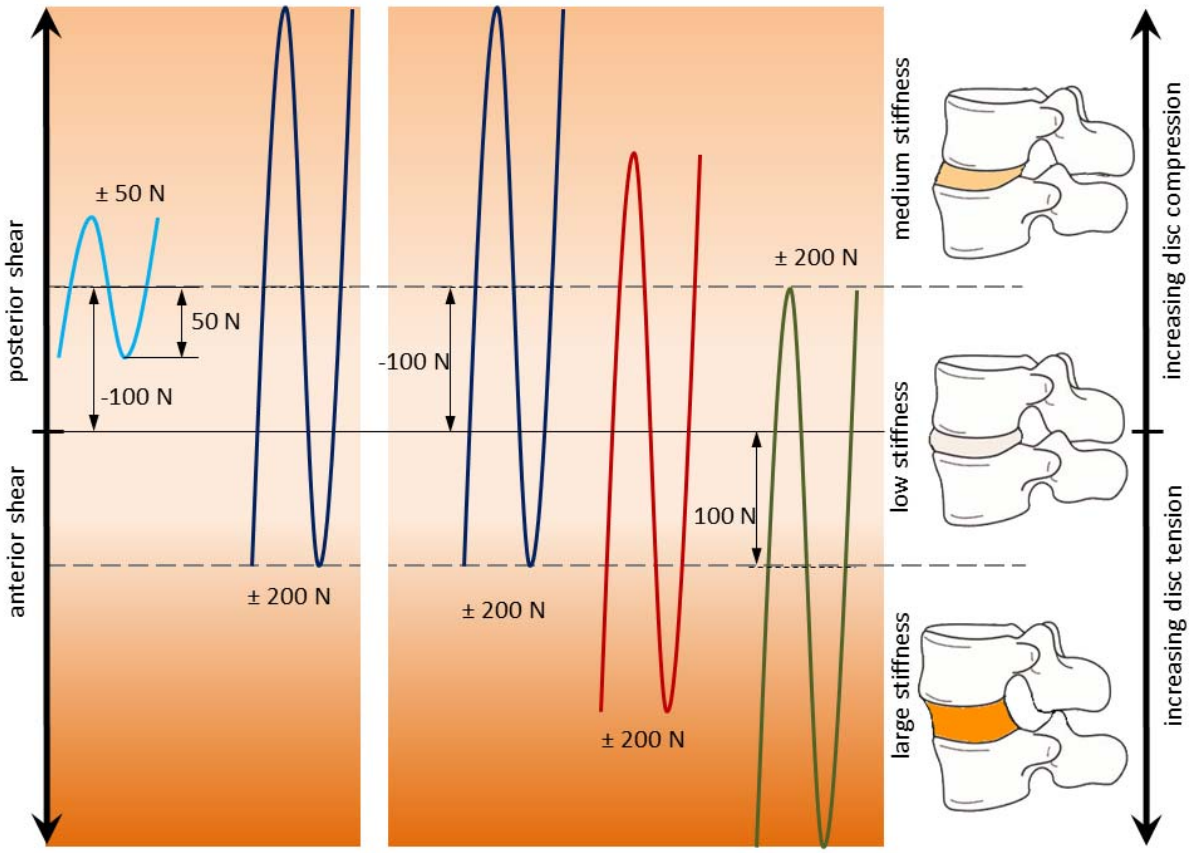

Fig. 4-2 Applied load patterns in dynamic shear; stiffness magnitude due to displacement of the upper vertebra is represented by three areas and indicated by different color intensity, on the left side the different amplitudes and on the right side the different offsets are displayed. Position of peak values is decisive for determined apparent stiffness.

The reference measurements (quasistatic and dynamic) did not exhibit any significant changes in the specimen's behaviour after the end of the quasistatic testing sequence. The first quasistatic load ID and the reference measurement after the quasistatic block showed similar apparent stiffness. This indicates that the discs were sufficiently preconditioned after the initial reference measurement.

4.2 Fatigue Measurements

HIGH and SHEAR load lead to failure within a reasonable number of cycles. A cyclic load magnitude of 40 to 50 % of the ultimate strength results in failure during the 300,000 load cycles.

The failures caused by compression and shear fatigue load differ. It is more complex to determine shear failure than compression failure. While axial failure appears to be predictable using the VC, no correlation was found between VC and shear failure.

4.2.1 Compression Fatigue Failure

Post-test preparation revealed clefts in the annulus fibrosus and nucleus pulposus of the disc and also disc delamination for almost all of the unfailed specimens exposed to compression fatigue loading. However, similar damages were also found in a simultaneously prepared (embedded, frozen, separated by band saw and thawed afterwards) but not tested FSU. Although the disc quality of this single FSU was poor, the origin of the disc damages observed for the tested specimens was ambiguous and not necessarily due to fatigue loading.

Two specimens exhibited failure of the cancellous bone with intact endplates and cortical shell of the vertebral bodies (FSU 3017 L2-L3, FSU 3023 L4-L5). It is probable that the endplates of these specimens would have failed after a few more cycles. Both FSUs were from midlife donors assigned to the NORM group. However, their VC was in the range of the young male donors. In the case of FSU 3023 L4-L5, which had the lower VC of the two, a failure was also observed in the creep curve. It is the only specimen that was rated as failed although the endplates were intact. The failure occurred at an extraordinarily large number of cycles (233,300). All other specimens failed below 60,000 cycles. It cannot be ruled out that this late failure was also caused by degeneration processes resulting from the long test period.

Another specimen did not show signs of failure in the creep displacement measurements even though the nucleus had penetrated the endplate (3001 L4-L5). Consequently, missing discontinuities in the creep curve does not always imply an intact system; minor failures may already have taken place.

The analyses based on Seidel et al. (2008) and Brinckmann et al. (1989) account for offset force and peak-to-peak force, as well as for the VC. The fatigue cycles measured tended to be larger than predicted. However, the black box model (see chapter 3.3.1) emphasised the dominant influence of the amplitudes for the chosen load levels. This coincides with Wöhler's law (1870, cited in Schütz, 1996), which states that the amplitudes are decisive for the cohesion of a material. It should be noted that some specimens did not fail although both equations predicted failure below 300,000 cycles. There might be other factors apart from BMD and endplate area that contribute to the fracture strength of the specimens, such as the thickness of the cortical bone or the load history of the donors. The derived model should only be applied to the parameter range investigated in this study. Extrapolation is not justified.

4.2.2 Shear Fatigue Failure

Deformation of the FSU is a result of the elastic deformation and creeping of the soft and hard tissue and movement of the specimen in the embedding.

The damages that have been detected during post-test preparation can be divided into hard tissue failures (pedicle fracture), soft tissue failures (disc detachment, ligament detachment) and fixation failure. The various failure events detected, which have differing appearances in the creep curve indicate a multilayer failure mechanism.

It is important to take into account that the minor failures observed may arise from soft tissue failure, as well as from loosening of the potting. Both result in an increased clearance and consequent increased displacement range and creep.

The creep curve of the excluded specimen (FSU 3001 L2-L3) exhibited only one possible minor failure event. A failure of hard tissue could not be detected, but disc detachment and a failed fixation was observed. Since all the other specimens showed major events and pedicle fractures, we concluded that the major failure event indicated a failure of hard tissue, whereas the minor event indicated soft tissue or fixation failure or an overlap of both.

In three out of five cases of pedicle fracture, the corresponding failure event occurred as a final event with one or more of the prior minor soft tissue failures. Since these minor failures also occurred in the only case with intact fixation (FSU 3031 L2-L3), this leads to the assumption that the soft tissue failure observed happened, to some extent, prior to the hard tissue failure.

In two cases, hard tissue failure represents the first failure event in the creep curve. In one case (FSU 3007 L4-L5), this primary major event seemed to overlie with soft tissue or fixation screw failure. Broad fracture of the pedicles at this point is unlikely since a more distinct major failure occurred later. In the second case (FSU 3012 L2-L3), the specimen exhibited a relatively low VC of less than 1,900 cm^2mg K_2HPO_4 / ml which resulted in early failure.

The VC may play a role in the prediction of axial fatigue strength, but no significant correlation was found between the VC and shear failure cycles. However, there was an exponential trend detected for the correlation between shear cycles to failure and the IVD height. As stated in the discussion about shear stiffness, the thickness of the disc seems to play a role in the resistance to shear deformation. It is also reasonable that the fatigue resistance is higher if the disc height is larger, which indicates less advanced degeneration.

Unexpectedly soft tissue impairment appears to occur before hard tissue failure. That implies that shear displacement can exceed a soft tissue structure's maximal deformation, even if the bony pedicles and facet joints are still intact. Simon et al. (2012) determined a facet joint space of 1.93 ± 0.51 mm. This was not determined under extreme loading; however, basing on this data we consider the maximum facet joint space as substantially smaller than the displacement at failure and not solely responsible for the clearance. The elasticity and creep ability of the pedicles also has to be considered.

Two aspects have to be considered with regard to fixation of the specimens. First, the influence of insufficient fixation on the failure mechanism of the specimen has to be regarded. To estimate this, the bending moment within the FSU was determined. The determined zero crossing of the bending moment remained within the intervertebral disc for the test period of all specimens. This indicates that the type of loading on the FSU was almost consistent, although the fixation was insufficient. Furthermore, the controller for the loading force remained stable and resulted in unaltered cyclic loading. Therefore, a severe effect on the failure mechanism is not assumed despite the clearance that occurs in the fixation.

In future, improvements in fixation are necessary for studies on shear load and methods to distinguish between pedicle and soft tissue failure are needed. In addition, a constant compression load should be applied in the axial direction in order to simulate body weight. This would also improve the situation at the fixation and avoid tensile forces on the disc.

The presented method to calculate equivalent fatigue loading cycles was designed to enable comparison of in vitro results from slightly different studies. However, due to the lack of appropriate fracture prediction models, the portion of the fracture contribution of the initial parameter and reference measurements cannot be exactly determined. This is especially difficult, because the amount of load in vivo and during explantation is also not known. Nevertheless, the methods to calculate equivalent load cycles presented in this study can serve as a first approximation to judge if the influence might rather be low or high.

4.3 Ultimate Strength Measurements

All except for one object in this study exhibited a fracture force which was 20 % to 30 % higher than that predicted by Brinckmann et al. (1989). The force of this single outlier was only 10 % larger and could influence the model outcome disproportionally due to the low sample size. In terms of ultimate strength forces, the values in this study were greater by about 2 kN. The slope of the influence of the VC (β_1 = 0.0041 kN/(cm² mgK2HPO4/ml)) was in the same range as for the specimens in the study conducted by Brinckmann et al. (β_1 = 0.00308 kN/(cm² mgK2HPO4/ml)). The intercept of the linear regression was not significantly different from zero in this study (p = 0.96); presumably, this was also the case for Brinckmann et al. since the given standard error for the intercept was greater than the intercept itself (0.32 kN with SE 0.38 kN). However, there is little data available for large VC values.

There are certain differences between the determinations of VC between the two studies. Beside the differences in technical equipment and the chosen area of interest to determine the BMD, Brinckmann derived the BMD from CT scans of specimens in an unfrozen state, whereas in this study the CTs were taken from frozen specimens. The density of frozen water is 9 % less than the density of unfrozen water and consequently also has a lower attenuation. Also, the AREA determination was not completely similar between the two studies. Considering this, the results of these studies match rather well. The results of both studies are displayed in Fig. 4-3. A regression with the pooled data did not widely differ from Brinckmann’s model.

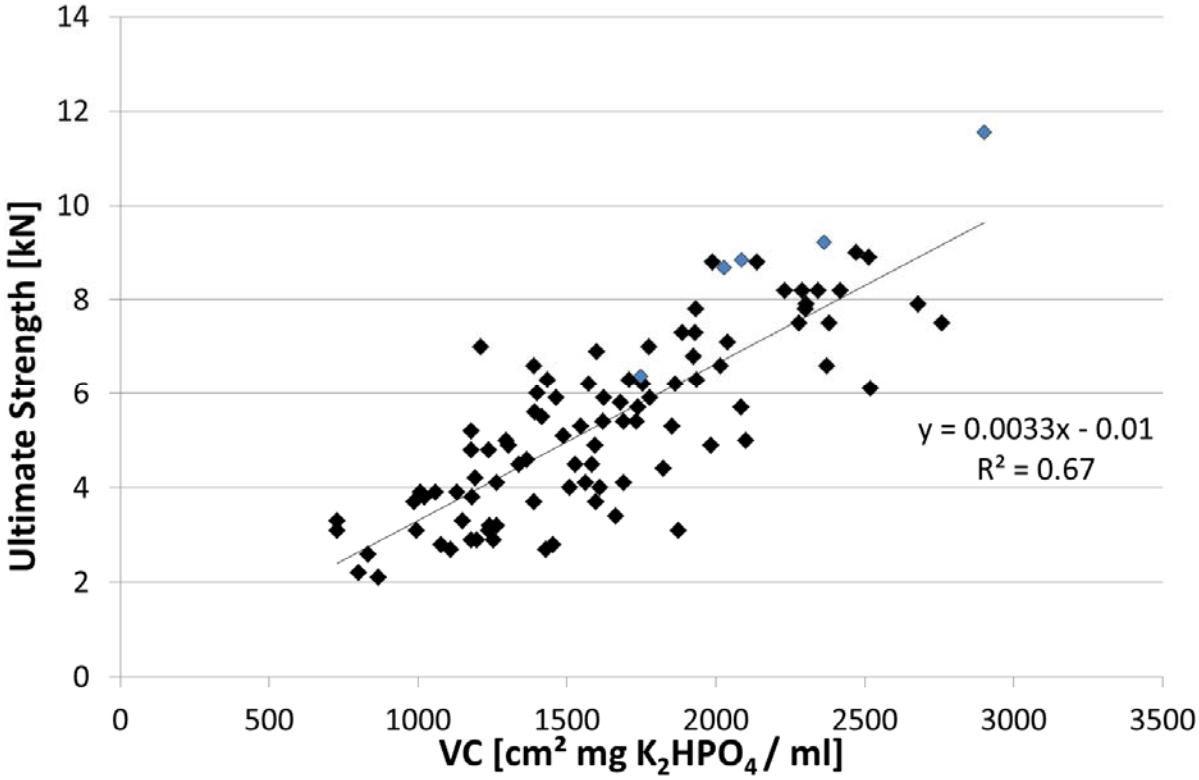

Fig. 4-3 Results for ultimate strength from this study (blue markers) combined with data from Brinckmann et al. (black markers) and the regression line for the pooled data.

5 Appendix

5.1 Specimen overview

Two different procedures were performed. For the main experiment (parameter measurements and fatigue testing), 36 FSUs were used. They came from three groups of donors: 12 FSUs from Midlife Male donors, 12 FSUs from Midlife Female donors and 12 FSUs from Young Male donors. Midlife corresponds to an age of 45 to 65 years and Young corresponds to an age of 25 to 44 years. For the measurements of the ultimate strength, 6 FSUs from Young Male donors. were used.

To receive these 42 FSUs (either L2-L3 or L4-L5), 32 lumbar spines (L2-L5) were collected by the Department of Legal Medicine, University Medical Centre Hamburg-Eppendorf. Two specimens were needed for pilot testing and seven had to be excluded, because of pathological state of the specimens. Four lumbar spines could be used partially (Fig. 5-1).

The specimens were collected from February 2009 until August 2011. About 550 counselling interviews with the next of kin of the donors were conducted for this purpose.

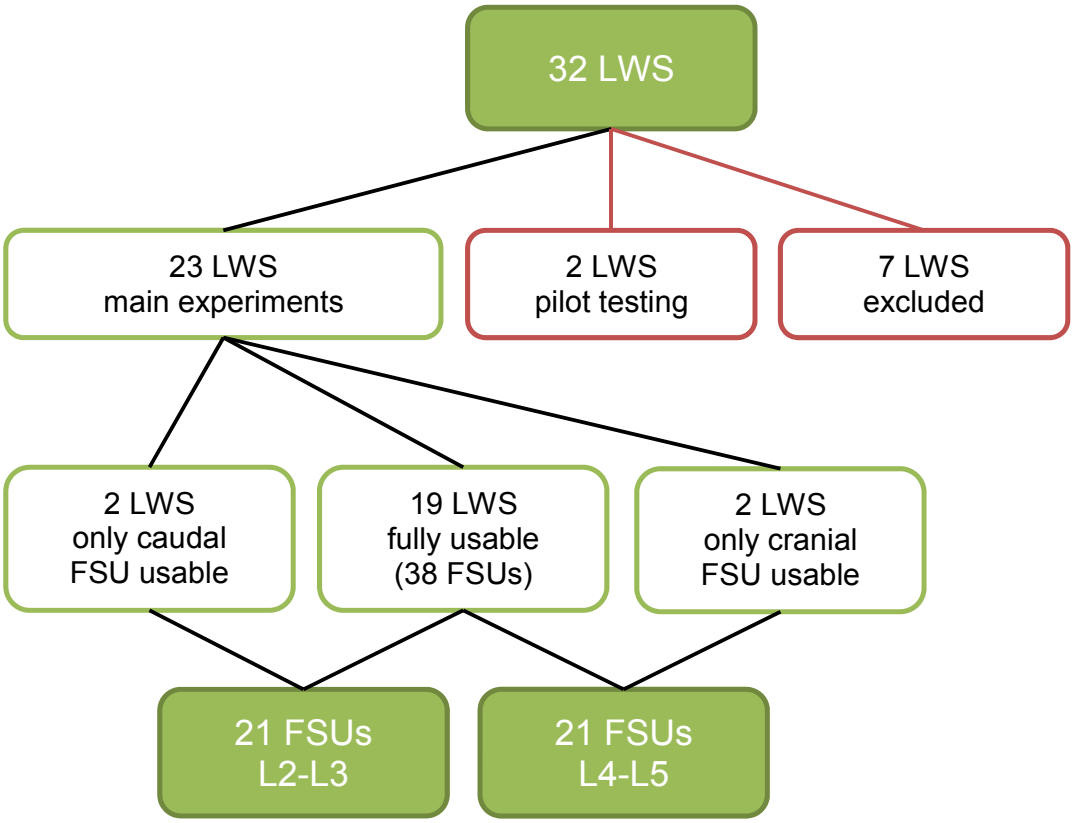

Fig. 5-1 Overview about the specimens collected for the purpose of this study

5.2 Test Rig Analysis

The test rig was used to apply a slightly different load set than in the last projects, especially with regard to the x direction. In order to analyse the dynamic behaviour of the test rig for the stiffness of the two load directions and different frequencies, a spring dummy was used (Fig. 5-2). The dummy exhibited a linear stiffness of 943 N/mm. The dummy could be mounted instead of embedding holders and specimens. The ends of the springs were not fixed to the flanges, therefore a preload of about -300 N was applied during the analysis experiments. This ensured that both springs would remain in contact with the flanges and the management of possible loads in the tensile direction without losing that contact.

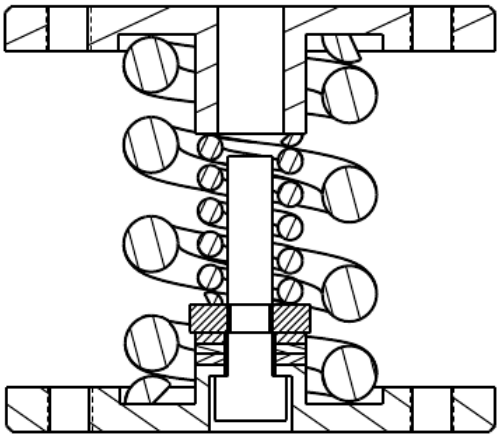

Fig. 5-2 Technical drawing of the spring dummy designed for test rig analysis.

The measured stiffness in the vertical direction increased from 0.02 Hz to 12 Hz by less than 2.7%. Considering the values from 1 to 12 Hz, the increase was only 1.9% (Fig. 5-3). The measured mean stiffness was 941 N/mm. The difference between spring stiffness and measured stiffness was due to the general stiffness of the vertical axis. Considering the vertical axis and the dummy as two collinear springs, the stiffness of the axis came to about 493,503 N/mm. This was more than 300 times the stiffness of the specimens and therefore sufficient for the planned testing.

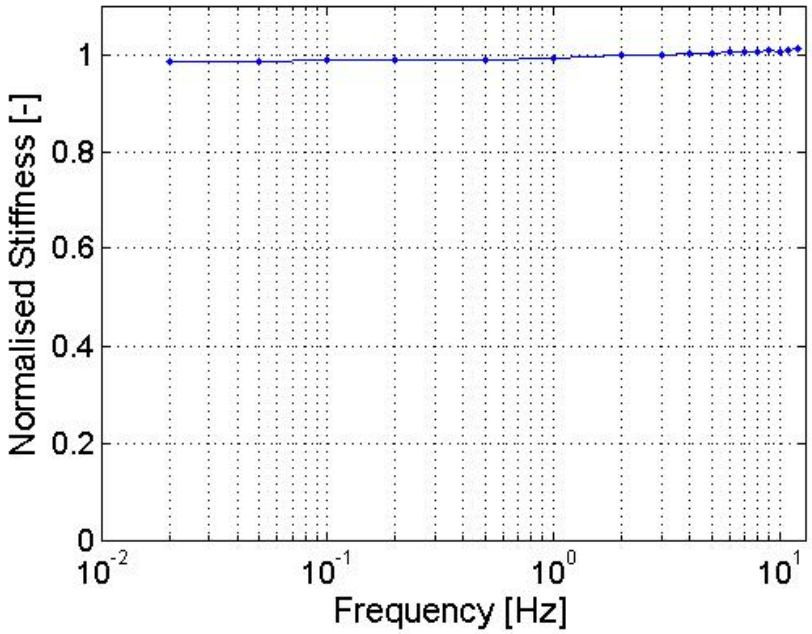

Fig. 5-3 Recorded stiffness in the vertical direction; measured stiffness normalised to nominal stiffness of the spring dummy (943 N/mm).

As described above, the dummy could only be reasonably loaded in its axial compression mode due to the unfixed ends. Therefore, a modified test setup was used to test the horizontal axis. The upper and lower attachment was complemented by brackets with a mounting option for the spring dummy so that cylinder pressure resulted in compression of the spring (Fig. 5-4).

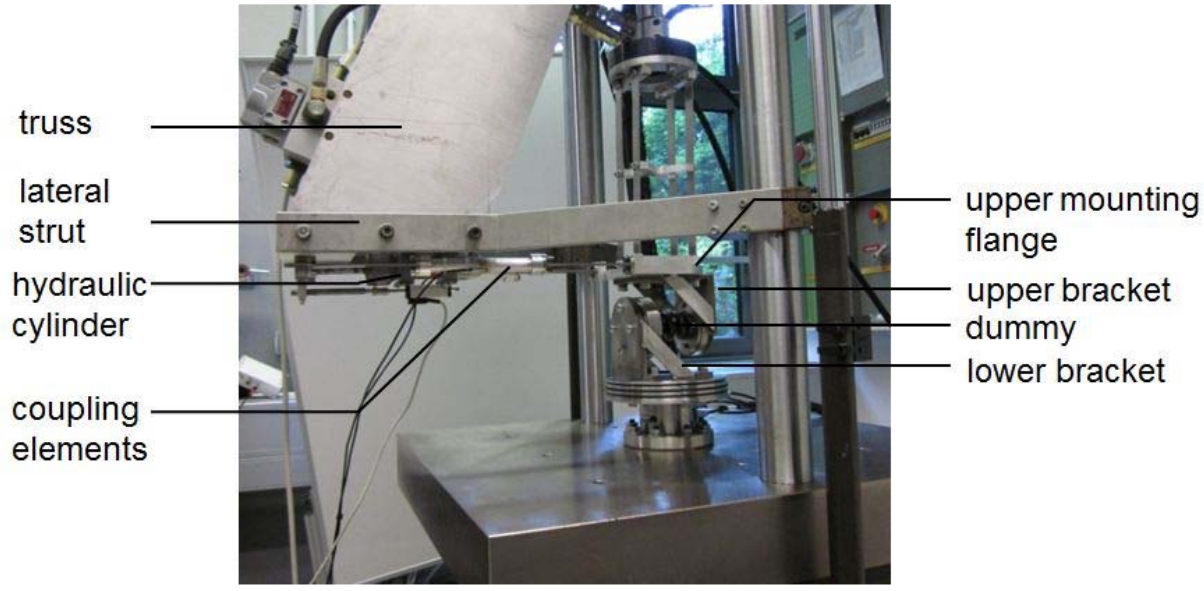

Fig. 5-4 Setup with brackets to test the horizontal axis; the spring dummy is mounted with horizontal orientation.

The measured horizontal stiffness increased by only 2.2%, from 0.02 Hz to 12 Hz. In considering the values from 1 Hz to 12 Hz, the increase was only 0.8% (Fig. 5-5). The measured mean stiffness in this setup was only 612 N/mm. That means that the

compliance of the horizontal direction contributes to the measured overall compliance by lowering it.

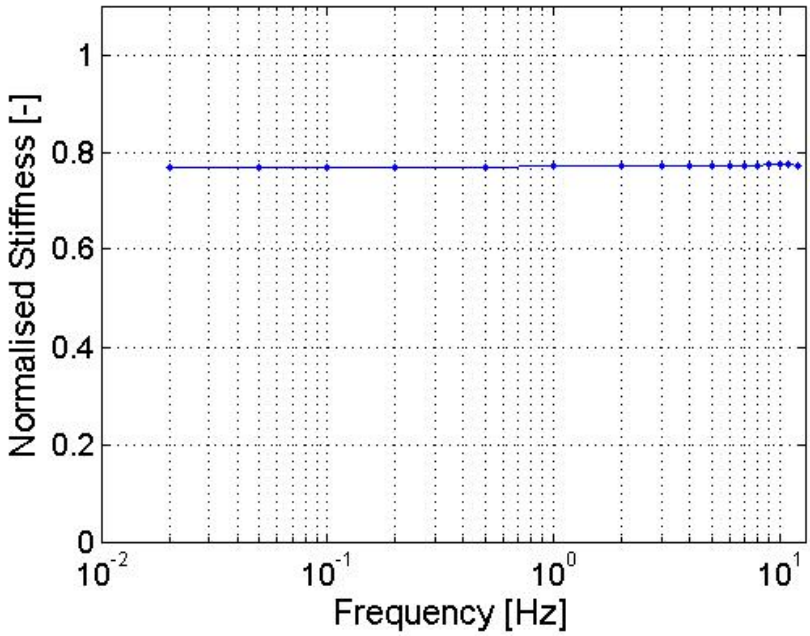

Fig. 5-5 Recorded stiffness in the horizontal direction; measured stiffness normalised to nominal stiffness of the spring dummy (943 N/mm).

The undesirably high compliance of the horizontal axis can be attributed to the rotated orientation of the specimen in the modified setup. Horizontal mounting of the spring dummy using the brackets resulted in a moment on the upper mounting flange (Fig. 5-4). Following the applied moment, the flange tilted slightly around the lateral axis.

To determine the contribution of the compliance of the axis and the bracket system, a laser vibrometer (OFV-50xVibrometer Sensor Head, OFV-5000 Modular Vibrometer Controller, Polytec, Waldbronn, Germany) was used. A load with a 1 Hz sinusoidal load signal was applied and the vibrations at five sites (A to D) at the test rig were each recorded in a separate measurement. In Fig. 5-6, the horizontal axis with the measure sites is displayed.

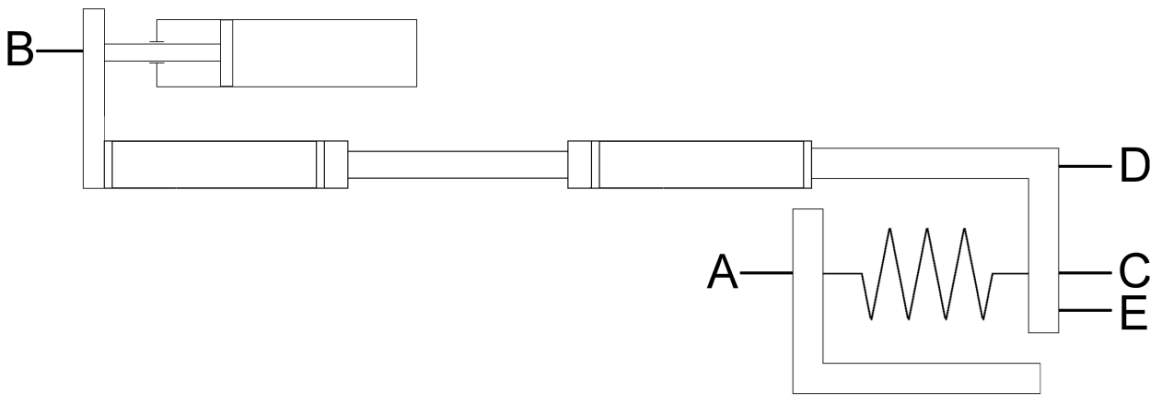

Fig. 5-6 Sketch of the horizontal axis with vibration measurement sites.

To analyse the stiffness of the horizontal axis, the displacements of site B (actuator pressure plate) and D (upper mounting flange) at 1,980 N load were evaluated and a stiffness of 10 kN/mm was determined. Considering the truss with 12 kN/mm and the axis as two collinear springs, the overall stiffness summed up to 5,450 N/mm. (Huber & Mischke, 2010) reported the shear stiffnesses of the FSUs at a maximum of about 450 N/mm. This was more than 10 times less than the test rig stiffness, therefore it was sufficient.

5.3 Shear Fatigue Measurements

Determination of the fatigue failure cycles in shear experiments turned out to be more complex than in the compression experiments. Two different mechanisms (change in peak-to-peak displacement and displacement gradient change) occurred and the differentiation between them was sometimes unclear. A MATLAB tool was developed to display mean displacement and peak-to-peak displacement in two additional diagrams. A clear gradient change with no or a slight change in peak to peak displacement was rated as a major failure.

Shear experiments exhibited a complex failure mechanism. To support the description in section 3.3.2, all displacement diagrams not displayed in the report are shown in Fig. 5-7 to Fig. 5-11.

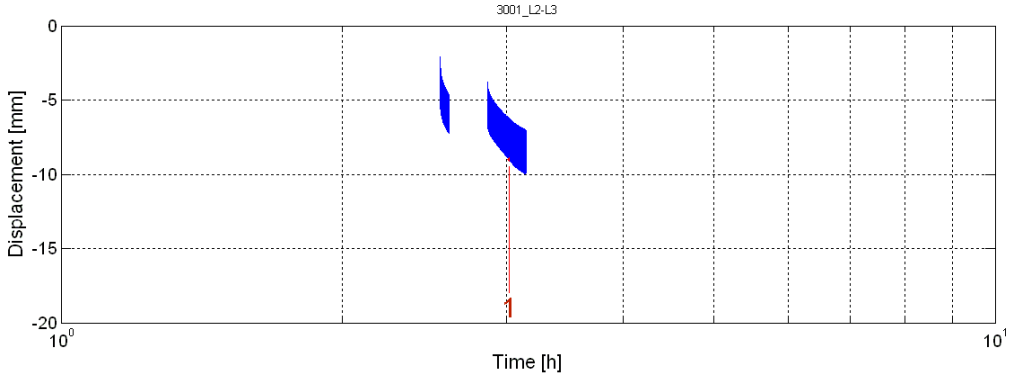

Fig. 5-7 Creep curve of LWS 3001 L2-L3: mark 1 indicates minor failure.

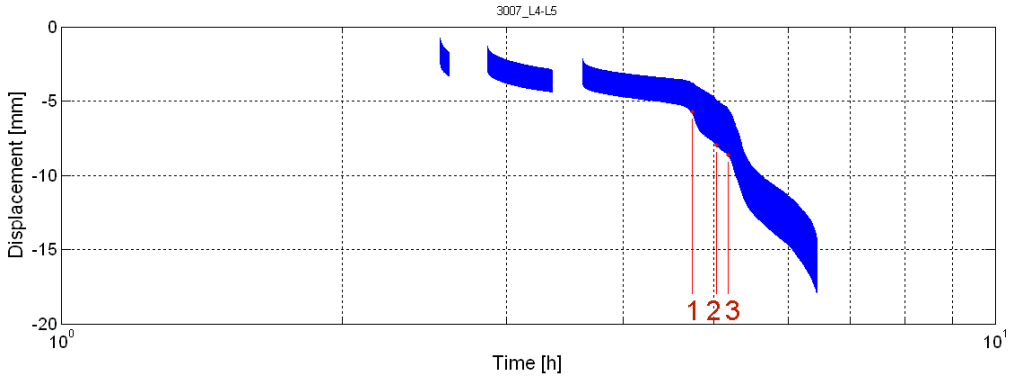

Fig. 5-8 Creep curve of LWS 3007 L4-L5: mark 1 indicates minor failure with overlapping major failure; mark 2 indicates a minor failure; and mark 3 indicates the major and final failure.

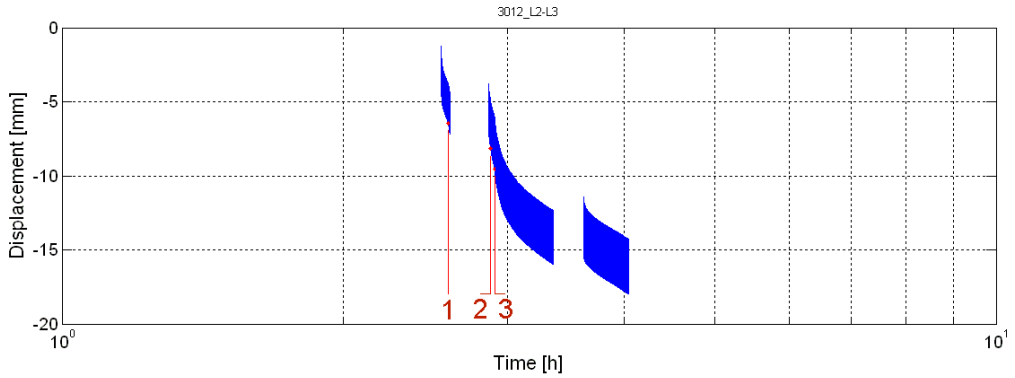

Fig. 5-9 Creep curve of LWS 3012 L2-L3: mark 1 indicates major failure; mark 2 and 3 indicate minor failures.

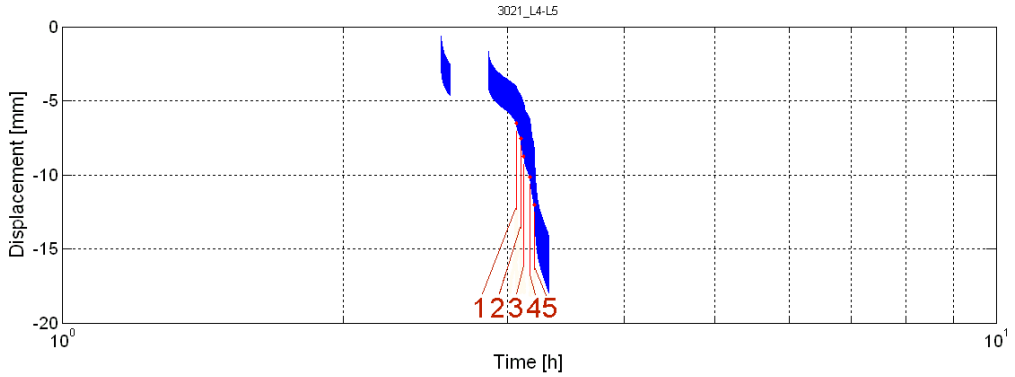

Fig. 5-10 Creep curve of LWS 3021 L4-L5: mark 1 to 3 indicate minor failures; mark 4 and 5 indicate major failures (failure at mark 5 with more distinct characteristics).

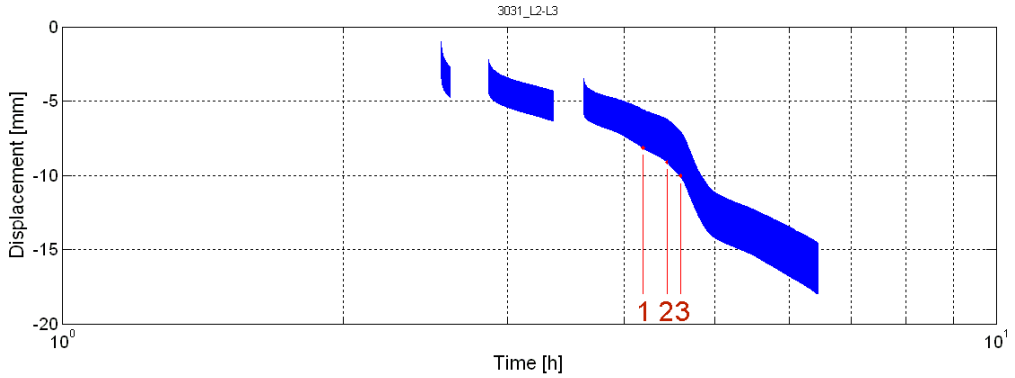

Fig. 5-11 Creep curve of LWS 3031 L2-L3: mark 1 and 2 indicate minor failures; mark 3 indicates the major and final failure.

5.4 Test Days

Tab. 5-1 Date of testing of fatigue-tested specimens (grey values indicate FSUs excluded from the statistics for fatigue testing).

Fatigue group	Donor group	ID	Level	Date of Testing
NORM	Midlife Male	3006	L4-L5	05.05.11
	Midlife Male	3009	L2-L3	22.09.11
	Midlife Male	3023	L4-L5	17.06.11
	Midlife Male	3028	L2-L3	12.09.11
	Midlife Female	3011	L4-L5	10.05.11
	Midlife Female	3014	L2-L3	24.05.11
	Midlife Female	3017	L2-L3	11.05.11
	Midlife Female	3026	L4-L5	18.08.11
OFFSET	Midlife Male	3006	L2-L3	04.05.11
	Midlife Male	3016	L4-L5	03.05.11
	Midlife Male	3025	L4-L5	11.08.11
	Midlife Male	3030	L2-L3	14.09.11
	Midlife Female	3004	L2-L3	30.05.11
	Midlife Female	3014	L4-L5	25.05.11
	Midlife Female	3026	L2-L3	17.08.11
	Midlife Female	3027	L4-L5	08.09.11
HIGH	Young Male	3001	L4-L5	22.08.11
	Young Male	3005	L2-L3	06.04.11
	Young Male	3013	L4-L5	22.06.11
	Young Male	3019	L2-L3	27.07.11
	Young Male	3031	L4-L5	20.09.11
	Young Male	3032	L2-L3	07.10.11
	Midlife Male	3016	L2-L3	02.05.11
	Midlife Male	3023	L2-L3	16.06.11
	Midlife Male	3028	L4-L5	13.09.11
	Midlife Male	3030	L4-L5	15.09.11
	Midlife Female	3004	L4-L5	31.05.11
	Midlife Female	3017	L4-L5	12.05.11
	Midlife Female	3011	L2-L3	09.05.11
	Midlife Female	3018	L2-L3	14.06.11
SHEAR	Young Male	3001	L2-L3	23.08.11
	Young Male	3007	L4-L5	31.08.11
	Young Male	3012	L2-L3	28.08.11
	Young Male	3021	L4-L5	30.08.11
	Young Male	3031	L2-L3	21.09.11
	Young Male	3032	L4-L5	07.10.11

6 References

Brinckmann, P.; Biggemann, M.; Hilweg, D.: Prediction of the compressive strength of human lumbar vertebrae. Clinical Biomechanics 4 (1989), Suppl. 2

Costi, J.J.; Hearn, T.C.; Fazzalari, N.L.: The effect of hydration on the stiffness of intervertebral discs in an ovine model. Clinical Biomechanics 17 (2002), 6, 446-455

Cripton, P.; Berleman, U.; Visarius H.; Begeman, P.C.; Nolte, L.P.; Prasad, P.: Response of the lumbar spine due to shear loading. In: Wayne State University - Injury Prevention Through Biomechanics 4.-5. May 1995, Symposium Proceedings, 111-126, Detroit

Dhillon, N.; Bass, E.C.; Lotz, J.C.: Effect of frozen storage on the creep behavior of human intervertebral discs. Spine 26 (2001), 8, 883-888

Frobin, W.; Brinckmann, P.; Biggemann, M.; Tillotson, M.; Burton, K.: Precision measurement of disc height, vertebral height and sagittal plane displacement from lateral radiographic views of the lumbar spine. Clinical Biomechanics 12 (1997), Suppl. 1

Gleizes, V.; Viguier, E.; Féron, J.M.; Canivet, S.; Lavaste, F.: Effects of Freezing on the Biomechanics of the Intervertebral Disc. Surgical and Radiologic Anatomy 20 (1998), 6, 403-407

Huber, G.; Mischke, Ch.; Skrzypiec, D.M.; Seidel, H.: Dependence of spinal segment mechanics on age and posture. Bundesanstalt für Arbeitsschutz und Arbeitsmedizin. Dortmund: 2010. Forschungsprojekt F 2069

Huber, G.; Paetzhold, H.; Püschel, K.; Morlock, M.M.: Verhalten von Wirbelsäulensegmenten bei dynamischer Belastung. Bundesanstalt für Arbeitsschutz und Arbeitsmedizin. Dortmund: 2005. Forschungsprojekt F 1899

Huber, G.; Skrzypiec, D.M.; Klein, A.; Püschel, K.; Morlock, M.M.: High cycle fatigue behavior of functional spinal units. Industrial Health 48 (2010) 5, 550-556

Jürgens, H.W.: Erhebung anthropometrischer Maße zur Aktualisierung der DIN 33 402-Teil 2. Bremerhaven: Wirtschaftsverlag NW, 2004. (Schriftenreihe der Bundesanstalt für Arbeitsschutz und Arbeitsmedizin)

Schütz, W.: A history of fatigue. Engineering Fracture Mechanics 54 (1996), 2, 263-300

Schust, M.; Menzel, G.; Hofmann, J.; Forta, N.G.; Pinto, I.; Hinz, B.; Bovenzi, M.: Measures of internal lumbar load in professional drivers – dependence on posture, anthropometry, age, duration of exposure and type of machine. Proceedings of the 5th International Conference on Whole Body Vibration Injuries, Amsterdam, 5-7 June 2013.

Seidel, H.; Pöpplau, B.; Morlock, M.M.; Püschel, K.; Huber, G.: The size of lumbar vertebral endplate areas - Prediction by anthropometric characteristics and significance for fatigue failure due to whole-body vibration. International Journal of Industrial Ergonomics 38 (2008), 9-10, 844-855

Seidel, H.; Hinz, B.; Hofmann, J.; Menzel, G.: Intraspinal forces and health risk caused by whole-body vibration – Predictions for European drivers and different field conditions. Int J Ind Ergonomics 38 (2008), 856-867

Simon, P.; Espinoza Orías, A.A.; Andersson, G.B.J., An, H.S.; Inoue, N.: In vivo topographic analysis of lumbar facet joint space width distribution in healthy and symptomatic subjects. Spine 37 (2012), 12, 1058-1064

Skrzypiec, D.M.; Klein, A.; Bishop, N.E.; Stahmer, F.; Püschel, K.; Seidel, H.; Morlock, M.M.; Huber, G.: Shear strength of the human lumbar spine. Clinical Biomechanics 27 (2012), 7, 646-651

Thompson, J.; Pearce, R.; Schechter, M.; Adams, M.; Tsang, I.; Bishop, P.: Preliminary evaluation of a scheme for grading the gross morphology of the human intervertebral disc. Spine. 15 (1990), 5, 411-415

van Dieën, J.H.; van der Veen, A.; van Royen, B.J.; Kingma, I.: Fatigue failure in shear loading of porcine lumbar spine segments. Spine 31 (2006), 15, 494-498

van Solinge, G.B.; van der Veen, A.J.; van Dieën, J.H.; Kingma, I.; van Royen, B.J.: Anterior shear strength of the porcine lumbar spine after laminectomy and partial facetectomy. European Spine Journal 19 (2010), 12, 2130-2136

7 Acknowledgement

The kind support of Dr. Jan Kolb, Dr. Daniel Skrzypiec, Kay Sellenschloh, Matthias Vollmer, Julian Gührs and Berry Pöpplau is deeply appreciated.